Revealing the molecular picture of surface ligand-interactions in thiocyanate-capped nanocrystals by 2D IR spectroscopy

by

SAMADHAN HARIDAS DESHMUKH

10CC18A26005

A thesis submitted to the

Academy of Scientific & Innovative Research

for the award of the degree of

DOCTOR OF PHILOSOPHY

in

SCIENCE

Under the supervision of

Dr. Sayan Bagchi

CSIR- National Chemical Laboratory, Pune

Academy of Scientific and Innovative Research

AcSIR Headquarters, CSIR-HRDC campus

Sector 19, Kamla Nehru Nagar,

Ghaziabad, U.P. – 201 002, India

July, 2023

Certificate

This is to certify that the work included in this Ph.D. thesis entitled, "***Revealing the molecular picture of surface-ligand interactions in thiocyanate-capped nanocrystals by 2D IR spectroscopy***", submitted by ***Mr. Samadhan Haridas Deshmukh*** to the Academy of Scientific and Innovative Research (**AcSIR**) in partial fulfilment of the requirements for the award of the Degree of ***Doctor of Philosophy in Science***, embodies original research work carried-out by the student. I/We, further certify that this work has not been submitted to any other University or Institution in part or full for the award of any degree or diploma. Research material(s) obtained from other source(s) and used in this research work has/have been duly acknowledged in the thesis. Image(s), illustration(s), figure(s), table(s) etc., used in the thesis from other source(s), have also been duly cited and acknowledged.

Samadhan Haridas Deshmukh

(Research Student)

Date: 31/07/2023

Dr. Sayan Bagchi

(Research Supervisor)

Date: 31/07/2023

STATEMENTS OF ACADEMIC INTEGRITY

I Mr. Samadhan Haridas Deshmukh, a Ph.D. student of the Academy of Scientific and Innovative Research (AcSIR) with Registration No. 10CC18A26005 hereby undertake that, the thesis entitled "Revealing the molecular picture of surface ligand-interactions in thiocyanate-capped nanocrystals by 2D IR spectroscopy" has been prepared by me and that the document reports original work carried out by me and is free of any plagiarism in compliance with the UGC Regulations on *"Promotion of Academic Integrity and Prevention of Plagiarism in Higher Educational Institutions (2018)"* and the CSIR Guidelines for *"Ethics in Research and in Governance (2020)"*.

Signature of the Student

Date : 31.07.2023

Place : Pune

It is thereby certified that the work done by the student, under my supervision is plagiarism-free in accordance with the UGC Regulations on *"Promotion of Academic Integrity and Prevention of Plagiarism in Higher Educational Institutions (2018)"* and the CSIR Guidelines for *"Ethics in Research and in Governance (2020)"*.

Signature of the Supervisor

Dr. Sayan Bagchi

Date : 31.07.2023

Place : Pune

This thesis is dedicated to

My parents, Mrs. Nanda Deshmukh, & Mr. Haridas Deshmukh

and, My niece Radha

for their endless support and inspiration.

Acknowledgments

Throughout my doctoral research journey, I have been fortunate to have the company, support, and guidance of numerous individuals. I would like to seize this moment to extend my deepest gratitude and heartfelt appreciation to each and every person who has accompanied and supported me throughout my doctoral research journey.

I would like to begin by expressing my deep appreciation to my supervisor Dr. Sayan Bagchi for his unwavering support and guidance throughout this journey. His constant presence and valuable insights have been indispensable to my progress. I am deeply grateful for the immeasurable impact that his unparalleled expertise, wise guidance, and generous support have had on my doctoral journey. Through his invaluable contributions, I have not only grown as a researcher but have also matured into a thoughtful and responsible individual. I consider myself incredibly fortunate to be a member of Dr. Sayan Bagchi's esteemed research group at CSIR-National Chemical Laboratory. It is an immense privilege to work alongside him and be a part of such a distinguished team. Being a part of Dr. Bagchi research group at CSIR-National Chemical Laboratory has been transformative. It is here that I have imbibed the values of hard work and discipline, shaping both my professional and personal growth. Under his guidance, I have not only honed my scientific skills but also learned to think creatively and innovatively. What I have gained and learned from him can never be repaid in any possible form. I strongly believe that the best way to express gratitude is by making significant contributions to the scientific community in the future. Working alongside him has been an extraordinary opportunity that has enriched my life in countless ways.

I extend my sincere gratitude to my doctoral advisory committee (DAC) members, Dr. Sarika Bhattacharyya, Dr. Arnab Mukherjee and Dr. Jayaraj Nithyanandhan, for their constant support, guidance, and valuable suggestions throughout my Ph.D. I am also thankful to the student academic office of NCL for their unwavering assistance. I acknowledge Dr. Sunita Barve, Mr. Gati Krushna Nayak, and the library staff for their support and granting access to resources. Additionally, I would like to express my appreciation to the NCL administrative staff for their continual support whenever needed.

I am grateful to Prof. Dr. Ashish K. Lele (Director, CSIR-NCL), Prof. Dr. Ashwini K. Nangia (Former Director, CSIR-NCL), Prof. Dr. B. L. V Prasad (Former HoD, Division of Physical & Materials Chemistry, CSIR-NCL) and Dr. T.G. Ajithkumar (HoD, Division of Physical & Materials Chemistry, CSIR-NCL) for giving me this opportunity and providing me with advanced research infrastructure and facilities. I sincerely thank our collaborator, Dr. Sameer Sapra (IIT Delhi), and his student, Dr. Sushma Yadav. I owe a special thanks to Dr. Angshuman Nag (IISER Pune) and Dr. Arup Rath (NCL Pune) for their productive conversations, helpful comments, and kind suggestions. I would like to extend a special thanks to Dr. Arup Rath and his students Chandan, Neha, and Dr. Debranjan Mandal for their invaluable help and guidance in the field of nanocrystal synthesis. Their support has been instrumental in my research journey.

I am delighted to express my heartfelt gratitude to my labmates, Srijan Chatterjee, Tubai Chowdhury, Shivshankar Kore, Akhil Pathania, Akhil B Mon, Sucheta Ghosh, Dr. Somnath Kashid, Dr. Pranab deb, Dr. Tapas Haldar, Dr. Sushil Sakpal, Deborin da and Kaushik da, for their selfless dedication and invaluable suggestions. Their generosity in sharing their time and knowledge has been truly invaluable to me. I express my special thanks to all my roommates, friends and seniors in NCL for their kind help, support, and best wishes.

I would like to express my sincere acknowledgment to the Council of Scientific and Industrial Research (CSIR) for granting me the fellowship that enabled me to pursue my Ph.D. at CSIR-NCL. Additionally, I am grateful to the Academy of Scientific and Innovative Research (AcSIR) for the opportunity to present my research work in the form of a thesis. Their support has been invaluable in facilitating my academic journey.

My heartfelt appreciation and gratitude go to my family, who have consistently showered me with unconditional love, care, and unwavering support. I owe my achievements to the freedom and encouragement provided by my mother Mrs. Nanda Deshmukh, my father Mr. Haridas Deshmukh and my sister Balika Deshmukh, who have played an integral role in shaping my life and defining the person I am today. A smile possesses a remarkable power to dispel all worries that burden our lives. The beaming smile of my niece, Radha, has the magical ability to effortlessly erase the anxieties and stresses of this bustling lifestyle.

I am indebted to all my teachers who have played vital roles in my life. I sincerely extend my respect and gratitude to them for their invaluable contributions

Finally, with deep reverence and profound gratitude, I humbly acknowledge the blessings bestowed upon me by the divine. I am grateful for every experience in my Ph.D. journey, both the positive and the challenging, for they have shaped me and taught me valuable lessons. I am thankful for all my accomplishments and accept the few losses I have encountered along the way. Each moment has been a mix of blessings and lessons, deserving of appreciation and reflection.

Samadhan Haridas Deshmukh

Table of Contents

Chapter 1 ……..1

1.1 Basic of nanocrystals……5

1.2 Synthesis of nonocrystals…….8

1.3 Surface chemistry of nanocrystals……..…10

1.4 Ultrafast spectroscopy……12

1.5 Outline of the thesis…….....14

1.6 References…….15

Chapter 2 ……..…22

2.1 UV-Visible Absorption Spectroscopy……..23

2.2 X-ray diffraction spectroscopy…….……23

2.3 Transmission Electron Microscopy…….….24

2.4 Fourier Transform Infrared Spectroscopy (FTIR)……24

2.5 Two-dimensional Infrared Spectroscopy (2D IR) spectroscopy….....26

2.5.1 2D IR Experimental setup, pulse sequence……..…..27

2.5.2 Spectral signature 2D IR spectrum……..…..29

2.5.3 Spectral diffusion of 2D IR peak…….……..31

2.6 Quantum Espresso calculations……..….33

2.7 Zeta potential……...34

2.8 References……..….34

Chapter 3…….36

3.1 Introduction…….....37

3.2 Materials and Method…….…38

3.2.1 Chemicals…….…….38
3.2.2 Synthesis of CdS nanocrystals……..39
3.2.3 Ligand exchange……...39
3.2.4 IR spectroscopy…….40
3.2.5 2D IR spectroscopy……...40
3.2.6 Material characterisation……..…….41
3.3 Results and discussion……..….41
3.4 Conclusion……....50
3.5 References…….51
Chapter 4……55
4.1 Introduction……...….56
4.2 Materials and Method…….…...58
4.2.1 Chemicals……..58
4.2.2 CdSe nanocrystals synthesis…….……58
4.2.3 Ligand exchange……...……59
4.2.4 IR spectroscopy……..……..59
4.3 Results and discussion…….……..…59
4.4 Conclusion…….……66
4.5 References……....…67
Chapter 5……...70
5.1 Introduction…….....71
5.2 Materials and Method…….…...…...73
5.2.1 Chemicals…….….....73
5.2.2 CdSe nanocrystals synthesis…….…….....74
5.2.3 Ligand exchange…….……..….74
5.2.4 IR spectroscopy…….…….……...…74

5.2.4 Pump probe spectroscopy……..75
5.3 Results and discussion…….…...75
5.4 Conclusion……...……...84
5.5 References…….…….....84
Chapter 6……...…….…..87
6.1 Summary……...…….….88
6.2 Future Scope……...….…..89
6.2.1 Understanding the molecular level picture of azide (different ligand) capped nanocrystals……..……..….90
6.2.2 Estimation of effect the organic and inorganic capped ligands on Cd nuclei of CdS and CdSe nanocrystals by Cd NMR spectroscopy...90
6.2.3 Probing the electric field exerted by size dependent NCs by 4MBN as ligand and Vibrational reporter……..……..…91
6.3 References…….....….92

Chapter 1

Introduction

The semiconductor nanocrystals (NCs) or quantum dots (QDs) are the artificial tiny particles of 1-10 nm in size which have been widely explored in last few decades. NCs are the important nucleus of modern nanotechnology revolution. Scientific and industrial community got attracted toward NCs due to high surface-to-volume ratio, and their tunability in size, shape, electronic, magnetic, and optical properties.[1-5] The quantum confinement effect of nanocrystals underpins their size dependent electronic properties, which change from molecular material to bulk like material. The increase in the size of NCs enable their valuable size tuneable optical properties. Surface covering organic/inorganic ligands determine their solubility in nonpolar/polar solvents.[6] Colloidal stability of NCs is maintained by the steric/electrostatic interactions of the surface ligands in solutions.[6] The judicious choice of surface covering ligands, semiconducting materials, and the size, shape, morphology, and dimensions of the NCs provides distinctly tunable optical and electronic properties.[7-11] These properties make them potential candidates for a wide range of applications, including photovoltaics, optoelectronics, photocatalytics, and biodiagnostics.[12-17] Generally, long bulky ligands (C8 to C18 hydrocarbon chains) are used for colloidal nanocrystal synthesis. These bulky insulating ligands, attached to the surface of NCs, create a layer around the NCs which saturates the dangling bonds and separates the NCs from their surrounding environments. This allows designing of NCs of a high degree of size, phase homogeneity, and desired shape. [18] Furthermore, these ligands help controling the nucleation rate and growth kinetics of NCs. It is clear from these examples that the ligands play an essential role throughout the NC synthesis and processing.

Surface modification of nanocrystals is a highly intense area of research due to its important role in various applications across a broad range of disciplines. The surface properties of NCs significantly affect their chemical and physical characteristics, which in turn determine their behaviour in different environments. Surface modification techniques, such as functionalization and coating, can be used to modify the surface properties of NCs for specific applications.[19-21] Functionalization can improve the stability, biocompatibility, and solubility of the NCs, However, changing the surface ligand can enhance their optical, electronic, and catalytic properties.[22] As a result, surface modification of NCs is crucial in fields of biomedicine, environmental science, energy, and electronics. For example, functionalized NCs can be used as drug delivery agents, sensors, and imaging probes for biomedical applications, while surface-coated NCs can be employed in solar cells, batteries, and catalysis.[21, 23] Charge carrier mobility within the NCs is extreme important when they

condense as a solid film for specific applications. To enhance the efficiency of the NC-based devices, there is a growing need to replace the long chain, bulky insulating organic ligands with shorter ones.[22, 24] This change can improve the charge carrier mobility and conductivity of the nanocrystals, leading to a more efficient device performance. The long chain ligands create a significant barrier to the charge transport, and hinder the performance of the device due to the longer interparticle distance and the weak electronic communication. By replacing the long chain ligands with shorter variants, the surface-to-volume ratio of the nanocrystals increases, creating a closer approach for NCs. The strong inter-particle association allows better charge transport and improved device efficiency.

Bulky organic ligands are replaced with shorter inorganic ligands, such as halides, pseudohalides, and chalcogenides to improve the electronic communication between nanocrystals and to enhance the charge carrier mobility.[6, 22, 25-26] These ligands help to minimize the large interparticle distance between nanocrystals, promoting efficient charge transfer and improving the performance of nanocrystal-based devices. In addition to these ligands, chalcogenidometallates, halometales, and polyoxomatallates are also being explored as potential replacements for bulky organic ligands.[6, 27-28] These inorganic ligands offer several advantages, including improved stability, better solubility, and enhanced electronic communication between the nanocrystals. Solution-based ligand exchange has emerged as a popular approach for replacing long-chain organic ligands with shorter inorganic variants. Bulky ligands like oleic acid create inorganic (core) - organic (ligands) interface at the surface of nanocystals, however short inorganic ligands make inorganic- inorganic interface at the NC surface.

Fundamental understating of surface-ligand interaction is very important to optimize, modify, and strengthen the working window of technology-based devices. Despite the surface of nanocrystals being a critical feature in nanotechnology, our fundamental understanding of the interactions between ligands and nanocrystals is limited due to a lack of molecular-level information. However, recently, tremendous interest in this interface of the ligands and the nanocrystal surface has grown considerably. Surface chemistry studies have employed ^{1}H and ^{31}P NMR spectroscopy to investigate the binding of bulky ligands to the surface of nanocrystals, as well as the dynamic nature of these ligands and the equilibrium between bound and free ligands.[29-31] Thiocyanate, a short inorganic ligand, has been used recently to enhance device performance.[6, 22, 25] ^{1}H NMR spectroscopy can't be used to investigate the surface ligand interactions of thiocyanate-capped nanocrystals, as thiocyanate ligand lacks a hydrogen atom that can be detected by ^{1}H NMR spectroscopy. ^{13}C NMR might provide

insights into the surface science of the thiocyanate ligands.[22] Distinctive features such as spectral broadening, shift, and new spectral signature can be plausibly utilized to differentiate between thiocyanate-capped nanocrystals and free thiocyanate in ^{13}C NMR spectroscopy. Due to the low natural abundance of ^{13}C, isotope-labelled thiocyanate is used for ligand exchange to achieve a significant signal in ^{13}C NMR spectroscopy by Kagan *et al*. However, analysis of the resulting ^{13}C NMR spectrum of thiocyanate-capped nanocrystals shows a single peak that is similar to the spectrum of free thiocyanate. Interpreting the ^{13}C NMR spectrum of thiocyanate-capped nanocrystals and free thiocyanate is challenging because of the similar results obtained in both cases, making it difficult to draw any plausible conclusions. The nature of the surface-ligand interaction in inorganic ligand capped NCs has not been reported to date due to the lack of appropriate experimental technique.

Vibrational spectroscopies can be utilized to report on both organic and inorganic-capped nanocrystals. FTIR and Raman spectroscopy have been utilized to gain insights into the chemical environment of the ligand shell surrounding nanocrystals, including the identity of the ligands and their binding nature.[22, 32-34] In addition to the steady state experiments, time-resolved vibrational spectroscopy can provide additional complementary information about the NC-ligand surface. Recently transient IR spectroscopy was used to study oleic acid-capped nanocystals.[35-36]

During my graduate research, I have used ultrafast two dimensional infrared (2D IR) spectroscopy, a time-resolved spectroscopy technique, to obtain an in-depth understanding of the ligand–NC surface interactions in inorganic ligand (thiocyanate) capped nanocrystals. 2D IR is a widely used ultrafast technique to understand structural dynamics in complex condense phase media, materials, and biology.[37-40] Thiocyanate plays a dual role, it acts a surface ligand and a vibrational reporter. Thiocyanate is an often-used vibrational marker to probe a variety of system involving electrolytes, green solvents, materials, and biology.[40-43] Combining steady state vibrational spectroscopy, time-resolved vibrational spectroscopies, and quantum chemical calculations can reveal the molecular level picture of surface-ligand interactions in thiocyanate-capped nanocrystals.

Above, I have introduced the importance of nanocrystals and the surface-ligand interactions in NCs. Additionally, I have mentioned that replacing the bulky organic ligands by short inorganic ligands improves the charge carried mobility in NCs. Next, I will provide a general, and a more elaborate introduction of the fundamentals of NCs, their synthesis, the surface chemistry of NCs, and ultrafast vibrational spectroscopy.

1.1 Basic of nanocystals

The energy gap is the spacing between the fully occupied valence band and the unoccupied conduction band, which is one of the defining features of semiconductor nanocrystals. During light absorption, electrons (phonon) from the valence band can jump into the conduction band due to a small band gap separation. This phenomenon creates an empty space in the valence band, referred to as a hole. (Figure 1.1) Excited electron and hole form an electron-hole pair, called exciton, which stays together due to Coulombic attraction, and the distance between electron and hole is known as 'exciton Bohr radius.'

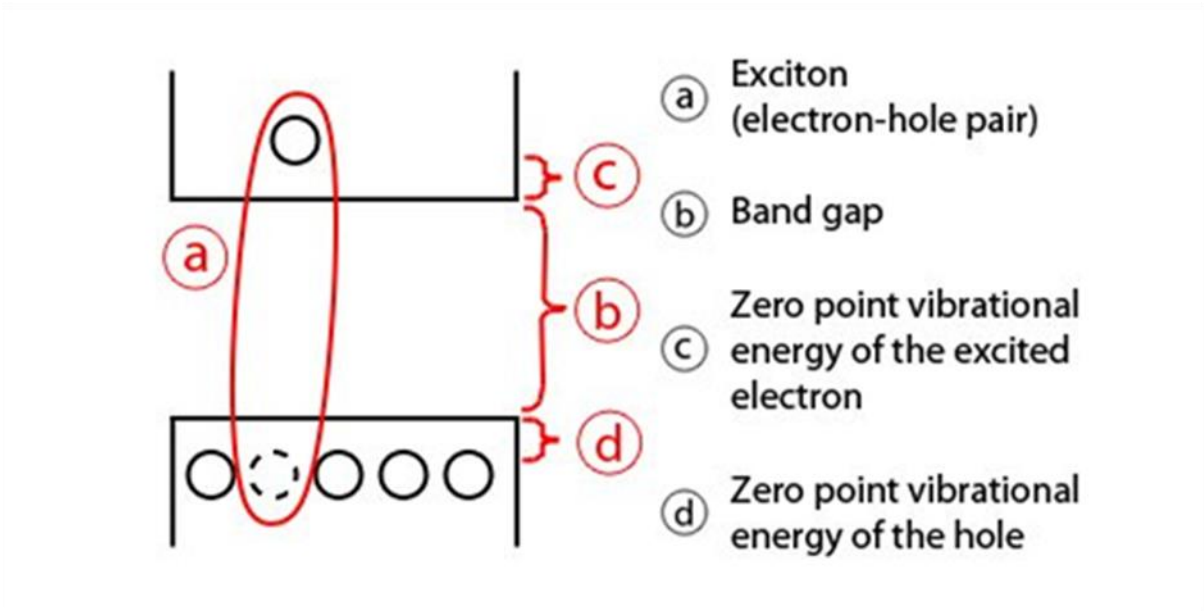

Figure 1.1: Schematic representation of excited state electron and hole.

For bulk semiconductors, the band gap is fixed and determined by the structure and composition of the respective materials because, in bulk semiconductors, there are infinite semiconducting crystals having a periodic arrangement of atoms. If this large number of atoms comes together to form a bulk like crystal, then their atomic orbitals can overlap with each other to make a band-like electronic structure. However, in the case of small semiconductor nanocrystals, the number of atoms per nanocrystal is limited, so it can't form a continuous band like structure, but rather discrete energy levels. (Figure 1.2) In nanoscale semiconductor crystals (typically less than 10–20 nm in size), the band gap, which is the energy difference between the valence and conduction bands, is influenced by the dimensions

of the crystal due to the tight spatial confinement of electron and hole wave functions. The size range in which this effect plays an important role is known as the region of quantum confinement. The semiconductor nanoparticles that fall within this size window are known as quantum dots or nanocrystals. In other words, when the size of a semiconducting

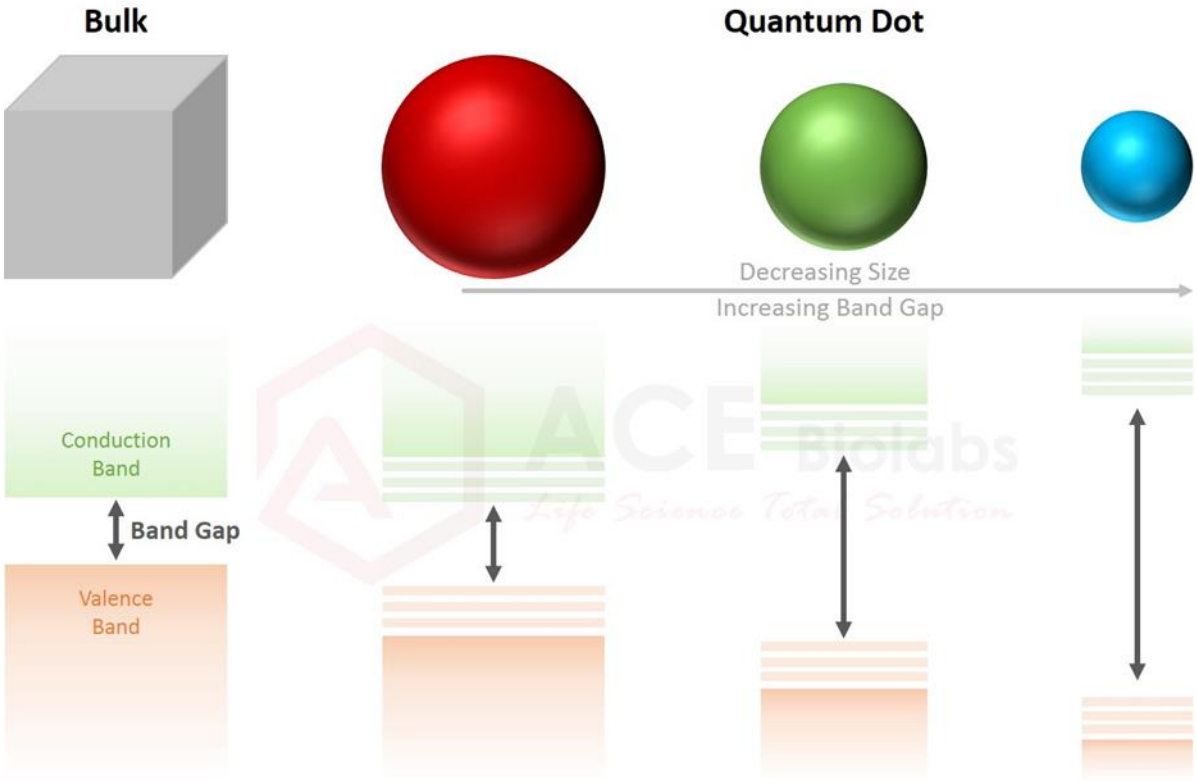

Figure 1.2: Schematic representation of band structure from bulk material to quantum dots and change in band gap.

particle is smaller than the exciton Bohr radius, excitons are physically confined to this size, and the band gap increases with the decrease in size of the semiconductor along with the quantized energy levels of the conduction and valence bands. This effect is called the quantum confinement effect. The semiconductor nanoscale particle that exhibits the quantum confinement effect is known as the quantum dot.

Fundamentally, nanocrystals rely on the concept of quantum confinement, in which electrons and holes are confined within nanoscale structures, resulting in distinct quantum properties.[44] The simplest and easiest example for understanding the quantum confinement effect is a particle in a 1D box. In microelectronics, there are small semiconductor nanocrystals that

having electron hole pairs. This is a real world "particle in box" system where indeed the electrons stay always inside the in a box. Inside the box, particles can only move to and fro due to the unpassable barrier at both ends. The potential energy at the wall of the box is infinity (V=∞ for x<0 or x>L) and inside the box is zero (V=0 for 0<x<L). This implies that the particle has zero probability of being located at the edge of the wall or outside the box. Within the confines of the box, the particle experiences no external forces and is able to move freely.

The wavefunction provides the fundamental description of a particle's behaviour. The Schrödinger equation is solved to obtain the wavefunction. The measurable properties, like its energy, position, and momentum, can be obtained from the wavefunction. The wavefunction of a free particle exhibits a travelling wave behaviour (equation 1.1) and the energy of this particle is a continuous quantity (equation 1.2).

$$\psi k\ (x) = Ae^{iKx} \quad \text{.....} \quad (1.1)$$

Here ψ_k is the wavefunction, x is the position of the particle, K is the wave vector, i is the imaginary part, and A is the amplitude of the wavefunction.[45]

$$E = \frac{\hbar^2 k^2}{2m_0} = \frac{p^2}{2m_0} \quad \text{.....} \quad (1.2)$$

Here, E is the energy of the particle, k is the wavenumber, and $\hbar$ is the reduced Planck's constant. Momentum p = mv putting this value we get equation 1.2. If free particle inside the 1D box has an infinite potential window, then the wavefunction of that particle changes from the travelling wavefunction to the standing wavefunction equation 1.3

$$\psi_n(x) = \sqrt{\frac{2}{L}}\, sin\frac{n\pi x}{L} \quad \text{.....} \quad (1.3)$$

The energy associated with the particle undergoes a transition from a continuous energy level to discrete energy level.[46] (equation 1.4)

$$E_n = \frac{(\hbar n\pi)^2}{2m_0 L^2} \quad \text{.....} \quad (1.4)$$

L is the length of 1D box, and *n* is a positive integer (1,2,3…..) Interestingly, the energy gap (ΔE) between two discrete levels decreases with an increase in the length of the box. The spherical box equations were derived by Louis Brus.

Semiconducting nanocrystals are a highly growing research field in academia and industry due to their unique properties arising from the confinement effect and high surface-to-volume ratio. Their size and shape-tunable optical, magnetic, and electronic properties have made them widely utilised in the fields of photovoltaics, light emitting diodes, photodetectors, and active materials in electronics, magnetics, catalysis, and biomedicine.

1.2 Synthesis of nanocrystals

The interest in the science of low-dimensional systems called nanoscience is a recognition of the famous statement made by Feynman that "There's Plenty of Room at the Bottom." When the dimensions of bulk materials are reduced to the nanoscale, dramatic changes in properties are observed. Nanoscale materials have been differentiated based on the nanoscale reduction of nanostructure dimensions to merely one, two, or three dimensions. Quantum well structures are nanostructures that have only one of their three dimensions reduced. If there are two dimensions at the nanoscale, then it is called a quantum wire, and if all dimensions are converted to the nanoscale, the structure is referred to as a quantum dot or nanocrystal. These three categories of nanostructures have the common word "quantum" because changes in their properties result from the physics of quantum mechanics. The synthesis of nanocrystals plays an important role in nanoscience. When nanocrystal materials are available with the desired size, shape, morphology, crystal structure, and chemical composition, new chemical and physical properties and usages of nanocrystals for a wide range of applications are possible. Two approaches, top-down and bottom-up, have been used to synthesise quantum dots (QDs) or nanocrystals (NCs). (Figure 1.3) In the top-down approach for nanocrystal synthesis, larger bulk materials are broken down into smaller nanoscale particles. This method involves the physical or chemical manipulation of a bulk material to create nanoscale particles with specific properties. The top-down method is simple for producing the desired structure with appropriate properties. However, the biggest problem with this method is the imperfection of the surface structure. This surface imperfection has a significant impact on the physical and chemical properties of the nanostructure. The bottom-up approach has the

ability to create less waste; as a result, this method is more economical compared to the top-down method. In the bottom-up method, the build-up of nanostructure is done from the bottom, like atom by atom, molecule by molecule, or cluster by cluster. Among these two methods, the bottom-up method is widely used in the synthesis of nanostructures due to many merits like homogeneous chemical composition, less waste, and better ordering.

The synthesis of colloidal NCs requires precursors, organic surfactants (long-chain acids), and high-boiling solvents. At high temperatures, the precursor materials break down into monomers, leading to a state of supersaturation. After that, nucleation starts to give NC growth. Reaction temperature, growth time, and concentration affect the growth of NCs. Let us first consider the temperature effect: at too high temperatures, secondary nucleation is initiated, which creates a broad

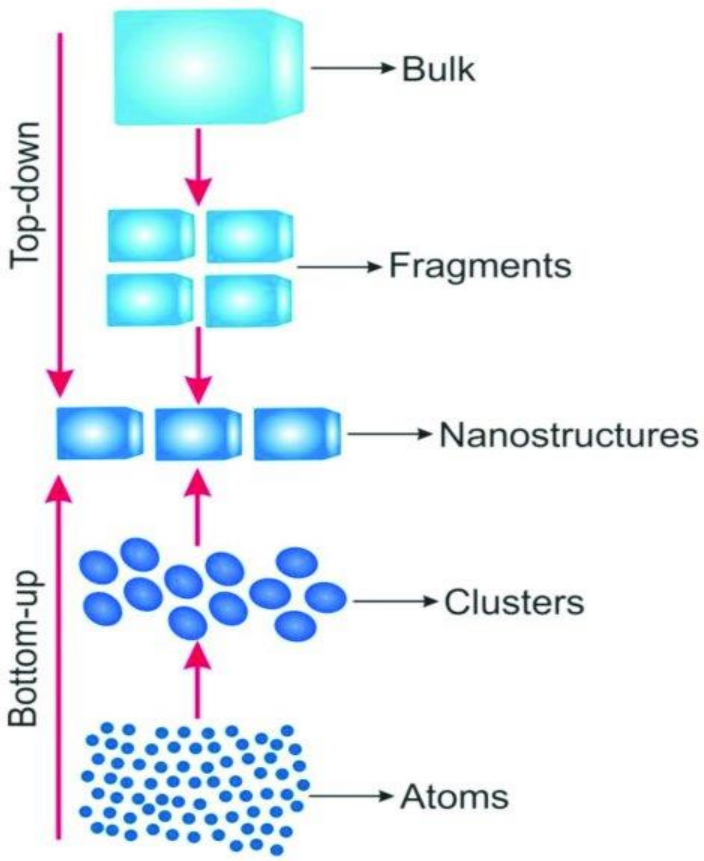

Figure 1.3: Schematic representation of Top-down and Bottom up approach for synthesis of nanocrystals.

size distribution of NCs; however, at too low temperatures, NC growth is not efficient and might produce poor crystallinity and quality NCs. Secondly The growth time of nanocrystals, which refers to the duration during which nanocrystals are allowed to form, can have significant effects on their properties. A longer growth time leads to larger NCs, while shorter growth times yield smaller nanocrystals. Short growth times prepare more uniform and monodisperse nanocrystals with a narrower size distribution. On the other hand, longer growth times can lead to more variability in size and shape, which creates a polydisperse and broader size distribution. Lastly, high monomer concentrations create small critical sizes and monodisperse colloidal NCs. On the other hand, at low monomer concentrations, synthesis has a large critical size and Oswald ripening, which leads to polydisperse size distribution. As the size and shape of NCs play a pivotal role, numerous reports are available to control size and shape by adjusting the reaction temperature the growth time, concentration, and surface ligands. In this thesis, all the NCs were synthesised by the hot injection method, which is a bottom-up approach.

1.3 Surface chemistry of nanocrystals

The characteristics and applications of nanoscale materials are heavily influenced by their surface chemistry, which plays a critical role in determining their properties. For bulk materials, only a small concentration of atoms is present at the surface; thus, the contribution of externally broken chemical bonds to material characteristics is negligible. For any material, the surface-to-volume ratio varies inversely with the linear dimension. With decreasing material size, the role of surface increases and, in the end, becomes dominant. Surfaces can substantially change some characteristics and produce entirely new effects at the nanoscale.[47-48] Traditional surface research has demonstrated that surface reconstruction moves surface atoms away from lattice locations to reduce the energy of massive crystal surfaces.[49] Surfaces with dangling bonds can create new electronic states and external molecules also affect the reactivity and energy of crystal surfaces.[50-51] All these surface effects of large crystals apply to NCs even though they have small facet sizes and multiple edge and corner sites.

The optoelectronics and solar photochemistry research communities have shown a great interest in colloidal QDs or nanocrystals due to their size-tunable electrical characteristics and high surface area-to-volume ratios.[52-54] As the ratio of surface to core atoms increases in colloidal nanocrystals, the properties of the surface atoms start to dominate the overall

particle properties. Surface atoms differ chemically from core atoms due to the termination of the semiconductor lattice at the NCs surface. Colloidal nanocrystals undergo photochemical or photocatalytic transformations at their surfaces, where the ligand-nanocrystal boundaries play a crucial role in mediating the primary energy and charge transfer processes.[55-57] The structure and surface chemistry of ligand-nanocrystal boundaries critically influence the energetic height and width of barriers governing energy and charge transfer processes in colloidal nanocrystals. Surface ligand dynamics and their electronic communication with the NC surface also have a significant impact on the photochemical transformation.[58-59] The electronic states of NCs can be significantly influenced by the surface chemistry and electronic interactions of ligands attached to nanocrystal surfaces.[60-62] Ligands play a significant role in the catalytic activity of nanocrystals, particularly in the solution phase. NCs-ligand shells can either inhibit or facilitate the adsorption of catalytic substrates and electron transfer, depending on the specific case. The surface chemistry of organic or inorganic ligand-capped NCs has a great impact on their catalytic reactivity. For the photo-reduction of nitrobenzene to aniline, capping ligands play multiple roles.[63] The efficiency of multi-phonon emission in NCs is attributed to size-dependent vibronic coupling factors to phonon modes, which rely on the size of NCs. The magnitude of this vibronic coupling factor depends upon the surface chemistry of the particles.[64]

Surface ligands tune the physical and chemical properties of NCs, resulting in maximum efficiency in device-based applications. Bulky capping surface ligands are routinely replaced by short inorganic ligands. Despite the important role of the surface chemistry of NCs, it has not been fully explored yet due to the limitations of conventional spectroscopy and chemical analysis to understand the surface chemistry of NCs. A bunch of spectroscopic techniques have been used to understand the heterogeneous NC surface chemistry. Vibrational spectroscopy, FTIR, and Raman are simple methods for getting surface ligand information.[22, 33-34] NMR spectroscopy (^{1}H, ^{13}C, ^{31}P) is also routinely engaged in NC surface analysis.[65-66]Small-angle X-ray scattering (SAXS) and dynamic light scattering (DLS) have been used to determine the effective thickness of NC's ligand capping layer.[6, 67] Understanding the structure and properties of NC's surface requires an intricate mix of concepts and modern methodological tools. Attempts to understand the surface chemistry of bulky organic ligand passivated NCs have been made[68] however, a detailed understanding of small inorganic ligand-capped NCs is still not explored.

1.4 Ultrafast spectroscopy

Spectroscopy is commonly used to study the interaction between light and matter. It reveals the quantized energy levels associated with electronic, vibrational, and rotational motions in all substances. Traditional spectroscopy allows us to investigate energy levels and chemical reactions within human-controlled time scales, provides information that is statistical in nature. However, for rapid processes like transition states, molecular motions, charge separation, and exciton transfer, high-resolution (in time) techniques are necessary. Dynamic information about the system under study can be measured by using pulsed light sources.

The investigation of processes in science is ultimately connected with the development of new tools that overcome the limitations of our natural sense to know natural processes. The processes that take place for longer than 50 milliseconds can be resolved visually. To understand the real time dynamical processes, one needs to use a very short time interval in which the motion of an object is frozen, allowing for a snapshot of the different evolutions of the system. The journey to time-resolved measurement started with the high speed photography experiment performed by Eadweard Muybridge in 1878. He used multiple cameras, along with fast shutter speeds, to capture millisecond movements. Muybridge captured different phases of motion for a running horse, and after connecting the camera snapshots, he created a movie in which we can see the motions of the horse's legs. This was the first step in a revolution in the time resolution of high speed photography. Edgerton invented stroboscopic photography in the mid-20th century with time resolution in the microsecond range.[69] Short light pulses can be used for monitoring and initiating dynamical processes. In 1899 Abraham and Lemoine reported the pump-probe technique in which two synchronised light pulses were used, pump pulse initiate the phenomenon of excitation and probe pulse observe the time dependent changes of an optical property of sample under study.[70] Norrish and Porter[71] another technique called as flash photolysis which consist two consist two electronically delayed light flashes having milli to micro second time resolution. They received the Nobel Prize in chemistry for their work in 1967. To know the time resolution necessary for molecular processes in real time, one can borrow the argument used in 1999 Nobel Prize lecture on the development of femtochemistry by Ahmed Zewail.[72]

Ultrafast spectroscopy is an experimental technique that uses ultrashort light pulses to investigate the dynamical processes in atoms, molecules, nanostructures and solids. This

research field has gained rapid growth in the last decade due to two main reasons: first one is the technological development of ultrashort light pulses technologically, including their length, frequency tunability and stability. The second reason is that the creation of complex spectroscopic methods that go beyond the traditional pump-probe setup has allowed for an increase in the amount of data available on the processes being studied. Ultrafast spectroscopy was revolutionised by the production of tunable, stable ultrafast pulses with widths of a few femtoseconds using solid state titanium sapphire lasers, chirped pulse amplification, and the pumping of optical parametric amplifiers. These advancements made it possible to apply the methodology to a considerably wider range of physical chemistry issues as well as to create new, more sophisticated experiments.

An abundance of structural, energetic, and dynamical knowledge about molecular, biological, and nanomaterial systems has been revealed through multidimensional optical spectroscopies. The phenomena covered by these investigations include bound exciton pair correlations in quantum wells,[73-77] exciton dissociation in photovoltaic thin films,[78-80] vibrational dynamics in solid-state materials, and quantum coherence in natural light harvesting. They have been useful in pinpointing the precise molecular movements involved in protein folding[81-83] and structural dynamics,[43, 84-85] as well as providing mechanistic insights into complex non-radiative relaxation[86-87] and chemical reaction or solvation dynamics.[88-90] The correlation between broadband excitation and emission frequencies as a function of system evolution is the primary benefit that two-dimensional (2D) ultrafast spectroscopies offer over one-dimensional counterparts, such as transient absorption or transient grating, and it makes it possible to resolve both homogeneous (anti-diagonal) and inhomogeneous (diagonal) line shape components. A 2D line's changing shape provides information about the frequency-frequency correlation function (FFCF). The dynamics of the FFCF provide details on the amplitudes and timeframes connected to changes in the optical frequencies under investigation, brought on by modifications to the molecular structure or the evolution of the solvent or protein environment.[91-93] These multidimensional experiments' increased information richness typically enables the simultaneous identification and resolution of overlapping ground state bleach/stimulated emission and excited state absorption features.

The quickest motions in the liquid state can be resolved by pulses of a few femtoseconds, which have also shown how these motions are connected to intermolecular interactions. The degree of pair correlation in polar molecular liquids and the type of contacts in ionic liquids,

as well as their relationship to macroscopic features was disclosed by ultrafast IR and Raman investigations.[94-95] Studies of the dynamics of straightforward probe molecules or ions in the liquid phase have been carried out using polarization-resolved IR pump-probe and two-dimensional IR (2D IR) techniques.[96] The 2D IR approach has been used to analyse fibrinogen to fibrin formation[97] as well as to investigate the architectures of amyloid fibrils, by using a site-specific aspartate residue as an IR probe.[98]. In this thesis, 2D IR and pump-probe spectroscopic methods used for investigation of thiocyanate capped nanocrystals surface-ligand interaction.

1.5 Outline of the thesis

The outline of thesis is as follows:

In this thesis we used ultrafast spectroscopic techniques to reveal the molecular level picture of inorganic ligand capped nanocrystals. This thesis work will help to optimize, maximize the efficiency of nanocrystal based devices.

Chapter 2 includes thorough details regarding the experimental and computational techniques employed in this thesis.

Chapter 3 includes an understanding of the surface ligand interaction of short inorganic ligand capped CdS nanocrystals. In this chapter, we used an experimental and theoretical approach to explore the surface capping of CdS by thiocyanate ions. After replacing the bulky ligands with short ligands of nanocrystals for better performance of devices, these short ligands provide colloidal stabilization for nanocrystals in the polar solvent. Surface coverage of bulky surface ligands has been revealed by NMR spectroscopy however, surface coverage of short inorganic ligands has not been explored yet due to the limitations of conventional spectroscopic methods. In this context, we performed 2D IR experiments on thiocyanate capped CdS nanocrystals. Ligand dynamic time scale reveals that there are three subpopulations of thiocyanate present in the colloidal stabilization of nanocrystals which are strongly bound, weakly bound, and free. Thiocyanate ions can be bound through the S or N ends to the surface of CdS, quantum chemical calculations are used to differentiate the binding mode of SCN^- ions. The combined experimental and theoretical investigation of thiocyanate capped CdS gives a molecular level picture of ligand-surface interactions.

Chapter 4 The electrostatic stabilisation of CdS and CdSe nanocrystals by thiocyanate ions is covered in this chapter. Short ligands stabilise the nanocrystals electrostatically, while lengthy, bulky surfactant ligands used during synthesis give colloidal stabilisation through steric interactions. The DLVO theory is used to analyse electrostatic interaction in colloidal suspension, zeta potential measurements, which take into account electrical double layers, are used to report electrostatic stabilisation in nanocrystals. Here, we carried out independent polarization-selective 2D IR investigations on CdS and CdSe with thiocyanate caps. It is supported by polarisation selective frequency-frequency correlation decay that thiocyanate ions interact electrostatically with the surface of naocrystals. Our findings give clear evidence that short inorganic ligands interact electrostatically with the NCs surface.

Chapter 5 The effect of particle size on the orientational dynamics of weakly interacting inorganic ligands is explored in this chapter. The orientation dynamics of bound organic and inorganic ligands have been studied however, the orientation dynamics of weakly interacting species in inorganic capped ligands have not been explored yet. We employed SCN^- passivated NCs of various particle sizes. The orientation dynamics of weakly interacting ligands are calculated using polarisation selective pump-probe spectroscopy. With an increase in NC size, reorientation dynamics (anisotropy decay) exhibit an increase in offset. The slowdown of the orientational dynamics suggests that as the NC size increases, the electric field in the layer farthest from the NC surface grows. When we take into account the size-dependent charge density of the NCs, this seems contradictory. We have demonstrated in this chapter that the considerable curvature of the bound thiocyanate layer prevents effective shielding of larger NCs. This fundamental finding will help improve the stability and working capacity of NCs for specific applications.

Chapter 6 discuss the future scope for all three working chapters (Chapter 3, Chapter 4 and Chapter 5) and the summary of the thesis.

1.6 References

1. Murray, C. B.; Norris, D. J.; Bawendi, M. G., Synthesis and characterization of nearly monodisperse CdE (E = sulfur, selenium, tellurium) semiconductor nanocrystallites. *J. Am. Chem. Soc.* **1993,** *115*, 8706-8715.

2. Yu, W. W.; Wang, Y. A.; Peng, X., Formation and Stability of Size-, Shape-, and Structure-Controlled CdTe Nanocrystals: Ligand Effects on Monomers and Nanocrystals. *Chem. Mater.* **2003,** *15*, 4300-4308.
3. Manna, L.; Milliron, D. J.; Meisel, A.; Scher, E. C.; Alivisatos, A. P., Controlled growth of tetrapod-branched inorganic nanocrystals. *Nat. Mater.* **2003,** *2*, 382-385.
4. Park, Y. I.; Piao, Y.; Lee, N.; Yoo, B.; Kim, B. H.; Choi, S. H.; Hyeon, T., Transformation of hydrophobic iron oxide nanoparticles to hydrophilic and biocompatible maghemite nanocrystals for use as highly efficient MRI contrast agent. *J. Mater. Chem.* **2011,** *21*, 11472-11477.
5. and, C. B. M.; Kagan, C. R.; Bawendi, M. G., Synthesis and Characterization of Monodisperse Nanocrystals and Close-Packed Nanocrystal Assemblies. *Annu. Rev. Mater. Sci.* **2000,** *30*, 545-610.
6. Boles, M. A.; Ling, D.; Hyeon, T.; Talapin, D. V., The surface science of nanocrystals. *Nat. Mater.* **2016,** *15*, 141-153.
7. Guo, J.; Kim, J.-Y.; Zhang, M.; Wang, H.; Stein, A.; Murray, C. B.; Kotov, N. A.; Kagan, C. R., Chemo- and Thermomechanically Configurable 3D Optical Metamaterials Constructed from Colloidal Nanocrystal Assemblies. *ACS Nano* **2020,** *14*, 1427-1435.
8. Wang, W.; Pan, Z.; Rao, H.; Zhang, G.; Song, H.; Zhang, Z.; Zhong, X., Proton Initiated Ligand Exchange Reactions for Colloidal Nanocrystals Functionalized by Inorganic Ligands with Extremely Weak Coordination Ability. *Chem. Mater.* **2020,** *32*, 630-637.
9. Mishra, N.; Vasavi Dutt, V. G.; Arciniegas, M. P., Recent Progress on Metal Chalcogenide Semiconductor Tetrapod-Shaped Colloidal Nanocrystals and their Applications in Optoelectronics. *Chem. Mater.* **2019,** *31*, 9216-9242.
10. Lee, W. S.; Kang, Y. G.; Woo, H. K.; Ahn, J.; Kim, H.; Kim, D.; Jeon, S.; Han, M. J.; Choi, J.-H.; Oh, S. J., Designing High-Performance CdSe Nanocrystal Thin-Film Transistors Based on Solution Process of Simultaneous Ligand Exchange, Trap Passivation, and Doping. *Chem. Mater.* **2019,** *31*, 9389-9399.
11. Koscher, B. A.; Nett, Z.; Alivisatos, A. P., The Underlying Chemical Mechanism of Selective Chemical Etching in CsPbBr3 Nanocrystals for Reliably Accessing Near-Unity Emitters. *ACS Nano* **2019,** *13*, 11825-11833.
12. Yang, J.; Cho, S. C.; Lee, S.; Yoon, J. W.; Jeong, W. H.; Song, H.; Oh, J. T.; Lim, S. G.; Bae, S. Y.; Lee, B. R.; Ahmadi, M.; Sargent, E. H.; Yi, W.; Lee, S. U.; Choi, H., Guanidinium-Pseudohalide Perovskite Interfaces Enable Surface Reconstruction of Colloidal Quantum Dots for Efficient and Stable Photovoltaics. *ACS Nano* **2022,** *16*, 1649-1660.
13. Cherniukh, I.; Rainò, G.; Sekh, T. V.; Zhu, C.; Shynkarenko, Y.; John, R. A.; Kobiyama, E.; Mahrt, R. F.; Stöferle, T.; Erni, R.; Kovalenko, M. V.; Bodnarchuk, M. I., Shape-Directed Co-Assembly of Lead Halide Perovskite Nanocubes with Dielectric Nanodisks into Binary Nanocrystal Superlattices. *ACS Nano* **2021,** *15*, 16488-16500.
14. Gheshlaghi, N.; Foroutan-Barenji, S.; Erdem, O.; Altintas, Y.; Shabani, F.; Humayun, M. H.; Demir, H. V., Self-Resonant Microlasers of Colloidal Quantum Wells Constructed by Direct Deep Patterning. *Nano Lett.* **2021,** *21*, 4598-4605.
15. Kelley, M. L.; Ahmed, F.; Abiodun, S. L.; Usman, M.; Jewel, M. U.; Hussain, K.; zur Loye, H.-C.; Chandrashekhar, M. V. S.; Greytak, A. B., Photoconductive Thin Films Composed of Environmentally Benign AgBiS2 Nanocrystal Inks Obtained through a Rapid Phase Transfer Process. *ACS Appl. Electron. Mater.* **2021,** *3*, 1550-1555.
16. Gréboval, C.; Chu, A.; Goubet, N.; Livache, C.; Ithurria, S.; Lhuillier, E., Mercury Chalcogenide Quantum Dots: Material Perspective for Device Integration. *Chem. Rev.* **2021,** *121*, 3627-3700.

17. Kairdolf, B. A.; Smith, A. M.; Stokes, T. H.; Wang, M. D.; Young, A. N.; Nie, S., Semiconductor Quantum Dots for Bioimaging and Biodiagnostic Applications. *Annu Rev Anal Chem* **2013,** *6*, 143-162.
18. Pradhan, N.; Reifsnyder, D.; Xie, R.; Aldana, J.; Peng, X., Surface Ligand Dynamics in Growth of Nanocrystals. *J. Am. Chem. Soc.* **2007,** *129*, 9500-9509.
19. Szendrei, K.; Jarzab, D.; Yarema, M.; Sytnyk, M.; Pichler, S.; Hummelen, J. C.; Heiss, W.; Loi, M. A., Surface modification of semiconductor nanocrystals by a methanofullerene carboxylic acid. *J. Mater. Chem.* **2010,** *20*, 8470-8473.
20. Moghaddam, N.; Dabard, C.; Dufour, M.; Po, H.; Xu, X.; Pons, T.; Lhuillier, E.; Ithurria, S., Surface Modification of CdE (E: S, Se, and Te) Nanoplatelets to Reach Thicker Nanoplatelets and Homostructures with Confinement-Induced Intraparticle Type I Energy Level Alignment. *J. Am. Chem. Soc.* **2021,** *143*, 1863-1872.
21. Heuer-Jungemann, A.; Feliu, N.; Bakaimi, I.; Hamaly, M.; Alkilany, A.; Chakraborty, I.; Masood, A.; Casula, M. F.; Kostopoulou, A.; Oh, E.; Susumu, K.; Stewart, M. H.; Medintz, I. L.; Stratakis, E.; Parak, W. J.; Kanaras, A. G., The Role of Ligands in the Chemical Synthesis and Applications of Inorganic Nanoparticles. *Chem. Rev.* **2019,** *119*, 4819-4880.
22. Fafarman, A. T.; Koh, W.-k.; Diroll, B. T.; Kim, D. K.; Ko, D.-K.; Oh, S. J.; Ye, X.; Doan-Nguyen, V.; Crump, M. R.; Reifsnyder, D. C.; Murray, C. B.; Kagan, C. R., Thiocyanate-Capped Nanocrystal Colloids: Vibrational Reporter of Surface Chemistry and Solution-Based Route to Enhanced Coupling in Nanocrystal Solids. *J. Am. Chem. Soc.* **2011,** *133*, 15753-15761.
23. Harris, R. D.; Bettis Homan, S.; Kodaimati, M.; He, C.; Nepomnyashchii, A. B.; Swenson, N. K.; Lian, S.; Calzada, R.; Weiss, E. A., Electronic Processes within Quantum Dot-Molecule Complexes. *Chem. Rev.* **2016,** *116*, 12865-12919.
24. Nag, A.; Kovalenko, M. V.; Lee, J.-S.; Liu, W.; Spokoyny, B.; Talapin, D. V., Metal-free Inorganic Ligands for Colloidal Nanocrystals: S2–, HS–, Se2–, HSe–, Te2–, HTe–, TeS32–, OH–, and NH2– as Surface Ligands. *J. Am. Chem. Soc.* **2011,** *133*, 10612-10620.
25. Koh, W.-k.; Saudari, S. R.; Fafarman, A. T.; Kagan, C. R.; Murray, C. B., Thiocyanate-Capped PbS Nanocubes: Ambipolar Transport Enables Quantum Dot Based Circuits on a Flexible Substrate. *Nano Lett.* **2011,** *11*, 4764-4767.
26. Kovalenko, M. V.; Scheele, M.; Talapin, D. V., Colloidal Nanocrystals with Molecular Metal Chalcogenide Surface Ligands. *Science* **2009,** *324*, 1417-1420.
27. Ocier, C. R.; Whitham, K.; Hanrath, T.; Robinson, R. D., Chalcogenidometallate Clusters as Surface Ligands for PbSe Nanocrystal Field-Effect Transistors. *J. Phys. Chem. C* **2014,** *118*, 3377-3385.
28. Huang, J.; Liu, W.; Dolzhnikov, D. S.; Protesescu, L.; Kovalenko, M. V.; Koo, B.; Chattopadhyay, S.; Shenchenko, E. V.; Talapin, D. V., Surface Functionalization of Semiconductor and Oxide Nanocrystals with Small Inorganic Oxoanions (PO43–, MoO42–) and Polyoxometalate Ligands. *ACS Nano* **2014,** *8*, 9388-9402.
29. De Roo, J.; Yazdani, N.; Drijvers, E.; Lauria, A.; Maes, J.; Owen, J. S.; Van Driessche, I.; Niederberger, M.; Wood, V.; Martins, J. C.; Infante, I.; Hens, Z., Probing Solvent–Ligand Interactions in Colloidal Nanocrystals by the NMR Line Broadening. *Chem. Mater.* **2018,** *30*, 5485-5492.
30. Singh, S.; Leemans, J.; Zaccaria, F.; Infante, I.; Hens, Z., Ligand Adsorption Energy and the Postpurification Surface Chemistry of Colloidal Metal Chalcogenide Nanocrystals. *Chem. Mater.* **2021,** *33*, 2796-2803.
31. Anderson, N. C.; Owen, J. S., Soluble, Chloride-Terminated CdSe Nanocrystals: Ligand Exchange Monitored by 1H and 31P NMR Spectroscopy. *Chemistry of Materials* **2013,** *25*, 69-76.

32. Cass, L. C.; Malicki, M.; Weiss, E. A., The Chemical Environments of Oleate Species within Samples of Oleate-Coated PbS Quantum Dots. *Anal. Chem.* **2013,** *85*, 6974-6979.
33. Zhang, J.; Zhang, H.; Cao, W.; Pang, Z.; Li, J.; Shu, Y.; Zhu, C.; Kong, X.; Wang, L.; Peng, X., Identification of Facet-Dependent Coordination Structures of Carboxylate Ligands on CdSe Nanocrystals. *J. Am. Chem. Soc.* **2019,** *141*, 15675-15683.
34. Pienpinijtham, P.; Han, X. X.; Ekgasit, S.; Ozaki, Y., Highly Sensitive and Selective Determination of Iodide and Thiocyanate Concentrations Using Surface-Enhanced Raman Scattering of Starch-Reduced Gold Nanoparticles. *Anal. Chem.* **2011,** *83*, 3655-3662.
35. Leger, J. D.; Friedfeld, M. R.; Beck, R. A.; Gaynor, J. D.; Petrone, A.; Li, X.; Cossairt, B. M.; Khalil, M., Carboxylate Anchors Act as Exciton Reporters in 1.3 nm Indium Phosphide Nanoclusters. *J. Phys. Chem. Lett.* **2019,** *10*, 1833-1839.
36. Kennehan, E. R.; Munson, K. T.; Doucette, G. S.; Marshall, A. R.; Beard, M. C.; Asbury, J. B., Dynamic Ligand Surface Chemistry of Excited PbS Quantum Dots. *J. Phys. Chem. Lett.* **2020,** *11*, 2291-2297.
37. Hunt, N. T., 2D-IR spectroscopy: ultrafast insights into biomolecule structure and function. *Chem. Soc. Rev.* **2009,** *38*, 1837-1848.
38. Ghosh, A.; Ostrander, J. S.; Zanni, M. T., Watching Proteins Wiggle: Mapping Structures with Two-Dimensional Infrared Spectroscopy. *Chem. Rev.* **2017,** *117*, 10726-10759.
39. Le Sueur, A. L.; Horness, R. E.; Thielges, M. C., Applications of two-dimensional infrared spectroscopy. *Anal.* **2015,** *140*, 4336-4349.
40. Nishida, J.; Breen, J. P.; Lindquist, K. P.; Umeyama, D.; Karunadasa, H. I.; Fayer, M. D., Dynamically Disordered Lattice in a Layered Pb-I-SCN Perovskite Thin Film Probed by Two-Dimensional Infrared Spectroscopy. *J. Am. Chem. Soc.* **2018,** *140*, 9882-9890.
41. Ren, Z.; Brinzer, T.; Dutta, S.; Garrett-Roe, S., Thiocyanate as a Local Probe of Ultrafast Structure and Dynamics in Imidazolium-Based Ionic Liquids: Water-Induced Heterogeneity and Cation-Induced Ion Pairing. *J. Phys. Chem. B* **2015,** *119*, 4699-4712.
42. Wei, Q.; Zhou, D.; Li, X.; Chen, Y.; Bian, H., Structural Dynamics of Dimethyl Sulfoxide Aqueous Solutions Investigated by Ultrafast Infrared Spectroscopy: Using Thiocyanate Anion as a Local Vibrational Probe. *J. Phys. Chem. B* **2018,** *122 50*, 12131-12138.
43. Fafarman, A. T.; Webb, L. J.; Chuang, J. I.; Boxer, S. G., Site-Specific Conversion of Cysteine Thiols into Thiocyanate Creates an IR Probe for Electric Fields in Proteins. *J. Am. Chem. Soc.* **2006,** *128*, 13356-13357.
44. Ashoori, R. C., Electrons in artificial atoms. *Nature* **1996,** *379*, 413-419.
45. Schmidt, H. M.; Weller, H., Quantum size effects in semiconductor crystallites: Calculation of the energy spectrum for the confined exciton. *Chem. Phys. Lett.* **1986,** *129*, 615-618.
46. Griffiths, D. J.; Schroeter, D. F., *Introduction to quantum mechanics*. Cambridge university press: 2018.
47. and, C. B. M.; Kagan, C. R.; Bawendi, M. G., Synthesis and Characterization of Monodisperse Nanocrystals and Close-Packed Nanocrystal Assemblies. *Annu. Rev. Mater. Sci.* **2000,** *30* (1), 545-610.
48. Ozbay, E., Plasmonics: Merging Photonics and Electronics at Nanoscale Dimensions. *Science* **2006,** *311*, 189-193.
49. Giessibl, F. J., Atomic Resolution of the Silicon (111)-(7×7) Surface by Atomic Force Microscopy. *Science* **1995,** *267*, 68-71.
50. Chadi, D. J., Atomic and Electronic Structures of Reconstructed Si(100) Surfaces. *Phys. Rev. Lett.* **1979,** *43*, 43-47.

51. Tarlov, M. J.; Burgess, D. R. F., Jr.; Gillen, G., UV photopatterning of alkanethiolate monolayers self-assembled on gold and silver. *J. Am. Chem. Soc.* **1993,** *115*, 5305-5306.
52. Nozik, A. J.; Beard, M. C.; Luther, J. M.; Law, M.; Ellingson, R. J.; Johnson, J. C., Semiconductor Quantum Dots and Quantum Dot Arrays and Applications of Multiple Exciton Generation to Third-Generation Photovoltaic Solar Cells. *Chem. Rev.* **2010,** *110*, 6873-6890.
53. Kramer, I. J.; Sargent, E. H., The Architecture of Colloidal Quantum Dot Solar Cells: Materials to Devices. *Chem. Rev.* **2014,** *114*, 863-882.
54. Pietryga, J. M.; Park, Y.-S.; Lim, J.; Fidler, A. F.; Bae, W. K.; Brovelli, S.; Klimov, V. I., Spectroscopic and Device Aspects of Nanocrystal Quantum Dots. *Chem. Rev.* **2016,** *116*, 10513-10622.
55. Malicki, M.; Knowles, K. E.; Weiss, E. A., Gating of hole transfer from photoexcited PbS quantum dots to aminoferrocene by the ligand shell of the dots. *ChemComm.* **2013,** *49*, 4400-4402.
56. Irgen-Gioro, S.; Yang, M.; Padgaonkar, S.; Chang, W. J.; Zhang, Z.; Nagasing, B.; Jiang, Y.; Weiss, E. A., Charge and energy transfer in the context of colloidal nanocrystals. *Chem. Phys. Rev.* **2020,** *1*.
57. Wu, K.; Zhu, H.; Lian, T., Ultrafast Exciton Dynamics and Light-Driven H2 Evolution in Colloidal Semiconductor Nanorods and Pt-Tipped Nanorods. *Acc. Chem. Res.* **2015,** *48*, 851-859.
58. Boldt, K.; Jander, S.; Hoppe, K.; Weller, H., Characterization of the Organic Ligand Shell of Semiconductor Quantum Dots by Fluorescence Quenching Experiments. *ACS Nano* **2011,** *5*, 8115-8123.
59. Morris-Cohen, A. J.; Vasilenko, V.; Amin, V. A.; Reuter, M. G.; Weiss, E. A., Model for Adsorption of Ligands to Colloidal Quantum Dots with Concentration-Dependent Surface Structure. *ACS Nano* **2012,** *6*, 557-565.
60. Frederick, M. T.; Amin, V. A.; Weiss, E. A., Optical Properties of Strongly Coupled Quantum Dot–Ligand Systems. *J. Phys. Chem. Lett.* **2013,** *4*, 634-640.
61. Brown, P. R.; Kim, D.; Lunt, R. R.; Zhao, N.; Bawendi, M. G.; Grossman, J. C.; Bulović, V., Energy Level Modification in Lead Sulfide Quantum Dot Thin Films through Ligand Exchange. *ACS Nano* **2014,** *8*, 5863-5872.
62. Kroupa, D. M.; Vörös, M.; Brawand, N. P.; McNichols, B. W.; Miller, E. M.; Gu, J.; Nozik, A. J.; Sellinger, A.; Galli, G.; Beard, M. C., Tuning colloidal quantum dot band edge positions through solution-phase surface chemistry modification. *Nat. Commun.* **2017,** *8*, 15257.
63. Jensen, S. C.; Bettis Homan, S.; Weiss, E. A., Photocatalytic Conversion of Nitrobenzene to Aniline through Sequential Proton-Coupled One-Electron Transfers from a Cadmium Sulfide Quantum Dot. *J. Am. Chem. Soc.* **2016,** *138*, 1591-1600.
64. Kelley, A. M., Electron−Phonon Coupling in CdSe Nanocrystals. *J. Phys. Chem. Lett.* **2010,** *1*, 1296-1300.
65. Gomes, R.; Hassinen, A.; Szczygiel, A.; Zhao, Q.; Vantomme, A.; Martins, J. C.; Hens, Z., Binding of Phosphonic Acids to CdSe Quantum Dots: A Solution NMR Study. *J. Phys. Chem. Lett.* **2011,** *2*, 145-152.
66. Hanrahan, M. P.; Chen, Y.; Blome-Fernández, R.; Stein, J. L.; Pach, G. F.; Adamson, M. A. S.; Neale, N. R.; Cossairt, B. M.; Vela, J.; Rossini, A. J., Probing the Surface Structure of Semiconductor Nanoparticles by DNP SENS with Dielectric Support Materials. *J. Am. Chem. Soc.* **2019,** *141*, 15532-15546.
67. Weir, M. P.; Toolan, D. T. W.; Kilbride, R. C.; Penfold, N. J. W.; Washington, A. L.; King, S. M.; Xiao, J.; Zhang, Z.; Gray, V.; Dowland, S.; Winkel, J.; Greenham, N. C.; Friend, R. H.; Rao, A.; Ryan, A. J.; Jones, R. A. L., Ligand Shell Structure in Lead Sulfide–Oleic

Acid Colloidal Quantum Dots Revealed by Small-Angle Scattering. *J. Phys. Chem. Lett.* **2019,** *10*, 4713-4719.
68. De Roo, J., The Surface Chemistry of Colloidal Nanocrystals Capped by Organic Ligands. *Chem. Mater.* **2023,** *35*, 3781-3792.
69. Edgerton, H. E.; Killian, J. R., Moments of vision: the stroboscopic revolution in photography. *(No Title)* **1979**.
70. Maiuri, M.; Garavelli, M.; Cerullo, G., Ultrafast Spectroscopy: State of the Art and Open Challenges. *J. Am. Chem. Soc.* **2020,** *142*, 3-15.
71. Norrish, R. G. W.; Porter, G., Chemical Reactions Produced by Very High Light Intensities. **1949,** *164*, 658-658.
72. Zewail, A. H., Femtochemistry: Atomic-Scale Dynamics of the Chemical Bond. *J. Phys. Chem. A* . **2000,** *104*, 5660-5694.
73. Engel, G. S.; Calhoun, T. R.; Read, E. L.; Ahn, T.-K.; Mančal, T.; Cheng, Y.-C.; Blankenship, R. E.; Fleming, G. R., Evidence for wavelike energy transfer through quantum coherence in photosynthetic systems. *Nature* **2007,** *446*, 782-786.
74. Calhoun, T. R.; Ginsberg, N. S.; Schlau-Cohen, G. S.; Cheng, Y.-C.; Ballottari, M.; Bassi, R.; Fleming, G. R., Quantum Coherence Enabled Determination of the Energy Landscape in Light-Harvesting Complex II. *J. Phys. Chem. B* **2009,** *113*, 16291-16295.
75. Collini, E.; Wong, C. Y.; Wilk, K. E.; Curmi, P. M. G.; Brumer, P.; Scholes, G. D., Coherently wired light-harvesting in photosynthetic marine algae at ambient temperature. *Nature* **2010,** *463*, 644-647.
76. Scholes, G. D.; Fleming, G. R.; Chen, L. X.; Aspuru-Guzik, A.; Buchleitner, A.; Coker, D. F.; Engel, G. S.; van Grondelle, R.; Ishizaki, A.; Jonas, D. M.; Lundeen, J. S.; McCusker, J. K.; Mukamel, S.; Ogilvie, J. P.; Olaya-Castro, A.; Ratner, M. A.; Spano, F. C.; Whaley, K. B.; Zhu, X., Using coherence to enhance function in chemical and biophysical systems. *Nature* **2017,** *543*, 647-656.
77. Romero, E.; Novoderezhkin, V. I.; van Grondelle, R., Quantum design of photosynthesis for bio-inspired solar-energy conversion. *Nature* **2017,** *543*, 355-365.
78. Song, Y.; Clafton, S. N.; Pensack, R. D.; Kee, T. W.; Scholes, G. D., Vibrational coherence probes the mechanism of ultrafast electron transfer in polymer–fullerene blends. *Nat. Commun.* **2014,** *5*, 4933.
79. Falke, S. M.; Rozzi, C. A.; Brida, D.; Maiuri, M.; Amato, M.; Sommer, E.; De Sio, A.; Rubio, A.; Cerullo, G.; Molinari, E.; Lienau, C., Coherent ultrafast charge transfer in an organic photovoltaic blend. *Science* **2014,** *344*, 1001-1005.
80. De Sio, A.; Troiani, F.; Maiuri, M.; Réhault, J.; Sommer, E.; Lim, J.; Huelga, S. F.; Plenio, M. B.; Rozzi, C. A.; Cerullo, G.; Molinari, E.; Lienau, C., Tracking the coherent generation of polaron pairs in conjugated polymers. *Nat. Commun.* **2016,** *7*, 13742.
81. Chung, H. S.; Ganim, Z.; Jones, K. C.; Tokmakoff, A., Transient 2D IR spectroscopy of ubiquitin unfolding dynamics. *Proc. Natl. Acad. Sci.* **2007,** *104*, 14237-14242.
82. Strasfeld, D. B.; Ling, Y. L.; Shim, S.-H.; Zanni, M. T., Tracking Fiber Formation in Human Islet Amyloid Polypeptide with Automated 2D-IR Spectroscopy. *J. Am. Chem. Soc.* **2008,** *130*, 6698-6699.
83. Shim, S.-H.; Gupta, R.; Ling, Y. L.; Strasfeld, D. B.; Raleigh, D. P.; Zanni, M. T., Two-dimensional IR spectroscopy and isotope labeling defines the pathway of amyloid formation with residue-specific resolution. *Proc. Natl. Acad. Sci.* **2009,** *106*, 6614-6619.
84. Chung, J. K.; Thielges, M. C.; Fayer, M. D., Dynamics of the folded and unfolded villin headpiece (HP35) measured with ultrafast 2D IR vibrational echo spectroscopy. *Proc. Natl. Acad. Sci.* **2011,** *108*, 3578-3583.
85. Ghosh, A.; Qiu, J.; DeGrado, W. F.; Hochstrasser, R. M., Tidal surge in the M2 proton channel, sensed by 2D IR spectroscopy. *Proc. Natl. Acad. Sci.* **2011,** *108*, 6115-6120.

86. Christensson, N.; Milota, F.; Hauer, J.; Sperling, J.; Bixner, O.; Nemeth, A.; Kauffmann, H. F., High Frequency Vibrational Modulations in Two-Dimensional Electronic Spectra and Their Resemblance to Electronic Coherence Signatures. *J. Phys. Chem. B* **2011,** *115*, 5383-5391.
87. Lukeš, V.; Christensson, N.; Milota, F.; Kauffmann, H. F.; Hauer, J., Electronic ground state conformers of β-carotene and their role in ultrafast spectroscopy. *Chem. Phys. Lett.* **2011,** *506*, 122-127.
88. Woutersen, S.; Mu, Y.; Stock, G.; Hamm, P., Hydrogen-bond lifetime measured by time-resolved 2D-IR spectroscopy: N-methylacetamide in methanol. *Chem. Phys.* **2001,** *266*, 137-147.
89. Zheng, J.; Kwak, K.; Asbury, J.; Chen, X.; Piletic, I. R.; Fayer, M. D., Ultrafast Dynamics of Solute-Solvent Complexation Observed at Thermal Equilibrium in Real Time. *Science* **2005,** *309*, 1338-1343.
90. Brinzer, T.; Berquist, E. J.; Ren, Z.; Dutta, S.; Johnson, C. A.; Krisher, C. S.; Lambrecht, D. S.; Garrett-Roe, S., Ultrafast vibrational spectroscopy (2D-IR) of CO2 in ionic liquids: Carbon capture from carbon dioxide's point of view. *J. Chem. Phys.* **2015,** *142*.
91. Kwak, K.; Park, S.; Finkelstein, I. J.; Fayer, M. D., Frequency-frequency correlation functions and apodization in two-dimensional infrared vibrational echo spectroscopy: A new approach. *J. Chem. Phys.* **2007,** *127*.
92. Kwak, K.; Rosenfeld, D. E.; Fayer, M. D., Taking apart the two-dimensional infrared vibrational echo spectra: More information and elimination of distortions. *J. Chem. Phys.* **2008,** *128*.
93. Roberts, S. T.; Loparo, J. J.; Tokmakoff, A., Characterization of spectral diffusion from two-dimensional line shapes. *J. Chem. Phys.* **2006,** *125*.
94. Yamada, S. A.; Bailey, H. E.; Fayer, M. D., Orientational Pair Correlations in a Dipolar Molecular Liquid: Time-Resolved Resonant and Nonresonant Pump–Probe Spectroscopies. *J. Phys. Chem. B* **2018,** *122*, 12147-12153.
95. Kakinuma, S.; Shirota, H., Femtosecond Raman-Induced Kerr Effect Study of Temperature-Dependent Intermolecular Dynamics in Pyrrolidinium-Based Ionic Liquids: Effects of Anion Species. *J. Phys. Chem. B* **2019,** *123*, 1307-1323.
96. Shin, J. Y.; Wang, Y.-L.; Yamada, S. A.; Hung, S. T.; Fayer, M. D., Imidazole and 1-Methylimidazole Hydrogen Bonding and Nonhydrogen Bonding Liquid Dynamics: Ultrafast IR Experiments. *J. Phys. Chem. B* **2019,** *123*, 2094-2105.
97. Dutta, B.; Vos, B. E.; Rezus, Y. L. A.; Koenderink, G. H.; Bakker, H. J., Observation of Ultrafast Vibrational Energy Transfer in Fibrinogen and Fibrin Fibers. *J. Phys. Chem. B* **2018,** *122*, 5870-5876.
98. Pazos, I. M.; Ma, J.; Mukherjee, D.; Gai, F., Ultrafast Hydrogen-Bonding Dynamics in Amyloid Fibrils. *J. Phys. Chem. B* **2018,** *122*, 11023-11029.

Chapter 2

Experimental and Computational Methods

2.1 UV-Visible Absorption Spectroscopy

Using a quartz cuvette with a 1 cm optical path length, the entire steady-state absorption spectra were recorded on a Shimadzu UV 3600 Plus spectrophotometer. For visible light, a tungsten lamp has been employed, and a deuterium lamp is used for the UV spectrum. Very diluted solutions at their excitation wavelength are employed for the absorption measurements in order to prevent the possibility of aggregation or re-absorption effects. Figure 2.1 shows a schematic representation of the UV-vis spectrophotometer. The light from the relevant sources is illuminated and split into its various wavelengths at the monochromator. The beam splitter receives this dispersed light and divides it into two beams. While the second beam is reflected by 90° and travels through the reference solution, the first beam is undeflected and interacts with the sample solution. An absorption versus wavelength plot illustrates the UV-vis signal caused by the differential absorption from the reference and the sample solutions.

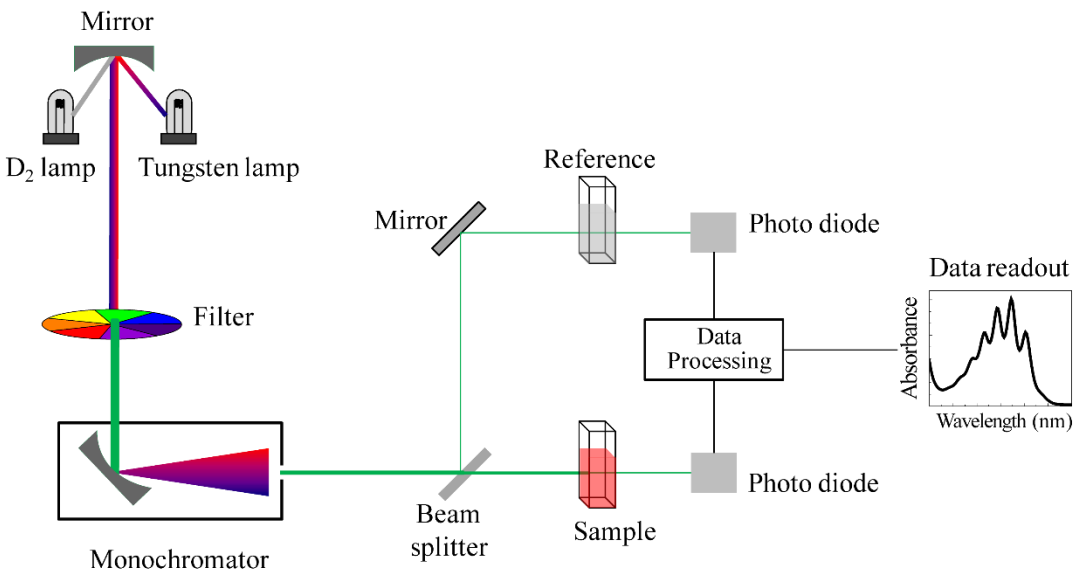

Figure 2.1 Schematic diagram of UV-Visible absorption spectrophotometer.

2.2 X-ray diffraction spectroscopy

X-Ray diffraction patterns were measured on Bruker D8 Advanced X-Ray Diffractometer using Cu Kα (λ = 1.54 Å) rays. All nanocrystal samples for XRD analysis were prepared by drop casting the as synthesized NCs on a clean glass substrate. A crystals atomic planes cause an incident X-ray beam to interfere with itself as it leaves the crystal. The condition is known as X-ray diffraction. It is a quick analytical method that can reveal the size of unit cells and is mostly used to determine a crystalline materials phase. X-ray diffraction involves the use of monochromatic X-rays generated by a cathode ray tube. These X-rays are filtered and collimated to concentrate them on a crystalline sample. When the X-rays interact with the sample, they produce diffracted rays through constructive interference, which satisfy Bragg's Law. By scanning the sample through a range of angles, all possible diffraction directions of the lattice can be attained.

2.3 Transmission Electron Microscopy

All the nanocrystals dispersed in hexane are diluted thousand times and drop-cast on the carbon-coated copper grids. The solvent is allowed to evaporate naturally under ambient conditions. TEM imaging is performed using HRTEM, JEOL JEM 2200FES. The transmission electron microscope (TEM) is a complex instrument that consists of three main systems, firstly an electron gun that generates the electron beam and a condenser system that focuses the beam onto the sample. Secondly an image-forming system consisting of an objective lens, a movable specimen stage, and intermediate and projector lenses that concentrate the electrons passing through the specimen to create a highly magnified and true image, and finally image-recording system, which typically includes a digital camera for long-term records and a fluorescent screen for viewing and focusing the image. Additionally, the TEM requires power supplies and a vacuum system comprising pumps, gauges, and valves to operate properly.

2.4 Fourier Transform Infrared Spectroscopy (FTIR)

The FTIR spectrometer offers several advantages over the conventional dispersive infrared spectrometer due to its inherent properties. In Figure 2.2, a schematic diagram of a Fourier transform infrared spectrophotometer (FTIR) is shown. Instead of using a monochromator

grating, the FTIR utilizes an interferometer to control the infrared light generated from a source.

In the FTIR setup, the infrared beam is directed towards a beam splitter within the interferometer. The beam splitter splits the incoming beam into two paths: one path remains undeflected, while the other is reflected at a 90° angle. The reflected beam falls onto a fixed mirror and is reflected back to the beam splitter. Simultaneously, the undeflected beam travels to a moving mirror and returns to the beam splitter. By moving the position of the moving mirror, the path length of the beam shined onto it can be altered. The reflected beams from both mirrors meet and recombine at the beam splitter. However, due to the different path lengths travelled by these beams, constructive and destructive interference phenomenon occurs.

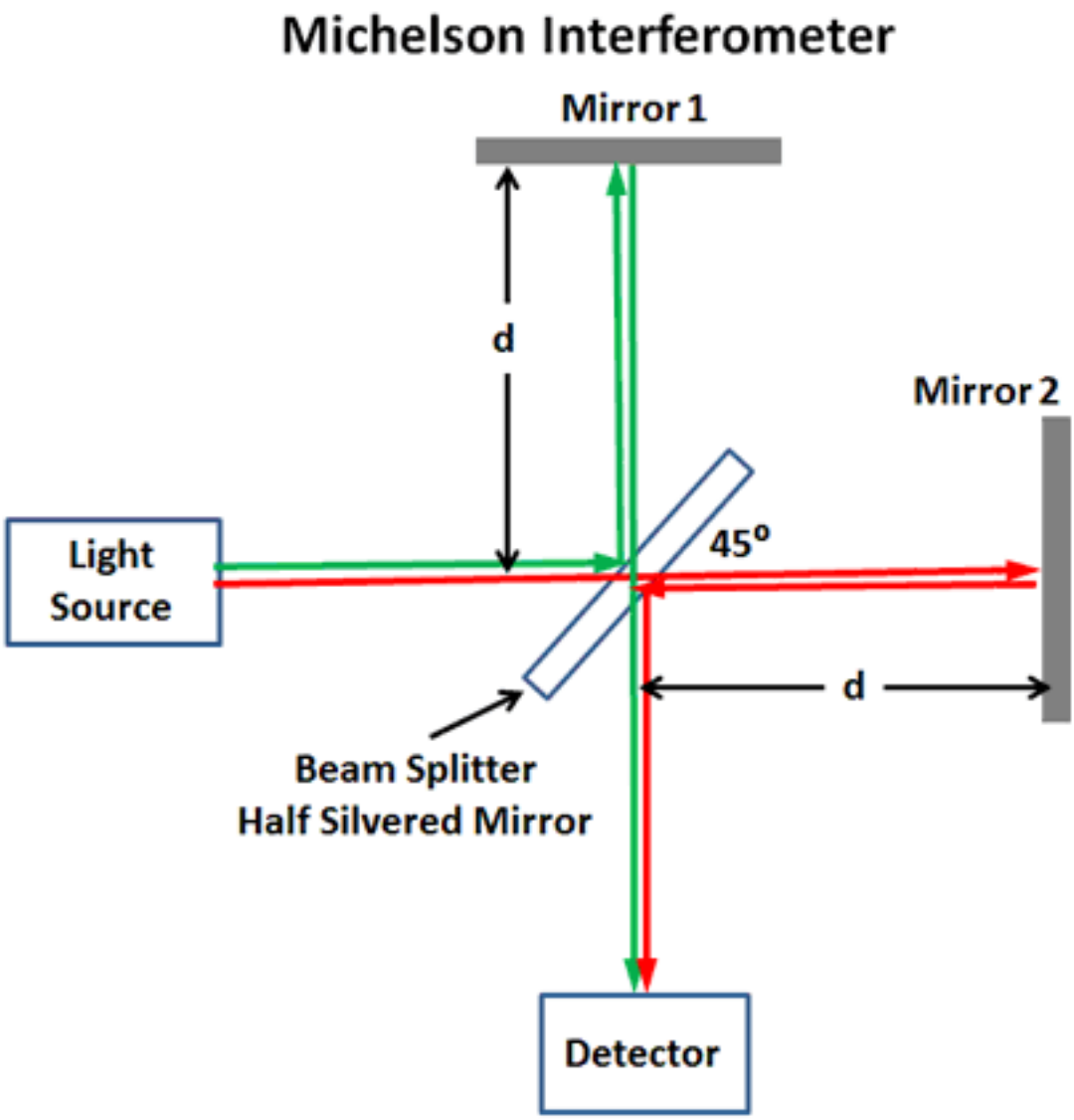

Figure 2.2 Schematic diagram of Fourier transform infrared (FTIR) spectrophotometer

This results in the formation of interference patterns within the combined beam, known as an interferogram. The interferogram is then focused onto the sample. As the infrared radiation passes through the sample, it absorbs specific wavelength based on the sample's characteristics. The transmitted radiation, now containing the interferogram signal in the time domain, continues its path and reaches the detector. The detector captures the interferogram signal, which provides information about the amount of energy absorbed at every wavelength. To convert the time-domain interferogram into a frequency-domain signal, the Fourier transformation formalism is employed. The key advantage of FTIR over dispersive IR spectroscopy is its faster data collection capability, along with other benefits such as superior spectral quality, ease of use, low maintenance requirements, and reproducibility of data. The IR absorption spectra shown in this thesis were acquired on a FTIR-Brucker Vertex 70 spectrometer at room temperature with 2 cm^{-1} frequency resolution. For each sample, ~90 μL of the sample solution was loaded into a demountable cell consisting of two windows (CaF_2, 3 mm thickness, Shenzen Laser Co. Ltd.), separated by a mylar spacer of 100 μm thickness.

2.5 Two-dimensional Infrared Spectroscopy (2D IR) spectroscopy

2D IR spectroscopy, developed two decades ago, is a powerful method for studying ultrafast structural dynamics in chemical, biological, and material systems. By increasing the dimensionality of the technique, similar to 2D NMR, it effectively untangles overlapping features in spectra. Using a sequence of infrared laser pulses, 2D IR spreads spectral information in two dimensions, allowing for the identification of interactions between vibrational modes and measurement of their temporal evolution. Unlike 2D NMR, which is limited to slower timescales range of ms to μs, 2D IR operates on a fast sub-picosecond timescale, enabling the detection of rapidly interconverting states and direct measurement of fast structural and environmental fluctuations. 2D IR spectroscopy is well suitable to study condensed phase samples where conformational fluctuations occur on fast timescales. Based on the vibrational frequencies that are highly sensitive to molecular environments, 2D IR spectroscopy provides information about the local sites and their fluctuations within complex systems. 2D IR spectroscopy conveys rich information on molecular systems such as

homogeneous and inhomogeneous spectral broadening effects, vibrational anharmonicity, spectral diffusion, intermode coupling strength and its temporal variation, energy relaxation, chemical exchange and conformational interconversions. Over the past two decades, 2D IR spectroscopy has been extensively used to study the structure and dynamics of small peptides, proteins, DNA, and lipid bilayers. Moreover, 2D IR has been utilized to interrogate ultrafast energy transfer in materials and biology, hydrogen-bond (H-bond) making and breaking in liquid water and in biomolecules, solvation dynamics arising from solute-solvent interactions and structural dynamics of inorganic ligand capped nanocrystals.

2.5.1 2D IR Experimental setup, pulse sequence

2D IR spectroscopy is a third-order non-linear spectroscopy technique, here sample is exposed to three consecutive femtosecond IR pulses, resulting in the generation of a vibrational echo pulse. 2D IR experiments performed in this dissertation by using the pulse shaper based spectrometer developed by Zanni and co-workers (Phasetech). The schematic representation of the 2D IR experimental setup is shown in Figure 2.3.

Ti:Sapphire regenerative amplifier (Libra, Coherent) generates ultrashort pulses of 50 femtosecond pulses outputs 800 nm light with a repetition rate of 1 KHz. This 800 nm output used as input for pumping the optical parametric amplifier (OPA). The signal and idler beams generated using 800 nm light source in the OPA, focused and combined at difference frequency generation (DFG) in a $AgGaS_2$ crystal, which produces IR pulses of ~ 50 fs duration. These IR pulses are further directed to the spectrometer, where it is split into a strong pump pulse (80%) and a weak probe pulse (20%). These two IR pulses used for both pump-probe and 2D IR experiments. The pump pulse is then passed through the acousto-optics modulator (AOM) based pulse shaper. Pulse shaper generates two temporally separated pump pulses from single pump pulse using the pulse shaping method which modulates the phase and amplitude of the pulses. The pump pulse further passes through a half waveplate and a polariser which allows us to perform a polarisation selective pump-probe and 2D IR experiments.

After pulse shaper, the pump pulses enter into a motorised delay stage that generates the time delays between the pump and probe pulses used to acquire the 2D IR and pump-probe spectrum. The pump and probe pulses focused at the sample using parabolic mirrors were spatially and temporarily overlapped inside the sample. The bandwidth of the pulses is wide

enough to stimulate both the v = 0 - 1 and v = 1 - 2 transitions at the same time. The interaction of both pump and probe pulses with the sample generates the vibrational echo signal in phase to the probe pulse. Furthermore, the signal dispersed on a monochromator (Princeton instruments) and finally detected by a liquid nitrogen cooled MCT IR 64 array detector (Infrared Associates).

Polarisation selective pump-probe experiment (PSPP) and 2D IR experiments were performed in the parallel $\langle XXXX \rangle$ and perpendicular $\langle XXYY \rangle$ polarization conditions, where the polarization of the pump beam was either parallel or perpendicular with respect to that of the probe beam. Pump polarization before the sample was controlled using the combination of a half-wave plate and a polarizer, as mentioned above. The polarization dependent 2D IR data were to check reorientation induced spectral diffusion (RISD), however polarization dependent pump-probe data were analysed to obtain the isotropic population decay and orientation dynamics of vibrational probe in system under investigation.

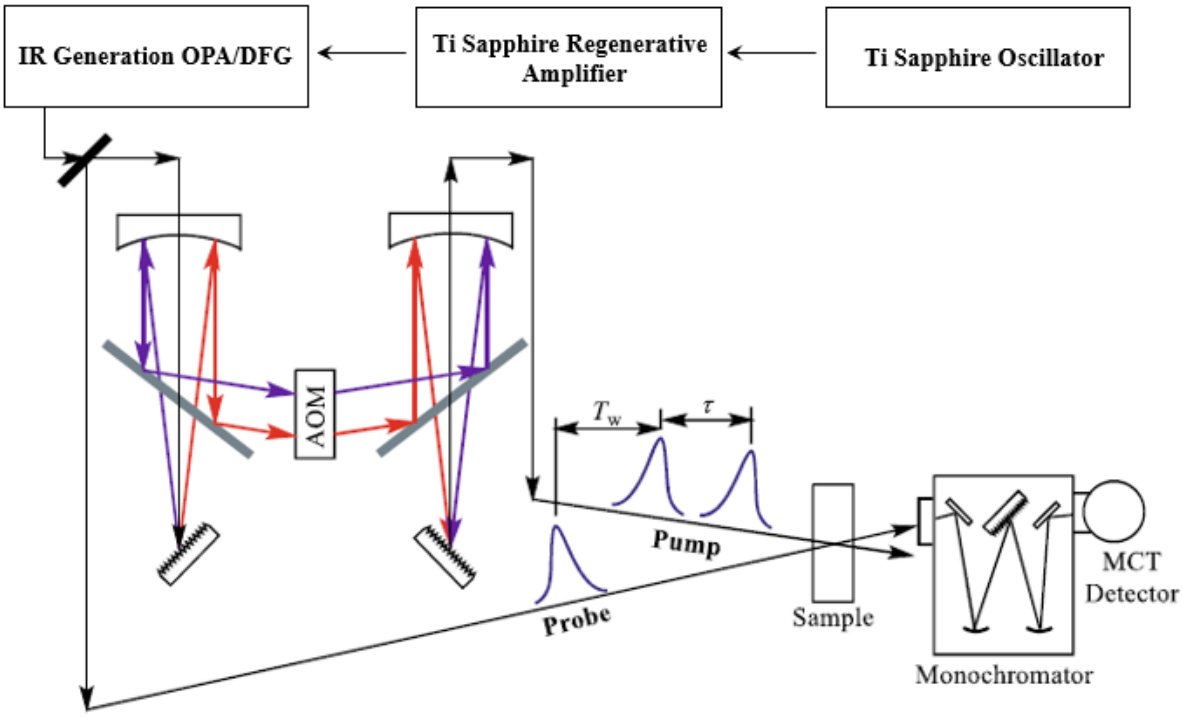

Figure 2.3 Experimental setup for the pulse shaper based 2D IR spectrometer.

In 2D IR experiments three successive femtosecond mid IR pulses interacts with sample shown in Figure 2.4. The first pulse interacts with the sample and creates coherence state between vibrational ground (v = 0) and excited (v = 1) states. The second pulse in the sequence restricts this coherence to a single vibrational state, limiting its influence to only

one of the two vibrational states. The time interval between pulse 1 and 2 is called a coherence time (τ). After second pulse there is time gap for structural changes happening in the samples called as waiting time (T_w). After waiting time (T_w), the third pulse create another coherence between v = 0 to v = 1 and v = 1 to v = 2 vibrational states at which all molecules are oscillating in phase. The controlled modulation of the time intervals between pulse 1 - 2 (τ) and pulse 2 - 3 (T_w) and the emitted vibrational echo frequency (ω_t) provides the experimental data for 2D IR spectroscopy. 2D IR data represented as a two-dimensional correlation map of the excitation (pump) frequency (ω_τ) versus detection (probe) frequency (ω_t), which describes the vibrational transitions that occur during the coherence and detection period. After waiting time (T_w), the third pulse create another coherence between v = 0 to v = 1 and v = 1 to v = 2 vibrational states at which all molecules are oscillating in phase. The controlled modulation of the time intervals between pulse 1 - 2 (τ) and pulse 2 - 3 (T_w) and the emitted vibrational echo frequency (ω_t) provides the experimental data for 2D IR spectroscopy. The vibrational transitions that take place throughout the coherence and detection period are described by a two-dimensional correlation map of the excitation (pump) frequency versus detection (probe) frequency in 2D IR data.

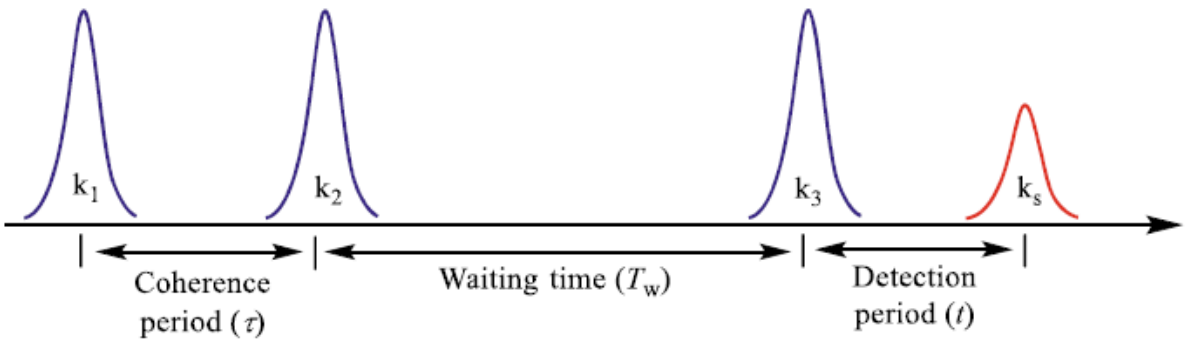

Figure 2.4 Pulse sequence used in the 2D IR experiment.

2.5.2 Spectral signature 2D IR spectrum

A single vibrational mode of vibrational probe is indicate as a peak pair in the 2D IR spectrum shown in in Figure 2.5 (b). Blue peak represent V=0-1 transition and red peak represent V=1-2 transition (figure 2.5 (a and b)), shift of red peak to lower frequency due vibrational anharmonicity of probe (figure 2.5 (b)). For a particular molecule in the ensemble, when the waiting time (T_w) is zero, the frequencies associated with the initial coherence (ω_τ) and the final coherence (ω_t) are identical, regardless of whether it pertains to the ground state

bleach (blue contour in Fig. 2.5 (b)) or the excited state emission (red contour in Fig. 2.5 (b)) signal of the molecule's vibrational mode. At zero waiting time excitation and detection pulses hits the sample at same time so that there is no time for structural reorganisation of system which leads to a single point along the diagonal on the 2D IR spectrum. 2D IR spectroscopy provides the all ensemble measurement of sample under study and the molecules within the ensemble exist in slightly different local microenvironment, the vibrational mode of interest produces a diagonally elongated frequency distribution covering such microenvironments. This diagonal elongation width of a 2D IR peak provides the heterogeneity in the microenvironment and thus provides the inhomogeneous broadening (figure 2.5 (c) black arrow). Homogeneous line broadening mechanisms, namely lifetime and dephasing, causes a small broadening in the peaks perpendicular to the diagonal (figure 2.5 (c) red arrow).

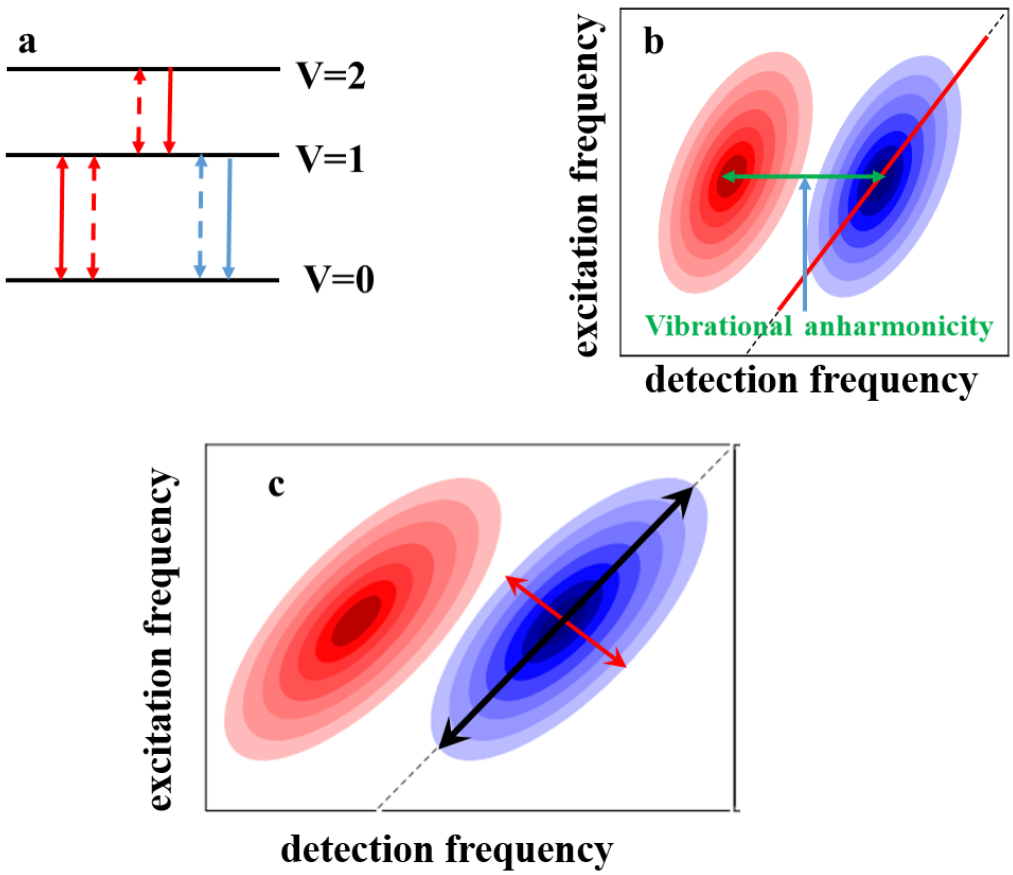

Figure 2.5 (a) Vibrational energy level and involved transitions in the 2D IR spectra. (b) A typical 2D IR spectrum peak pair separated by vibrational anharmonicity. (c) 2D IR spectrum inhomogeneous (black arrow) and homogeneous (red arrow) broadening at T_w=0.

2.5.3 Spectral diffusion of 2D IR peak

In Kubo lineshape theory, the homogeneous linewidth has an infinitely short timescale as transitions fluctuate instantaneously over a frequency bandwidth. The inhomogeneous linewidth, originating from static inhomogeneity, has an infinitely long timescale. This creates an intermediate regime known as spectral diffusion, which involves fluctuations on the measurement timescale.

The change in surroundings local environment of the probe molecules can change the shape of the 2D-IR spectra. When the local environment around the vibrational probe molecules changes, the frequency of the vibrational mode changes, which causes the loss of frequency correlation and the change in shape of the spectra happens. For early waiting times, the surrounding environment has very little time to evolve, and the correlation between the initial and final frequencies is high. As a result, the spectra are elongated along the diagonal direction. (Figure 2.6 (a)) At long waiting time, the local environment gradually evolves and loses the memory of its original configuration, which causes the spectra to have a rounder shape. Given sufficiently long time, all possible structural dynamics happens ultimately the correlation between initial and final frequency completely vanishes, and the spectra become round and no longer elongate along the diagonal axis. (Figure 2.6 (a)) This process is called as ‘spectral diffusion’. (Figure 2.6) Spectral diffusion provides insights into the timeframe within which the probe molecules fully explore the frequencies encompassed by the inhomogeneously broadened absorption line. It reveals the duration necessary for the systems structures to undergo changes that allow the probe to encounter all the configurations responsible for the inhomogeneous broadening.

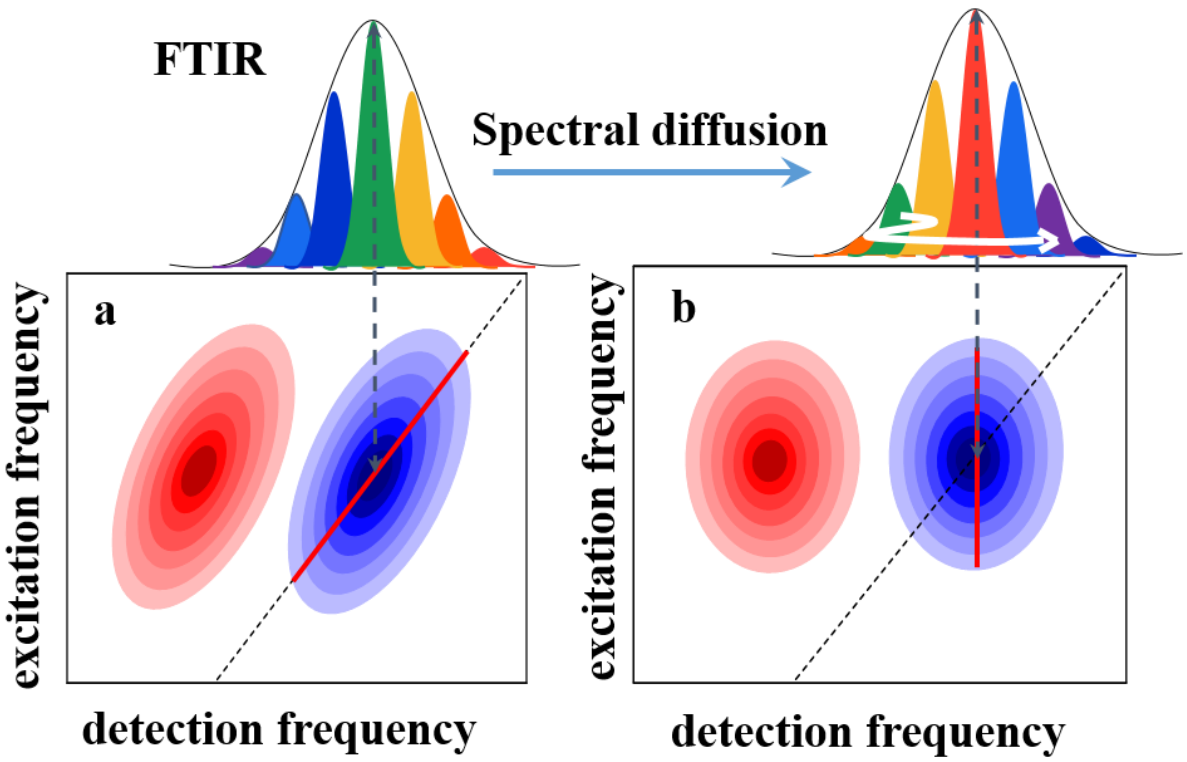

Figure 2.6 (a) 2D IR spectrum at early waiting time (b) 2D IR spectrum at long waiting time.

Spectral diffusion happens as a function of waiting time T_w which results the changes in peak shapes. 2D IR correlation spectrum shows peaks that represent the vibrational eigenstates and their interactions with the surroundings, characterized by different positions, signs, amplitudes, and line shapes. The line shapes observed in 2D IR experiments are highly responsive to the rapid structural fluctuations of molecules, peptides, proteins and materials in solution. The frequency-frequency correlation function (FFCF), also referred to as the vibrational solvation correlation function, serves as a crucial connection between experimental observations and the underlying structural fluctuations of molecules and intermolecular interactions. The amplitude and frequency fluctuation time scales of system under supervision as function of waiting time (T_w) quantitatively obtained by using frequency- frequency correlation function (FFCF). The FFCF represents the average probability that a vibrational oscillator, starting with a specific frequency at t = 0, will retain the same frequency at a later time t. It is calculated by considering all initial frequencies and their respective probabilities. Several methods has been developed to extract FFCF from 2D IR spectrum like nodal line, ellipticity etc.[1-2] The diagonal and off-diagonal peaks overlaps

with each other when vibrational anharmonicity is smaller, in his case analysing the 2D IR spectrum is more challenging task. To avoid this problem Michael Fayer (Stanford University) reported the center line slope (CLS) method. Instead of quantify changes in peak, new novel method has been developed Fayer and et al to simultaneously investigate spectral diffusion and the frequency-frequency correlation function (FFCF). This approach involves tracking variations in the frequency-dependent positions of peak maxima in slices obtained from 2D-IR data. In the center line slope method, a line is constructed by connecting the highest intensity point obtained from plotting lines along the ωτ axis parallel to the ωt axis. Insensitivity to pulse duration, sloping absorptive background, and overlap between diagonal and off-diagonal peaks are the key advantages of the CLS approach over other methods. FFCF of T_w-dependent evolution of the 2D IR spectral line shape was calculated with center line slope (CLS) method.[3] The CLS decay curves were fitted with bi-exponential functions mentioned below to extract the time constants.

$$C(t) = \sum_{i=1}^{2} a_i e^{\left(\frac{t}{\tau_i}\right)}$$

The CLS varies from 1 to 0 with spectral diffusion of time dependent 2D IR spectrum. Initial value of CLS determines the heterogeneity of the system around the solute under investigation. Larger the drop from unity lesser is the heterogeneity.

2.6 Quantum Espresso Calculations

Quantum Espresso is an integrated suite of open-source computer codes for electronic-structure calculations and material modeling at the nanoscale. It is based on the density-functional theory (DFT), plane waves, and pseudopotentials. Quantum Espresso has a wide range of practical uses. Its applications span from calculating ground-state energy and optimizing structures to simulating molecular dynamics and modeling properties related to response and spectroscopy. Quantum Espresso enables DFT simulations on crystal structures or supercells that exhibit periodicity. Its versatility extends to a wide range of materials, including insulators, semiconductors, and metals. The software provides flexible options for k-point sampling and energy state smearing. Additionally, Quantum Espresso incorporates different pseudopotentials and approximations for exchange-correlation functions to enhance computational efficiency. For thiocyanate capped CdS nanocrystals, understanding the binding mode of thiocyanate either by N end or S end. DFT calculations have been performed

using Quantum-Expresso on the (111) facet (cationic site) of zinc-blended shaped CdS nanocrystals. For simplification, a slab model has been used to optimize the NC structure.[4] PBE[5] was used as the exchange-correlation functional, and ultrasoft pseudopotentials described the electron–ion interaction.[6]

2.7 Zeta potential

There are six essential parts to a zeta potential measurement system. To begin, a laser is employed as a light source to illuminate the samples particles. The light source for zeta potential measurements is divided into an incident beam and a reference beam. The laser beam that was incident is transmitted the sample cells centre and the light that has been scattered at an angle of around 13° is detected Any particles travelling through the measurement volume will cause the intensity of light detected to fluctuate with a frequency corresponding to the particle speed when an electric field is applied to the cell. This information is transmitted to a digital signal processor, which is then sent to a computer. The electrophoretic mobility and subsequently the zeta potential are estimated from the frequency spectrum generated by the Zetasizer Nano programme. The detector can only accurately measure dispersed light whose intensity falls within a certain range. An attenuator, which modifies the intensity of the light that reaches the sample and, as a result, the intensity of the scattering, is used to do this. The installation of compensation optics ensures that the alignment is kept at its best by compensating for variations in the cell wall thickness and dispersant refraction.

Here in this thesis Zeta potential measurements were performed on Anton Paar Litesizer 500, Anton Paar, and GmbH, using an Omega cuvette. The sample was measured for 1 min and auto fitting of the correlation function was performed using the Anton Paar DLS software, Kalliope.

2.8 References

1. Asbury, J. B.; Steinel, T.; Kwak, K.; Corcelli, S. A.; Lawrence, C. P.; Skinner, J. L.; Fayer, M. D., Dynamics of water probed with vibrational echo correlation spectroscopy. *The Journal of Chemical Physics* **2004,** *121* (24), 12431-12446.
2. Lazonder, K.; Pshenichnikov, M. S.; Wiersma, D. A., Easy interpretation of optical two-dimensional correlation spectra. *Opt. Lett.* **2006,** *31* (22), 3354-3356.
3. Kwak, K.; Park, S.; Finkelstein, I. J.; Fayer, M. D., Frequency-frequency correlation functions and apodization in two-dimensional infrared vibrational echo spectroscopy: A new approach. *J. Chem. Phys.* **2007,** *127*.
4. Giannozzi, P.; Baroni, S.; Bonini, N.; Calandra, M.; Car, R.; Cavazzoni, C.; Ceresoli, D.; Chiarotti, G. L.; Cococcioni, M.; Dabo, I.; Dal Corso, A.; de Gironcoli, S.; Fabris, S.; Fratesi, G.; Gebauer, R.; Gerstmann, U.; Gougoussis, C.; Kokalj, A.; Lazzeri, M.; Martin-Samos, L.; Marzari, N.; Mauri, F.; Mazzarello, R.; Paolini, S.; Pasquarello, A.; Paulatto, L.; Sbraccia, C.; Scandolo, S.; Sclauzero, G.; Seitsonen, A. P.; Smogunov, A.; Umari, P.; Wentzcovitch, R. M., QUANTUM ESPRESSO: a modular and open-source software project for quantum simulations of materials. *J Phys Condens Matter* **2009,** *21* (39), 395502.
5. Perdew, J. P.; Burke, K.; Ernzerhof, M., Generalized Gradient Approximation Made Simple. *Phys. Rev. Lett.* **1996,** *77* (18), 3865-3868.
6. Vanderbilt, D., Soft self-consistent pseudopotentials in a generalized eigenvalue formalism. *Phys. Rev. B* **1990,** *41* (11), 7892-7895.

Chapter 3

Dynamics Time Scales Identify the Surface–Ligand Interactions in Thiocyanate-Capped Cadmium Sulfide Nanocrystals

3.1 Introduction

Semiconductor nanocrystals (NCs) are composed of a semiconductor lattice whose surface is passivated with molecular capping ligands. Selection of the capping ligands, semiconductor material, size, and dimension provides highly tunable optical and electronic properties of the NCs. These characteristics make the NCs an emerging class of building blocks in various optoelectronic, photovoltaic, photocatalytic, and biodiagnostic applications.[1-7] The last few decades have witnessed advances in controlling the reproducibility of size and shape dispersity in NC synthesis.[8] However, one of the most defining features of the properties and reactivity of the NCs is the surface, which acts as an interface between the semiconductor lattice and the capping ligands.[9] Unlike conventional molecules, heterogeneity exists across the surface of an individual NC. In addition, a dynamic equilibrium exists between the ligands bound to the NC surface and the free ligands in the surrounding media.[8, 10] Detailed insight into the heterogeneity in ligand–NC interactions is essential to improve the current NC-based technologies. Long-chain organic ligands are usually used for stabilizing NCs during their preparation. However, replacing the long chain ligands with shorter variants improves the conductivity and carrier mobility, thereby increasing NC-based device performance.[11-14] In the past decade, solution-based ligand exchange has routinely been used to replace the long-chain organic ligands with the shorter inorganic variants (e.g., halides, pseudohalides, azides, halometalates).[15-17] Thiocyanate (SCN^-) ligand has been recently utilized to prepare colloidal quantum ink, which showed superior carrier mobility.[15] Despite the importance of the NC surface, the heterogeneous ligand–NC interactions are poorly understood due to a lack of molecular-level information.[8] ^{1}H NMR has recently been utilized for long-chain organic ligands (acids and thiolates) to distinguish between surface-bound and freely diffusing ligands.[8-9, 18-23] However, ^{1}H NMR cannot be applied to short inorganic pseudohalide ligands like thiocyanates which are devoid of hydrogen atoms. The interactions

of these short ligands at the NC surfaces have been qualitatively explained based on the hard and soft acids and bases (HSAB) principle.[9, 16] However, a recent quantum chemical study has reported that the coordination of the SCN^- ligand only partly follows the HSAB principle, which cannot be generalized to inorganic solid materials.[24] Quantitative information on the binding modes and the coordination number of inorganic ligands is required to understand their influence on the NC properties.

The use of Fourier transform infrared (FTIR) and Raman spectroscopies has been reported to access purity, ligand identity, and static coordination environments at the NC surface.[15, 21, 25] Although most of the ligands (both long chain acids and short pseudohalides) have distinct vibrational signatures, these steady-state vibrational techniques are most helpful in understanding ligand−NC interactions when used in complement with other experiments and quantum calculations. Beyond probing the static coordination environments, transient IR (TRIR) spectroscopy has been successfully used for the long-chain oleic acid ligands.[26-27] However, no timeresolved IR studies have been reported on the short inorganic variants. Among the available time-resolved IR methodologies, two-dimensional infrared (2D IR) spectroscopy provides a unique route to obtain an in-depth understanding of the inorganic ligand−NC interactions. We choose the short SCN^- ligand because of its ability to form stable solution-phase NCs and its impressive electron mobility, which is required for optoelectronic applications.[15, 28] Moreover, SCN^- is a highly sensitive local vibrational probe of the surface heterogeneity.[29-30] Herein, we successfully demonstrate that the ligand dynamics time scales obtained from 2D IR spectroscopy in SCN^- capped CdS NCs quantitatively distinguish three distinct inorganic ligand−NC interactions within the heterogeneous ensemble.

3.2 Materials and Method

3.2.1 Chemicals

Cadmium oxide (CdO, 99.8%), oleic acid (OA, >98.9%), octadecene (ODE), sulphur powder (S, 99%) ammonium thiocyanate (NH_4SCN, 99.9%), isopropyl alcohol (IPA), dimethylformamide (DMF) Hexane and chloropropanethiol (CPT) were purchased from Sigma-Aldrich and used without further purification.

3.2.2 Synthesis of CdS nanocrystals (NCs)

CdS NCs has been synthesized by following previously reported method.[1] In a typical synthesis process CdO (0.16 g, 1.25 mmol), ODE (78.12 mmol) and OA (12.67 mmol) were taken in a three-neck flask. The mixture was heated at 280 °C under an inert (argon) atmosphere for 30 minutes. In a separate three-neck flask, 0.04 g of S powder was dissolved in 5ml ODE and the resulting solution (S-ODE) was heated under an inert atmosphere at 100 °C for 10 minutes. The S precursor solution was allowed to cool at room temperature. The cadmium precursor solution temperature was reduced to 250 °C and 5 ml of S-ODE was rapidly injected into the three-neck flask. The yellow coloration of the solution indicated the formation of CdS NCs. Five minutes later, the heating was switched off and the reaction mixture was allowed to cool to room temperature under an inert atmosphere. Then CdS NCs was precipitated and washed by using excess isopropyl alcohol. After washing precipitate was redispersed in hexane and stored in glove box for further use.

3.2.3 Ligand Exchange

NH_4SCN (7.6 mg, 0.1 mmol) was added to 1 ml DMF to make a 100 mM ammonium thiocyanate (NH_4SCN) stock solution. In a typical ligand exchange process, 0.5 ml of OA capped CdS NC (15-20 mg/ml) in hexane was added to 0.5 ml SCN stock solution with 0.5 µl CPT.[31-32] The above mixture was vortexed vigorously and the clear, colourless hexane phase

was discarded. The resulting thiocyanate passivated NCs solution was vortexed thrice with hexane. The final SCN capped CdS NCs solution was used for spectroscopic studies.

3.2.4 IR spectroscopy

IR absorption spectra was measured at room temperature on a Bruker Vertex 70 FTIR spectrometer. For each sample, ~90 μL of the sample solution was loaded into a demountable cell consisting of two windows (CaF_2, 3 mm thickness) separated by a mylar spacer of 100 μm thickness. The reported peak frequencies were obtained by fitting the IR spectrum with Voigt line shape function. The 2D IR experiments were performed with the same solutions in the same sample cell.

3.2.5 2D IR spectroscopy

The 2D IR spectra were acquired by using a pulse shaper-based 2D IR spectrometer developed by PhaseTech Spectroscopy, Inc., USA. A detailed description of the setup used for this work has been described elsewhere.4 In brief, mid IR pulses, centred at ~2070 cm^{-1} , were generated with approximately ~60 fs pulse width. At beam splitter splits the mid IR pulse into a strong pump (80%) beam and a weak probe (20%) beam. A germanium acousticoptic modulator (AOM) based pulse shaper was used to generate two pump pulses with a delay interval of (τ) from single strong pump pulse. The spatially and temporarily τ overlapped pump and probe pulses were directed towards sample using parabolic mirrors. A motorised delay stage used for set the pump and probe delay (T_w). Each 2D IR spectra were acquired by scanning (τ) at fixed T_w. After the sample position, signal was collected using a monochromator (Princeton Instruments) and detected on a nitrogen-cooled 64-pixel HgCdTe (MCT) IR array (InfraRed Associates) detector. Final 2D IR spectra were constructed by

Fourier transforming the experimental data along the axis. Generally, 2D IR spectra is a plot of the initial frequencies versus the final frequencies. The 2D IR experiments were performed with the same solutions used for the IR absorption spectra, in the same sample cell. Waiting time dependent evolution of 2D IR line shape was analysed with the central line slope (CLS) method.[33] Multi exponential decay function was used to model the CLS decay.

$$C(t) = \sum_i a_i e^{\left(\frac{t}{\tau_i}\right)}$$

CLS decay provides solvation dynamics time scale and also the heterogeneity associated with different ligand sub-ensemble.

3.2.6 Material Characterisation

Optical absorption measurements were done by using Shimadzu UV-vis-IR (UV-3600 Plus) spectrophotometer. High-resolution images of NCs were captured by high resolution transmitted electron microscope (HRTEM, JEOL JEM 2200FES). Powder X-ray diffraction (PXRD) patterns are collected by using a Bruker D8 Advance diffractometer in Bragg–Brentano geometry and operating with Cu Kα radiation. Zeta potential measurements were performed on Anton Paar Litesizer 500, Anton Paar, and GmbH, using an Omega cuvette. The sample was measured for 1 min and auto fitting of the correlation function was performed using the Anton Paar DLS software, Kalliope.

3.3 Results and discussion

Figure 3.1a shows that the excitonic features of the CdS NCs were preserved after ligand exchange. The X-ray diffraction (XRD) pattern of the SCN^- capped CdS (CdS-SCN) was identical to that of CdS-OA (Figure 3.1b). The size distributions of the NCs are shown in

Figure 3.1c. In agreement with the previous literature, the fringe spacing and XRD correspond to (111), (220), and (311) planes of the zinc blend structure.[34] The XRD pattern reveals (111) to be the predominant facet. HRTEM images of CdS NCs (Figure 3.2a) before and after ligand exchange exhibit good crystallinity with well-defined lattice fringes. After ligand exchange, ^{1}H NMR shows no characteristic peak for vinyl hydrogen of oleate around 5 to 6 ppm confirming full removal of oleate from the NCs surface (Figure 3.2b).

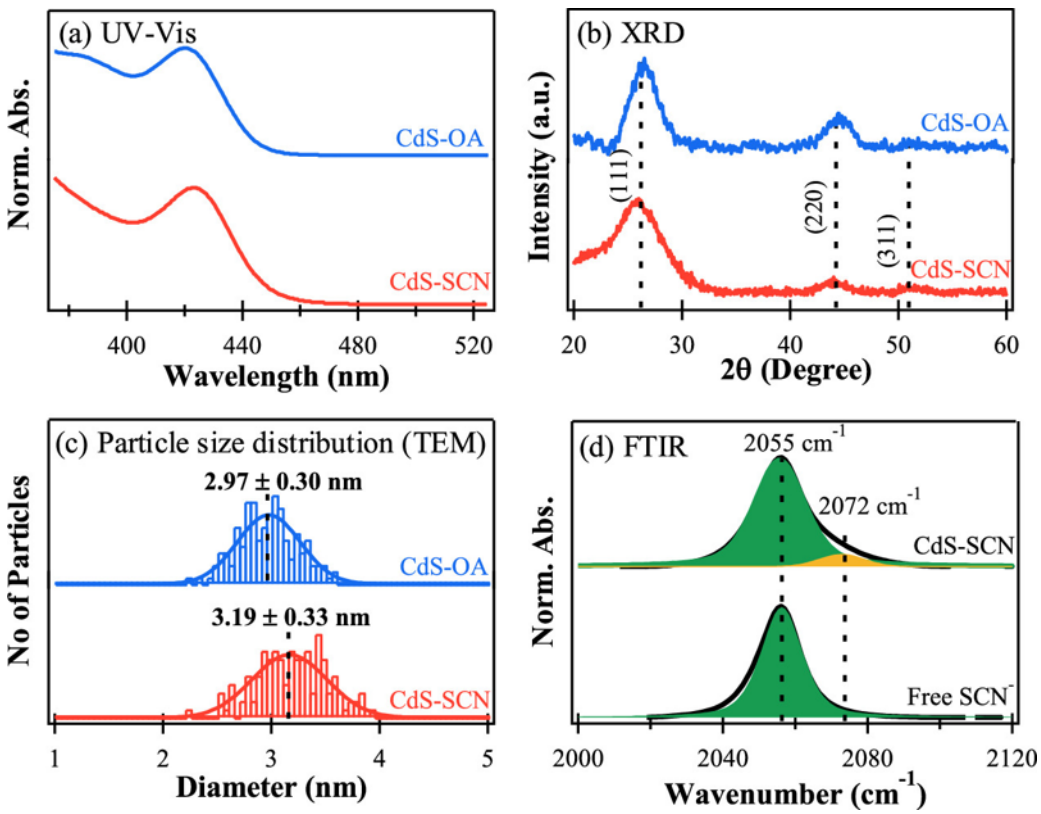

Figure 3.1 (a) UV-Vis absorption spectra, (b) XRD patterns and (c) particle size distributions obtained from HRTEM analysis of CdS NC before (blue) and after (red) ligand exchange. (d) FTIR spectra of the nitrile stretch ($\bar{\nu}_{CN}$) of SCN^- in presence (up) and absence (down) of NCs.

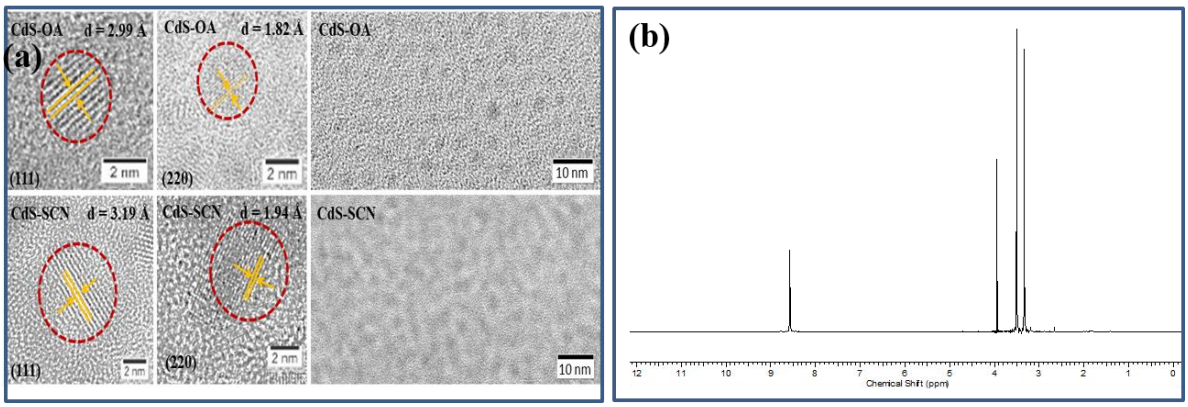

Figure 3.2 (a) HRTEM images of oleic acid capped (top panel) and NH_4SCN capped (bottom panel) CdS NCs.(b) ^1H NMR spectra of thiocyanate capped CdS NCs in DMF.

The FTIR spectrum of the CdS-SCN in DMF shows an asymmetric peak in the CN stretch $\bar{\nu}_{CN}$ region (Figure 3.1d) which could be fitted (Table 3.1) to two Gaussians centered at 2055 cm^{-1} ($\bar{\nu}_L$) and 2072 cm^{-1} ($\bar{\nu}_H$) The full width at half maximum (fwhm) of the peaks at ($\bar{\nu}_L$) and ($\bar{\nu}_H$)are 16.5 and 14.6 cm^{-1}, respectively.

Table 3.1. FTIR, anharmonicity and CLS fitting parameters of the nitrile stretch of free SCN^- and in CdS-SCN.

System	FTIR peak positions (cm^{-1}) and FWHM (cm^{-1})	Anharmonicity of SCN^- (cm^{-1})	CLS fitting parameters			
			a_1	τ_1 (ps)	a_2	τ_2 (ps)
NH_4SCN	2055.6, 13.5	26.5	0.10 ± 0.01	5.2 ± 0.5	-	-
CdS-SCN	2055.6, 16.5	26.2	0.38 ± 0.02	4.5 ± 0.4	0.08 ± 0.02	39.4 ± 5.1
	2072.9, 14.6	23.7	0.11 ± 0.06	1.3 ± 1.2	0.74 ± 0.02	114.2 ± 10.8

In the absence of NCs, NH_4SCN shows a symmetric peak at 2055 cm^{-1} ($\bar{\nu}_F$) in DMF with a fwhm of 13.5 cm^{-1} (Figures 3.1d). Previous studies of M^+ SCN^- (M = Li^+, Na^+, Mg^{2+}) in different solvents reported a blue-shift in ($\bar{\nu}_{CN}$) due to the formation of contact ion pairs.[35-40]Thus, the peaks at ($\bar{\nu}_L$) and ($\bar{\nu}_H$) in CdS-SCN can plausibly be assigned to the freely

diffusing ligands and the ligands interacting with the NCs, respectively. However, these assignments based on peak positions are speculative. Further, it should be noted that although the presence of NCs makes the fwhm of the peak at ($\bar{\nu}_L$) larger by 3 cm^{-1} than that of the peak at ($\bar{\nu}_F$) (Table 3.1), the origin of this broadening cannot be explained from FTIR results.

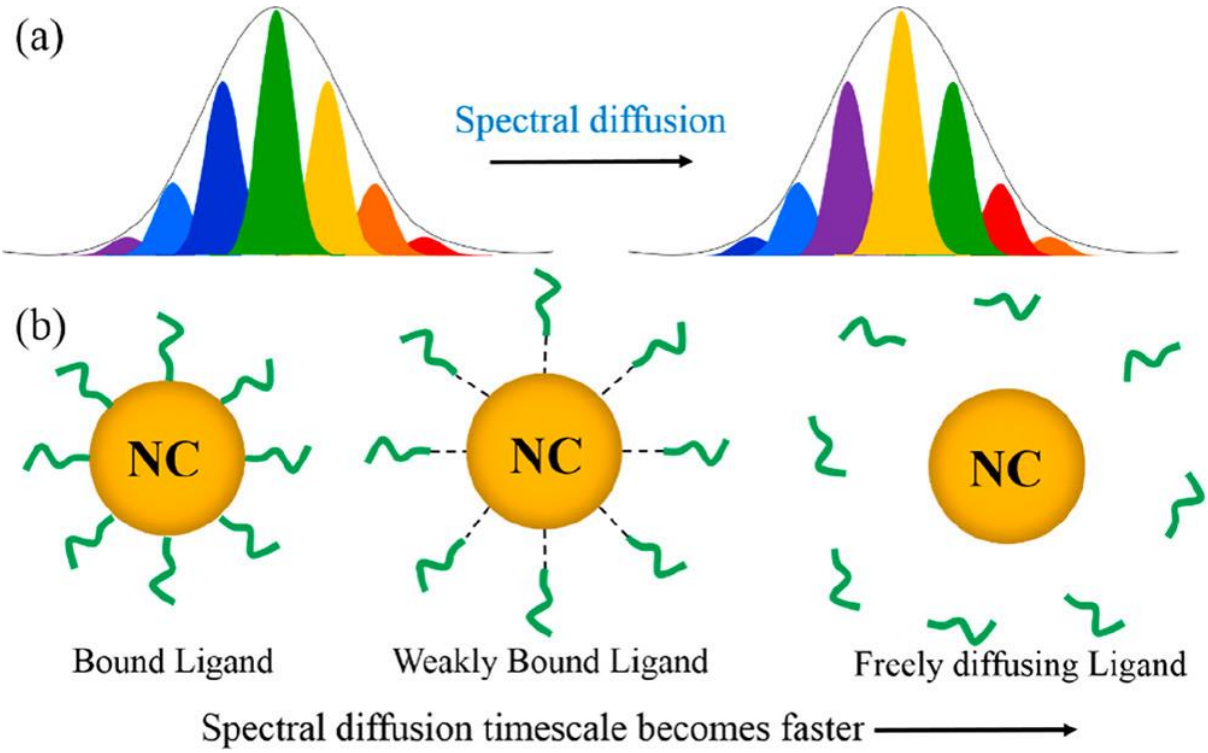

Figure 3.3 Schematic representations of (a) the exchanging heterogeneous subensembles (different colors) within a symmetric frequency distribution (solid black line representing an absorption band) leading to spectral diffusion and (b) the changes in the spectral diffusion time scales with variations in ligand–NC interactions.

A particular mode of ligand-NC interaction is manifested as a symmetric peak in the FTIR spectrum. Due to the inherent heterogeneity in the NC ensemble, subensembles exist within each absorption band. These subensembles exchange on specific time scales (spectral diffusion) depending on the strength of interaction of the ligand to the NC surface (Figure 3.3a). The stronger the ligand-NC interaction, the slower the time scale (Figure 3.3b). The changes in the 2D IR line shapes can directly provide the spectral diffusion time scales and

identify the relative strength of the ligand-NC interaction. We have acquired 2D IR spectra of CdS-SCN at different time delays (T_w) to obtain a detailed understanding of the ligand−NC interactions. A typical 2D IR spectrum consists of a peak pair corresponding to ground-state bleach and stimulated emission (blue peak, v = 0 to v = 1) and excited state absorption (red peak, v = 1 to v = 2) separated by vibrational anharmonicity. The existence of multiple binding modes introduces multiple overlapping peak pairs (2D IR) in the spectra. The 2D IR spectrum shows two peak pairs (Figure 3.4a, left column), with the blue peaks centered at frequencies corresponding to the FTIR peak positions ($\bar{\nu}_L$ and $\bar{\nu}_H$) and the red peaks shifted along the detection axis by the respective anharmonicities. The spectral diffusion (within each peak) lowers the diagonal tilt of the peaks with increasing T_w without changing the peak positions (white lines in Figure 3.4a). The spectral diffusion time scales are quantified using center line slope (CLS) formalism where the inverse of the T_w-dependent white lines' slopes are fitted to exponential decays.[33] We have performed additional control experiments and analyses in the absence of NCs on NH_4SCN in DMF (Figure 3.4a, right column). The CLS of the peak at ($\bar{\nu}_H$) fits well to a single exponential decay indicating that the spectral diffusion with this ligand population happens at a 114 ps time scale (Figure 3.4a). The CLS of the peak at ($\bar{\nu}_L$) shows a biexponential decay, consisting of two decay time scales, 5 and 39 ps (Figure 3.4b). The faster (5 ps) time scale shows an excellent agreement with that obtained from the CLS of the peak ($\bar{\nu}_F$) in the absence of NCs, thereby confirming the existence of freely diffusing ligands.

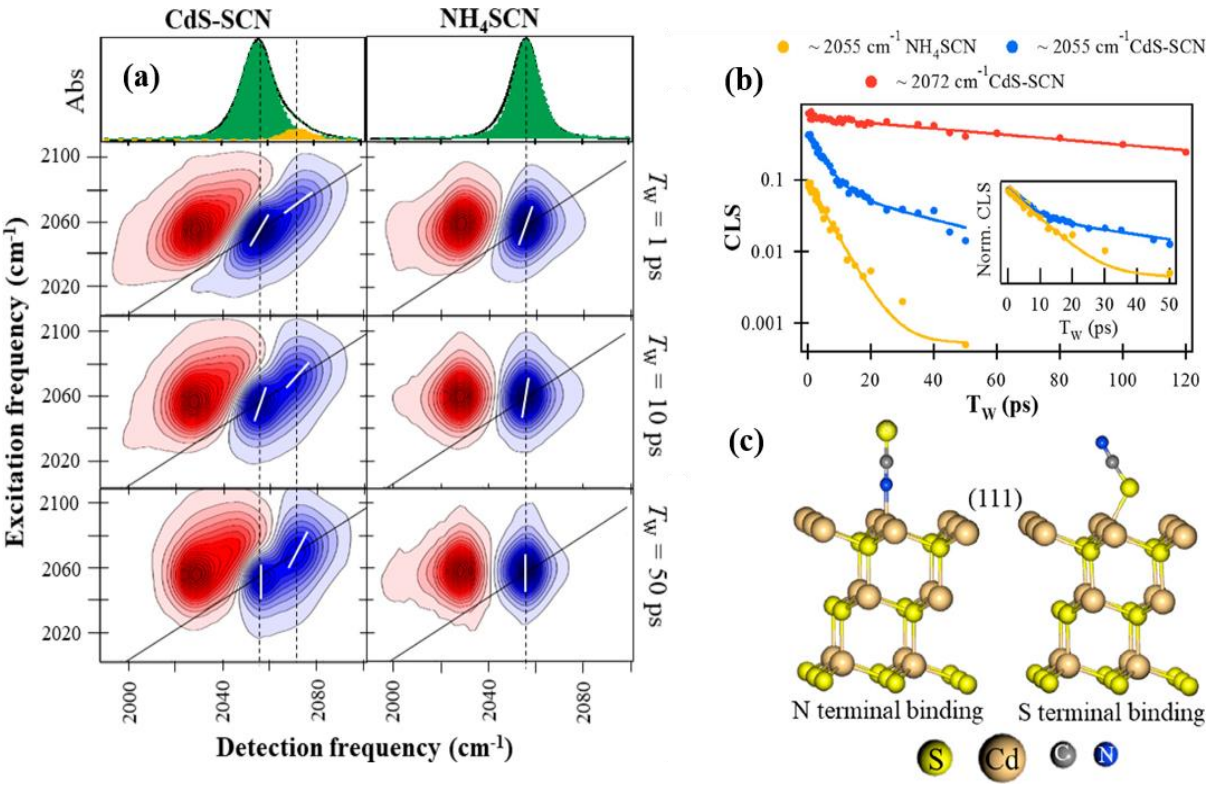

Figure3.4 (a) 2D IR spectra of CdS-SCN (left column) and NH_4SCN (right column) in DMF at three different waiting times (T_w). T_w increases from the top to the bottom along each column. FTIR spectra are shown at the respective top panels such that the peak positions of the FTIR and 2D IR are vertically aligned. (b) T_w dependent CLS decays of the 2055 and 2072 cm^{-1} peaks of CdS-SCN are shown in blue and red, respectively. CLS decay of NH_4SCN (2055 cm^{-1}, yellow) has been appended for easy comparison with the blue decay. The *y*-axis is shown in log scale for clear visualization of the number of exponential decays. The inset represents the normalized CLS decays at 2055 cm^{-1} in the presence and absence of NCs. (c) Optimized slab structure of the N-terminated and S-terminated SCN^- capped (111) facet of the CdS crystal. We set $a = b = 8.40$ Å, $c = 60$ Å, and $\alpha = \beta = \gamma = 90°$ to construct the slab with chelating ligands. The vacuum spacing is about 45 Å, and thus the image effect is eliminated. The plane wave basis set is used with a kinetic energy cutoff of 25 Ry.

It is worth mentioning that the freely diffusing ligands can be paired with the NH_4^+ countercation. A previous study reported a much faster spectral diffusion in DMF (1 ps), albeit using transition metal carbonyl as the vibrational probe.[40] A future study involving variation in the cation size/charge density can provide a clearer picture. Direct binding to the NC surface should restrict the ligand movement and slow down the spectral diffusion. Thus, the slowest time scale corresponding to the peak at ($\bar{\nu}_H$) arises due the strongly bound ligands. The negatively charged SCN^- likely binds (making X-type interaction) to the Cd-rich

positively charged (111) surface, giving rise to this distinct ligand population. The intermediate time scale of 39 ps for the peak at ($\bar{\nu}_L$) indicates a ligand population which is neither freely diffusing nor strongly bound to the NC surface. The ligand interacting weakly with the NCs would be less restricted than those bound strongly to the NCs but would have slower dynamics than that of the freely diffusing ligands. The absorption of the weakly interacting ligands at a frequency similar to that of the freely diffusing ones makes these two ligand populations indistinguishable in the FTIR spectra. It has been previously reported that free thiocyanate anions cannot be spectrally distinguished from solvent separated ion pairs.[36, 40] The only indication in the steady-state spectrum was the broadening of the peak at ($\bar{\nu}_L$) as compared to that at ($\bar{\nu}_F$). However, the ligand dynamics time scales obtained from 2D IR allows us to directly identify the variations in the ligand populations.

Interestingly, the freely diffusing ligands do not have any apparent interaction with the NCs, as indicated from the spectral diffusion time scales. We tried decreasing the ligand concentration during ligand exchange to remove the freely diffusing ligands. However, only a partial transfer of the NCs to the DMF phase was observed, which shows identical normalized FTIR spectra (Figure 3.5) irrespective of the ligand concentration. This result suggests that the free-diffusing ligands are an integral part of the heterogeneous NC system. A zeta potential value of −57.6 mV for CdS-SCN indicates that the ligands can provide electrostatic stabilization to the NCs. Our results demonstrate that the electrostatically bound ligands (39 ps time scale) are in dynamic equilibrium with the freely diffusing ligands (5 ps time scale). Thus, the free ligands could not be eliminated by reducing the ligand concentration during ligand exchange.

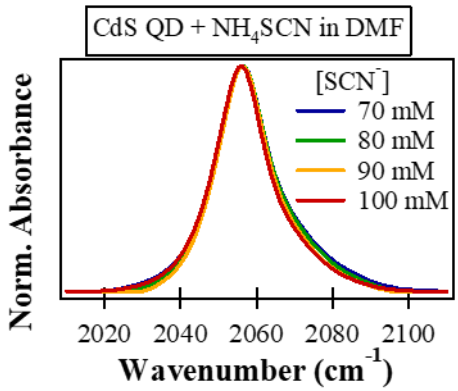

Figure 3.5 FTIR signals of the CN stretch in CdS NC systems after exchange with different thiocyanate concentrations.

In addition to the distinct time scale upon binding to the NCs, the separation between the respective blue and red peaks (vibrational anharmonicity) for SCN^- is known to decrease with proximity to the cations.[41] The estimated anharmonicity (Table 3.1) is the lowest for the peak at ($\bar{\nu}_H$), confirming that this peak arises from strongly bound ligands to the NCs. The anharmonicities of the weakly bound and the free ligands are the same, within the experimental error limit. Additional information is obtained from the amplitudes of the CLS decays (Figure 4b). Although the CLS value at $T_w = 0$ should be unity as no spectral diffusion is possible, it usually decreases from unity due to the presence of ultrafast homogeneous fluctuations. A larger decrease from unity at $T_w = 0$ indicates a larger homogeneous contribution to the line shape of the IR peak. It is intriguing to observe that the ultrafast fluctuations decrease with the increasing strength of ligand−NC interaction, thereby decreasing the homogeneous contribution to the IR line shape.

The ratio of the areas of the peaks at ($\bar{\nu}_H$) and ($\bar{\nu}_L$) is estimated to be 0.1 from the FTIR spectrum of CdS-SCN. In addition, the amplitudes of the biexponential CLS decay for the peak at ($\bar{\nu}_L$) show that the weakly bound ligands contribute ~20% while the rest comes from the freely diffusing ligands. Combining the two results, the population ratio of strongly bound ligands:weakly bound ligands:free ligands is estimated to be 1:2:7. A large fraction of free

ligands is needed to stabilize the NCs as the free ligands are in dynamic equilibrium with both the strongly bound and the weakly interacting ligands. Although the IR spectra of CdS-SCN show two peaks arising from three overlapping transitions, a single peak in ^{13}C NMR[15] confirms the presence of a dynamic equilibrium between the three ligands populations. We therefore estimate a nanosecond time scale for the exchange process, i.e., faster than the NMR time scale and slower than picoseconds as no cross peaks from chemical exchange are seen up to 80 ps in 2D IR.

Table 3.2: Quantum chemically calculated $\bar{\nu}_{CN}$ of different possible thiocyanate species of free SCN^-, $Cd(SCN)_2$ and CdS-SCN.

Compound/ion	Calculated $\bar{\nu}_{CN}$ (cm^{-1})
SCN^-	2051.32
$Cd(SCN)_2$ (-S directing)	2131.56
$Cd(SCN)_2$ (-N directing)	2092.10, 2094.03
SCN^- attached with (111) facet of CdS QDs through N atom	2079.36
SCN^- attached with (111) facet of CdS QDs through S atom	2105.57

Although we have identified the strongly bound ligand population directly from the ligand dynamics time scales, the ambidentate SCN^- can bind to the positively charged (111) NC surface (X-type interaction) either through the sulfur (S) or the nitrogen (N) atom. Density functional theory (DFT) calculations on $Cd2^+$-SCN^- ion pairs (see Table 3.2 for calculated frequencies) predict a blue-shift in $\bar{\nu}_{CN}$ for SCN^- interacting with Cd^{2+} either through the S end or through the N end. To mimic the experimental condition, additional DFT calculations have been performed using Quantum-Expresso on the (111) facet of zinc-blende shaped CdS-NC. For simplification, a slab model has been used to optimize the NC structure.[42] PBE[43] was used as the exchange-correlation functional, and ultrasoft pseudopotentials[44] described the electron–ion interaction. Two different models considering the binding nature of SCN^- (S-

bound and N-bound) have been constructed, and their optimized structures are presented in Figure 3.4c. Small fragments of the slabs were utilized to calculate the $\bar{\nu}_{CN}$ at the B3LYP/lanl2dz level of calculation with the Gaussian 16 package.[45] The calculated values of $\bar{\nu}_{CN}$ are presented in Table 3.2. A close resemblance of $\bar{\nu}_{CN}$ for the N bound SCN^- (2079.36 cm^{-1}) to the (111) surface has been observed with an experimental band at 2072 cm^{-1}, indicating that the ligands are bound to the NC surface through the N atom, making an X type interaction with the (111) facet.

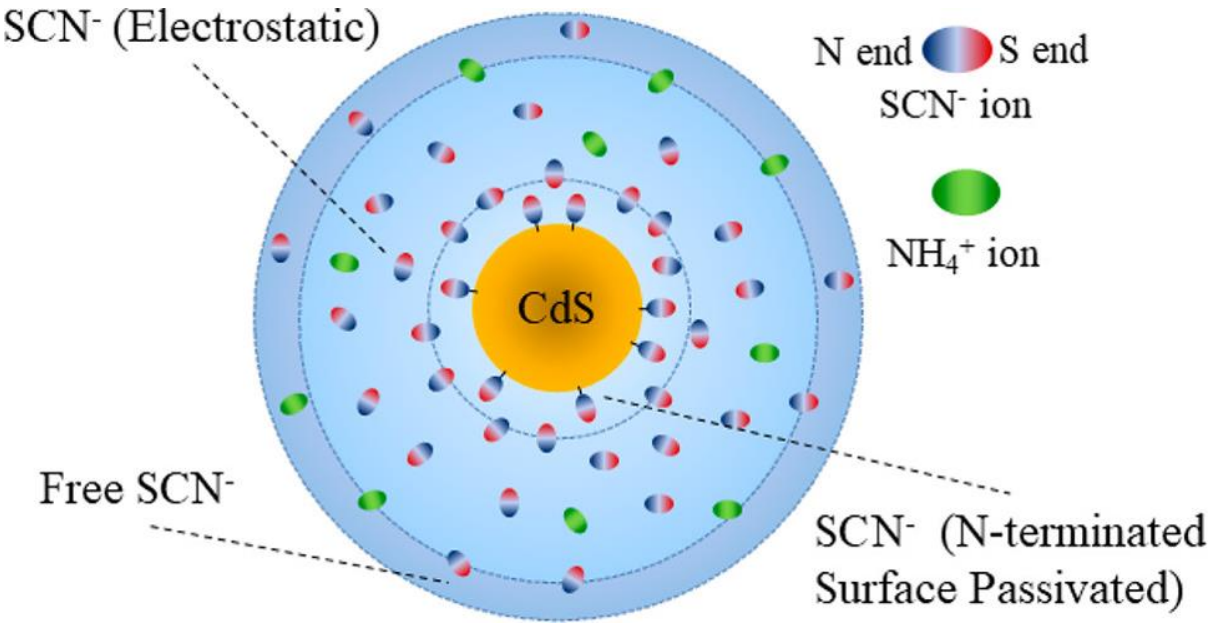

Figure 3.6 Schematic representation of different SCN^- populations in the CdS-SCN system.

3.4 Conclusion

Our results successfully demonstrate that the variations in the inorganic ligand–NC interactions at the NC surface can be successfully deciphered from the variations in the ligand dynamics (Figure 3.6). A unique spectral diffusion time scale, associated with any ligand–NC interactions, depends on how strongly the ligand is interacting with the NC. A stronger interaction slows down the spectral diffusion such that the excitation and detection

frequencies remain correlated for a longer time. We have identified three distinct populations of pseudohalide ligands-strongly bound, electrostatically interacting, and freely diffusing-in the CdS-SCN NCs. These ligand populations were found to be present in the NC system in the ratio 1:2:7. Furthermore, control experimental results indicate a dynamic equilibrium where all the three ligand populations exchange at nanosecond time scales. Interestingly, although the freely diffusing ligands do not apparently interact with NCs, the presence of the dynamic equilibrium between the various ligand populations make these free ligands an intrinsic part of the NC system. Results obtained from quantum chemical calculations show an excellent agreement with our 2D IR interpretations. In addition, the theoretical results indicate that the ambidentate SCN^{-} ligand binds through the N atom, making an X-type interaction with the NCs. This work demonstrates that 2D IR spectroscopy can directly provide a detailed molecular-level picture of how small inorganic ligands stabilize the NCs. In CdS-SCN, the stabilization of the NCs comes from passivating the surface charges through direct binding as well as electrostatic interaction. This study opens up a new avenue to investigate the interaction of small inorganic ligands with the NCs of varying shapes, sizes, and semiconductor materials.

3.5 References

1. Gur, I.; Fromer, N. A.; Geier, M. L.; Alivisatos, A. P., Air-Stable All-Inorganic Nanocrystal Solar Cells Processed from Solution. *Science* **2005,** *310*, 462-465.
2. Konstantatos, G.; Howard, I.; Fischer, A.; Hoogland, S.; Clifford, J.; Klem, E.; Levina, L.; Sargent, E. H., Ultrasensitive solution-cast quantum dot photodetectors. *Nature. 2006 Jul 13;442(7099):180-3. doi: 10.1038/nature04855.* **2006**.
3. Kovalenko, M. V.; Manna, L.; Cabot, A.; Hens, Z.; Talapin, D. V.; Kagan, C. R.; Klimov, V. I.; Rogach, A. L.; Reiss, P.; Milliron, D. J.; Guyot-Sionnnest, P.; Konstantatos, G.; Parak, W. J.; Hyeon, T.; Korgel, B. A.; Murray, C. B.; Heiss, W., Prospects of Nanoscience with Nanocrystals. *ACS Nano* **2015,** *9*, 1012-1057.
4. Talapin, D. V.; Lee, J.-S.; Kovalenko, M. V.; Shevchenko, E. V., Prospects of Colloidal Nanocrystals for Electronic and Optoelectronic Applications. *Chem. Rev. 110*, 389-458.

5. Gao, X.; Cui, Y.; Levenson, R. M.; Chung, L. W. K.; Nie, S., In vivo cancer targeting and imaging with semiconductor quantum dots. *Nat. Biotechnol.* **2004,** *22*, 969-976.
6. Howes, P. D.; Chandrawati, R.; Stevens, M. M., Colloidal nanoparticles as advanced biological sensors. *Science* **2014,** *346*, 1247390.
7. Bell, A. T., The Impact of Nanoscience on Heterogeneous Catalysis. *Science* **2003,** *299* (5613), 1688-1691.
8. Hartley, C. L.; Kessler, M. L.; Dempsey, J. L., Molecular-Level Insight into Semiconductor Nanocrystal Surfaces. *J. Am. Chem. Soc.* **2021,** *143*, 1251-1266.
9. Boles, M. A.; Ling, D.; Hyeon, T.; Talapin, D. V., The surface science of nanocrystals. *Nat. Mater.* **2016,** *15* (2), 141-153.
10. Anderson, N. C.; Hendricks, M. P.; Choi, J. J.; Owen, J. S., Ligand Exchange and the Stoichiometry of Metal Chalcogenide Nanocrystals: Spectroscopic Observation of Facile Metal-Carboxylate Displacement and Binding. *J. Am. Chem. Soc. 135*, 18536-18548.
11. Noone, K. M.; Strein, E.; Anderson, N. C.; Wu, P.-T.; Jenekhe, S. A.; Ginger, D. S., Broadband absorbing bulk heterojunction photovoltaics using low-bandgap solution-processed quantum dots. *Nano Lett.* **2010,** *10*, 2635-2639.
12. Lu, H.; Joy, J.; Gaspar, R. L.; Bradforth, S. E.; Brutchey, R. L., Iodide-passivated colloidal PbS nanocrystals leading to highly efficient polymer: nanocrystal hybrid solar cells. *Chem. Mater.* **2016,** *28*, 1897-1906.
13. Seo, J.; Cho, M. J.; Lee, D.; Cartwright, A.; Prasad, P. N., Efficient heterojunction photovoltaic cell utilizing nanocomposites of lead sulfide nanocrystals and a low-bandgap polymer. *Adv. Mater.*
2011, *23*, 3984-3988.
14. Itskos, G.; Papagiorgis, P.; Tsokkou, D.; Othonos, A.; Hermerschmidt, F.; Economopoulos, S. P.; Yarema, M.; Heiss, W.; Choulis, S., Size-dependent charge transfer in blends of PbS quantum dots with a low-gap silicon-bridged copolymer. *Adv. Energy Mater.* **2013,** *3*, 1490-1499.
15. Fafarman, A. T.; Koh, W.-k.; Diroll, B. T.; Kim, D. K.; Ko, D.-K.; Oh, S. J.; Ye, X.; Doan-Nguyen, V.; Crump, M. R.; Reifsnyder, D. C.; Murray, C. B.; Kagan, C. R., Thiocyanate-Capped Nanocrystal Colloids: Vibrational Reporter of Surface Chemistry and Solution-Based Route to Enhanced Coupling in Nanocrystal Solids. *J. Am. Chem. Soc.* **2011,** *133*, 15753-15761.
16. Nag, A.; Kovalenko, M. V.; Lee, J.-S.; Liu, W.; Spokoyny, B.; Talapin, D. V., Metal-free Inorganic Ligands for Colloidal Nanocrystals: S2–, HS–, Se2–, HSe–, Te2–, HTe–, TeS32–, OH–, and NH2– as Surface Ligands. *J. Am. Chem. Soc.* **2011,** *133*, 10612-10620.
17. Kovalenko, M. V.; Scheele, M.; Talapin, D. V., Colloidal Nanocrystals with Molecular Metal Chalcogenide Surface Ligands. *Science* **2009,** *324*, 1417-1420.
18. De Roo, J.; Yazdani, N.; Drijvers, E.; Lauria, A.; Maes, J.; Owen, J. S.; Van Driessche, I.; Niederberger, M.; Wood, V.; Martins, J. C.; Infante, I.; Hens, Z., Probing Solvent–Ligand Interactions in Colloidal Nanocrystals by the NMR Line Broadening. *Chem. Mater.* **2018,** *30*, 5485-5492.
19. Elimelech, O.; Aviv, O.; Oded, M.; Banin, U., A tale of tails: Thermodynamics of CdSe nanocrystal surface ligand exchange. *Nano Lett.* **2020,** *20*, 6396-6403.
20. Zherebetskyy, D.; Scheele, M.; Zhang, Y.; Bronstein, N.; Thompson, C.; Britt, D.; Salmeron, M.; Alivisatos, P.; Wang, L.-W., Hydroxylation of the surface of PbS nanocrystals passivated with oleic acid. *Science* **2014,** *344*, 1380-1384.
21. Zhang, J.; Zhang, H.; Cao, W.; Pang, Z.; Li, J.; Shu, Y.; Zhu, C.; Kong, X.; Wang, L.; Peng, X., Identification of Facet-Dependent Coordination Structures of Carboxylate Ligands on CdSe Nanocrystals. *J. Am. Chem. Soc.* **2019,** *141*, 15675-15683.

22. Fritzinger, B.; Capek, R. K.; Lambert, K.; Martins, J. C.; Hens, Z., Utilizing self-exchange to address the binding of carboxylic acid ligands to CdSe quantum dots. *J. Am. Chem. Soc.* **2010,** *132*, 10195-10201.
23. Giansante, C.; Infante, I., Surface traps in colloidal quantum dots: a combined experimental and theoretical perspective. *J. Phys. Chem. Lett. 2017* **2017,** *8*, 5209-5215.
24. Wang, Z.; Liu, T.; Long, X.; Li, Y.; Bai, F.; Yang, S., Understanding the Diverse Coordination Modes of Thiocyanate Anion on Solid Surfaces. *J. Phys. Chem. C 123*, 9282-9291.
25. Pienpinijtham, P.; Han, X. X.; Ekgasit, S.; Ozaki, Y., Highly Sensitive and Selective Determination of Iodide and Thiocyanate Concentrations Using Surface-Enhanced Raman Scattering of Starch-Reduced Gold Nanoparticles. *Anal. Chem.* **2011,** *83*, 3655-3662.
26. Leger, J. D.; Friedfeld, M. R.; Beck, R. A.; Gaynor, J. D.; Petrone, A.; Li, X.; Cossairt, B. M.; Khalil, M., Carboxylate Anchors Act as Exciton Reporters in 1.3 nm Indium Phosphide Nanoclusters. *J. Phys. Chem. Lett.* **2019,** *10*, 1833-1839.
27. Kennehan, E. R.; Munson, K. T.; Doucette, G. S.; Marshall, A. R.; Beard, M. C.; Asbury, J. B., Dynamic Ligand Surface Chemistry of Excited PbS Quantum Dots. *J. Phys. Chem. Lett.* **2020,** *11*, 2291-2297.
28. Sun, B.; Voznyy, O.; Tan, H.; Stadler, P.; Liu, M.; Walters, G.; Proppe, A. H.; Liu, M.; Fan, J.; Zhuang, T.; Li, J.; Wei, M.; Xu, J.; Kim, Y.; Hoogland, S.; Sargent, E. H., Pseudohalide-Exchanged Quantum Dot Solids Achieve Record Quantum Efficiency in Infrared Photovoltaics. *Adv Mater 29*, 1700749.
29. Wu, B.; Breen, J. P.; Xing, X.; Fayer, M. D., Controlling the Dynamics of Ionic Liquid Thin Films via Multilayer Surface Functionalization. *J. Am. Chem. Soc. 142*, 9482-9492.
30. Kim, H.; Cho, M., Infrared Probes for Studying the Structure and Dynamics of Biomolecules. *Chem. Rev.* **2013,** *113*, 5817-5847.
31. Mahajan, C.; Sharma, A.; Rath, A. K., Solution-Phase Hybrid Passivation for Efficient Infrared-Band Gap Quantum Dot Solar Cells. *ACS Appl. Mater. Interfaces* **2020,** *12*, 49840-49848.
32. Choi, M.-J.; GarcÃ-a de Arquer, F. P.; Proppe, A. H.; Seifitokaldani, A.; Choi, J.; Kim, J.; Baek, S.-W.; Liu, M.; Sun, B.; Biondi, M.; Scheffel, B.; Walters, G.; Nam, D.-H.; Jo, J. W.; Ouellette, O.; Voznyy, O.; Hoogland, S.; Kelley, S. O.; Jung, Y. S.; Sargent, E. H., Cascade surface modification of colloidal quantum dot inks enables efficient bulk homojunction photovoltaics. *Nat. Commun.* **2020,** *11*, 103.
33. Kyungwon, K.; Sungnam, P.; Ilya, J. F.; Fayer, M. D., Frequency-frequency correlation functions and apodization in two-dimensional infrared vibrational echo spectroscopy: A new approach. *J. Chem. Phys.* **2007,** *127*, 124503.
34. Kumar, N.; Alam, F.; Dutta, V., Photoluminescence study of oleic acid capped and hexanoic acid washed CdS quantum dots. *RSC Adv.* **2016,** *6*, 28316-28321.
35. Yuan, R.; Yan, C.; Fayer, M., Ionâ€"Molecule Complex Dissociation and Formation Dynamics in LiCl Aqueous Solutions from 2D IR Spectroscopy. *J. Phys. Chem. B* **2018,** *122*, 10582-10592.
36. Kyung-Koo, L.; Kwang-Hee, P.; Donghyun, K.; Jun-Ho, C.; Hyewon, S.; Sungnam, P.; Minhaeng, C., Ion-pairing dynamics of Li+ and SCNâˆ' in dimethylformamide solution: Chemical exchange two-dimensional infrared spectroscopy. *J. Chem. Phys.* **2011,** *134*, 064506.
37. Firman, P.; Xu, M.; Eyring, E. M.; Petrucci, S., Thermodynamics of dimerization of sodium thiocyanate in some acyclic polyethers studied by infrared spectroscopy. *J. Phys. Chem.* **1992,** *96*, 8631-8639.

38. Saar, D.; Petrucci, S., Infrared and ultrasonic spectra of sodium thiocyanate and lithium thiocyanate in tetrahydrofuran. *J. Phys. Chem.* **1986,** *90*, 3326-3330.
39. Sun, Z.; Zhang, W.; Ji, M.; Hartsock, R.; Gaffney, K. J., Contact Ion Pair Formation between Hard Acids and Soft Bases in Aqueous Solutions Observed with 2DIR Spectroscopy. *J. Phys. Chem. B* **2013,** *117*, 15306-15312.
40. Park, S.; Ji, M.; Gaffney, K. J., Ligand Exchange Dynamics in Aqueous Solution Studied with 2DIR Spectroscopy. *J. Phys. Chem. B 114*, 6693-6702.
41. Roy, V. P.; Kubarych, K. J., Interfacial Hydration Dynamics in Cationic Micelles Using 2D-IR and NMR. *J. Phys. Chem. B* **2017,** *121*, 9621-9630.
42. Giannozzi, P.; Baroni, S.; Bonini, N.; Calandra, M.; Car, R.; Cavazzoni, C.; Ceresoli, D.; Chiarotti, G. L.; Cococcioni, M.; Dabo, I.; Dal Corso, A.; de Gironcoli, S.; Fabris, S.; Fratesi, G.; Gebauer, R.; Gerstmann, U.; Gougoussis, C.; Kokalj, A.; Lazzeri, M.; Martin-Samos, L.; Marzari, N.; Mauri, F.; Mazzarello, R.; Paolini, S.; Pasquarello, A.; Paulatto, L.; Sbraccia, C.; Scandolo, S.; Sclauzero, G.; Seitsonen, A. P.; Smogunov, A.; Umari, P.; Wentzcovitch, R. M., QUANTUM ESPRESSO: a modular and open-source software project for quantum simulations of materials. *J Phys Condens Matter* **2009,** *21* (39), 395502.
43. Perdew, J. P.; Burke, K.; Ernzerhof, M., Generalized Gradient Approximation Made Simple. *Phys. Rev. Lett.* **1996,** *77* (18), 3865-3868.
44. Vanderbilt, D., Soft self-consistent pseudopotentials in a generalized eigenvalue formalism. *Phys. Rev. B* **1990,** *41* (11), 7892-7895.
45. Frisch, M.; Trucks, G.; Schlegel, H.; Scuseria, G.; Robb, M.; Cheeseman, J.; Scalmani, G.; Barone, V.; Petersson, G.; Nakatsuji, H., Gaussian 16, Revision A. 03, Gaussian, Inc., Wallingford CT. *Gaussian16 (Revision A. 03)* **2016**.

Chapter 4

Directly Probing the Electrostatic Interaction in Inorganic Ligand Capped Nanocrystals by 2D IR Spectroscopy

4.1 Introduction

In the previous chapter, we investigated thiocyanate-capped CdS nanocrystals. Recently, thiocyanate ions have gained attention as effective short capping ligands for enhancing device performance.[1-9] The previous chapter provided a fundamental understanding of how these inorganic ligands stabilize nanocrystals (NCs) in solutions. Through a combination of FTIR, 2D IR, and quantum mechanical calculations, we identified that three types of ligands are present: freely diffusing, weakly bound, and strongly bound to the CdS 111 surface.[10] These findings suggest that thiocyanate ions stabilize the quantum dots either by directly binding to the NCs surface or through electrostatic stabilization.

Interestingly, the 2D IR results revealed the presence of a weakly bound thiocyanate layer that appeared spectroscopically indistinguishable from freely diffusing thiocyanate anions. This observation led us to propose the hypothesis that an electrical double layer is necessary for NC stabilization. Although the NC community has assumed this hypothesis due to anions forming a double layer close to positively charged metal surfaces, [11-14] direct experimental proof has been lacking until now.

Given that our results were obtained on CdS nanocrystals, the question naturally arises whether the same stabilization pattern holds for other quantum dots. To address this, we extended our study to CdSe NCs, in which the Cd core remains intact, but the S is replaced with Se. CdSe is also one of the most extensively studied NC materials.[1, 15-19] By investigating CdSe NCs, we aim to gain further insights into the generalizability of the stabilization mechanisms observed in CdS nanocrystals. Understanding these aspects will contribute to the broader comprehension and potential applications of NCs in various devices.

Following a similar approach to the previous study, the bulky organic ligands of the as-synthesized NCs were replaced with thiocyanate ligands through a ligand exchange protocol, resulting in the formation of CdSe-SCN NCs dissolved in DMF. The size of the synthesized CdSe nanocrystals closely resembled that of the CdS quantum dots mentioned earlier. Figure 4.1a Shows the UV–vis spectra of the CdSe NCs dispersed in hexane (before exchange) and DMF (after exchange) solutions. The X-ray diffraction (XRD) pattern of the SCN^- capped CdSe (CdSe-SCN) was identical to that of CdS-OA (Figure 4.1b). HRTEM image of CdSe NCs shown in figure 4.1c.The size distributions of the NCs are shown in Figure 4.1d. In agreement with the previous literature, the fringe spacing and XRD correspond to (111), (220), and (311) planes of the zinc blend structure.[20] The XRD pattern reveals (111) to be the predominant facet.

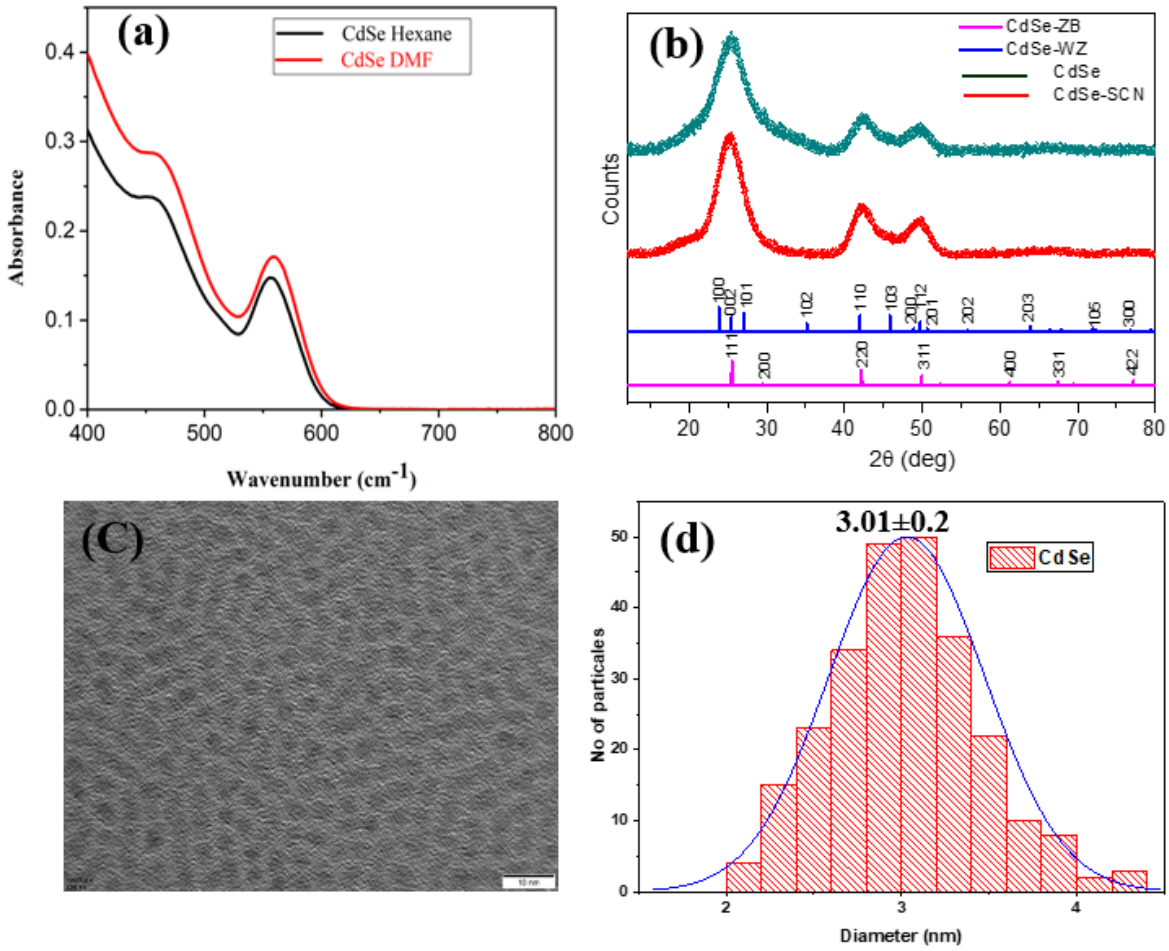

Figure 4.1 (a) UV–vis absorption spectra in hexane and DMF, (b) XRD patterns, and (c) HRTEM image of CdSe NCs (d) particle size distributions obtained from HRTEM analysis of CdSe NCSs

4.2 Materials and Method

4.2.1 Chemicals

Cadmium oxide (CdO, 99.5%), Trioctylphosphine oxide (TOPO, 99%), Trioctylphosphine (TOP,90%), 1-octadecene (ODE, 90%), Oleic acid (90%), Selenium powder mesh (99.99%), Octaadecylamine (ODA, >95%), toluene, hexane, methanol, acetone chloropropanethiol (CPT).

4.2.2 CdSe nanocrystal synthesis

The mixture of 1 mmol (0.128 g) CdO, 4 mmol (1.27 mL) oleic acid and 14 mL of ODE in a 50 mL three-neck flask was degassed first at room temp. Then temperature is increased to 100 °C under vacuum and degassed at 120 °C for 20 min. Then heated to about 240 °C under inert gas until a clear solution is obtained under constant stirring. After this, solution was cooled to 90 °C and ODA (1.5 g) and 1.0 g TOPO were added into the flask. Temperature is increased to 280 °C. At this temperature, TOP-Se solution (0.4 M, 2.5 mL) was injected swiftly into the Cd-oleate solution. The temperature fell down to 268 °C and the reaction was allowed to proceed at 280 °C for 8 min. The solution was cooled down in water bath. The resultant NCs are washed twice in a 1:1 mixture of hexane-methanol, to remove unreacted precursors. The nanocrystals were precipitated by adding acetone and redispersed in hexane.

4.2.3 Ligand Exchange

The ligand exchange procedure was performed using the method reported by Kagan et al., with some modifications.[1] In a typical procedure, 1 mL of 130 mM NH_4SCN in acetone was prepared, and this solution was added drop-wise to 0.5 mL of a dispersion of as-synthesized CdSe NCs in hexane (15-20 mg/ml) until precipitation was formed. The resulting solution was then centrifuged for 3 minutes at 4000 rpm. After that, the supernatant was discarded, and the resulting NCs were washed with acetone. Finally, the CdSe NCs were dried and dispersed in 0.5 mL of DMF with 0.5 μl of CPT.[21-22] This SCN-capped CdSe was used for spectroscopic studies.

4.2.4 IR spectroscopy

IR absorption spectra was measured at room temperature on a Bruker Vertex 70 FTIR spectrometer. For each sample, ~90 μL of the sample solution was loaded into a demountable cell consisting of two windows (CaF_2, 3 mm thickness) separated by a mylar spacer of 100 μm thickness. Same sample cell used for 2D IR experiments.

4.3 Results and discussion

Figure 4.2b displays the FTIR spectrum of CdSe-SCN nanocrystal, exhibiting an asymmetric peak. This peak was analyzed by fitting it with two Gaussian lineshape functions, centered at

2055 cm^{-1} and 2072 cm^{-1}, respectively. Notably, these peak positions exactly match those observed for CdS-SCN NCs discussed in the preceding chapter. Consequently, it can be inferred that similar to CdS-SCN, CdSe-SCN also comprises a small bound population, represented by the higher frequency peak centered at 2072 cm^{-1} in Figure 4.2b.

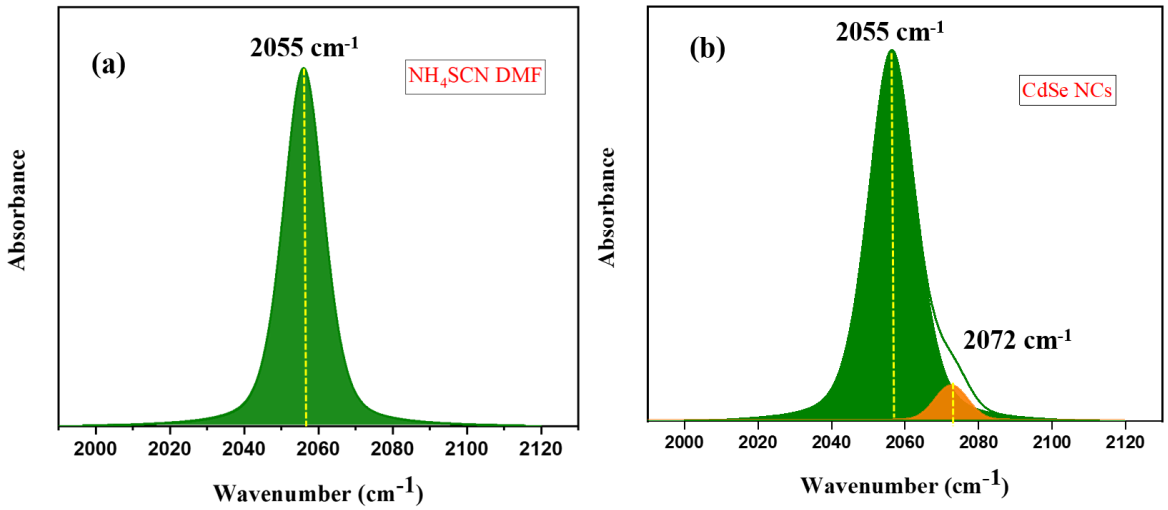

Figure 4.2 (a) FTIR spectra of the nitrile stretch of SCN^- in the DMF. (b) FTIR spectra of the nitrile stretch of CdSe-SCN in the DMF.

Comparing the peak at 2055 cm^{-1} to the peak frequency of NH_4SCN in DMF (Figure 4.2 a), we find an exact match. However, it is worth noting that the full width at half maximum (FWHM) of the peak for CdSe-SCN is larger than that of the free thiocyanate anion by ~3 cm^{-1}. As described in the previous chapter, it is important to acknowledge that FTIR spectra cannot resolve weakly bound populations, as they are known to overlap with free, solvent-shared, and solvent-separated ions, making them indistinguishable through FTIR spectroscopy.[23-24]

To gain a deeper insight into the peak at 2055 cm^{-1} in CdSe-SCN NCs, we conducted 2D IR spectroscopy at different time delays (T_w values). Figure 4.3 illustrates the T_w-dependent 2D IR spectra, displaying two peak pairs resulting from v = 0 to v = 1 transitions and v = 1 to v = 2

transitions, separated by the detection frequency axis due to vibrational anharmonicity. The peak pairs diagonally elongated at shorter T_w values. As the waiting time increases, the lower frequency peak pair approaches a circular shape, while the higher frequency peak retains elongation along the diagonal. This distinct change in peak evolution suggests that the fluctuation dynamics of the higher frequency peak are much slower than those of the lower frequency peak. This behavior is similar to what was observed for CdS-SCN NCs.

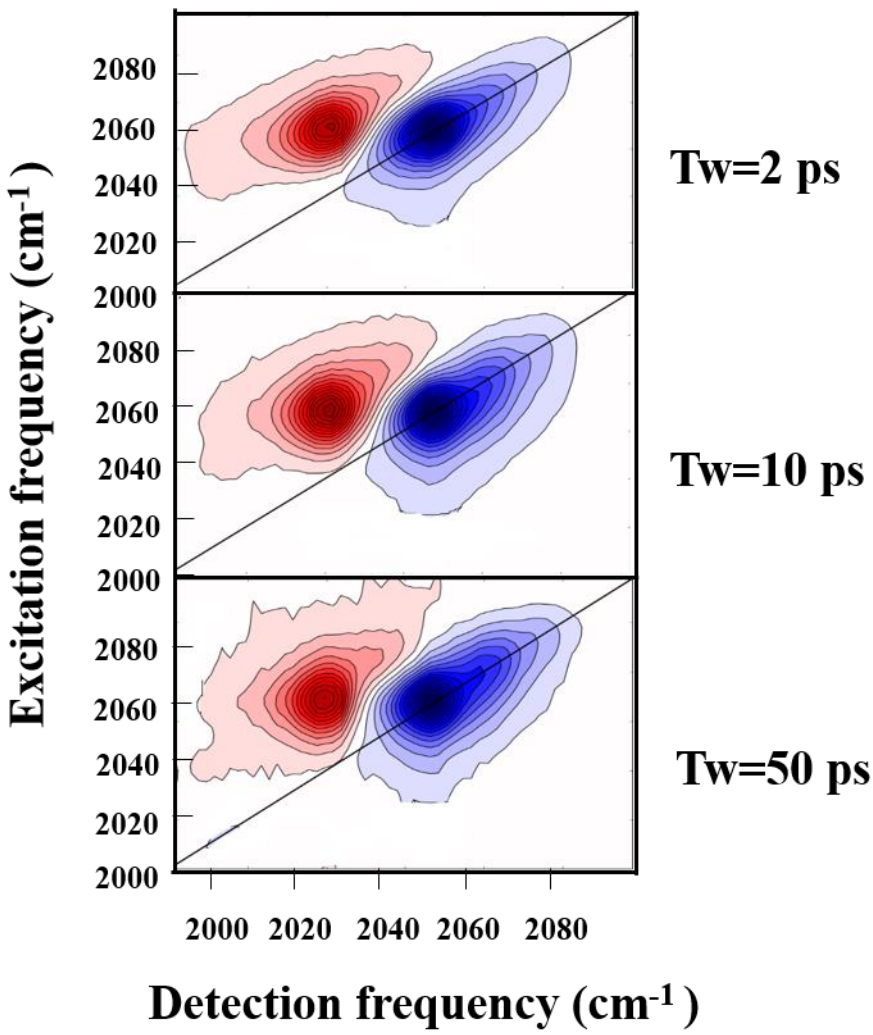

Figure 4.3 2D IR spectra of CdSe-SCN in DMF at three different waiting times (T_w). T_w increases from the top to the bottom.

To investigate the structural dynamics of the thiocyanate ligands, we analyzed the T_w-dependent changes in the 2D IR peak shapes using the CLS method[25] (Figure 4.4). The peak at 2072 cm^{-1} indeed shows a slow decay with a time component of 124 ps (Table 4.1). Similarly, as observed in the previous chapter, the peak at 2072 cm^{-1} exhibits a bi-exponential decay with time constants of 1.3 ps and 114 ps. Intriguingly, despite the replacement of S with Se, the timescales show a nearly quantitative match.

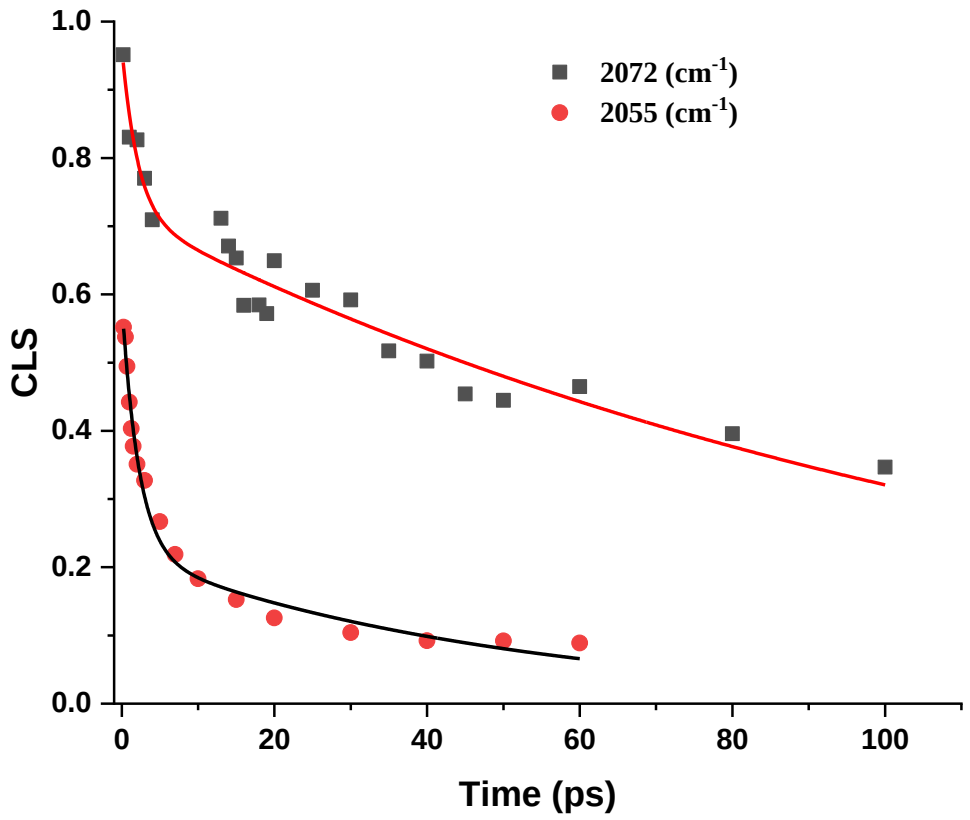

Figure 4.4 T_w dependent CLS decays of the 2072 cm^{-1} peaks (black) and 2055 cm^{-1} (red) of CdSe-SCN

This result indicates that the modes of passivation by the thiocyanate ligands remain the same for both CdS-SCN and CdSe-SCN NCs. This finding can be rationalized because the Cd^{2+} rich 111 surface, which binds the thiocyanate anions, remains unchanged for NCs containing both S and Se. Although our results suggest three different types of ligand interactions (strongly bound, weakly bound, and free) in CdS-SCN and CdSe-SCN NCs, direct experimental proof of the electrical double layer is still lacking. Furthermore, it would be intriguing to gain a deeper understanding of the exact origin of the double layer phenomenon.

Table 4.1 Experimental CLS parameters of free and bound peak

SCN Stretch	a_1	τ_1 (ps)	a_2	τ_2 (ps)
2055 cm^{-1}	0.36±0.02	2.2±0.3	0.22±0.02	49.6±9.9
2072 cm^{-1}	0.24±0.04	2.05±0.7	0.71±0.02	124±13.1

To confirm the presence of the electrical double layer, we conducted polarization-selective 2D IR spectroscopy and generated the normalized frequency-frequency correlation function (FFCF) using the CLS method for both parallel and perpendicular polarization conditions (Figure 4.5). Surprisingly, the FFCF obtained for perpendicular polarization exhibited a faster decay compared to the parallel polarization condition. Such an observation is commonly attributed to reorientation-induced spectral diffusion (RISD).[26-28] Generally RISD effect takes accounts of orientation of probe molecule relative to local electric field of the respective medium.

When the solute reorientation is slower than the environment fluctuation, the FFCF is agnostic to the polarization condition.[29] RISD occurs when the solutes reorientation is faster than the

fluctuations in its surrounding environment.[30] In such cases, the solute can reorient while the environment is considered static.[31] Although the environment does not fluctuate on the solutes reorientation timescale, the solute experiences a new environment due to its reorientation, resulting in a change in the solute's absorption frequency. Consequently, the solute reorientation contributes to the FFCF, leading to the occurrence of RISD.

In our system, probe molecules that remain aligned with the initial pump polarization (parallel) experience lesser frequency changes compared to those that undergo rotation and are probed with perpendicular polarization. This difference in frequency changes caused the FFCF for the perpendicular polarization condition to decay more rapidly. In other words, for perpendicular polarization, spectral diffusion happens fast compared to parallel polarization because this polarization measure the spectral diffusion of significantly rotated molecules as molecules rotate angle between transitions dipole moments and electric field changes which changes the vibrational frequency of probe molecules.[29] The parallel polarization samples those molecules which retains their orientation which shows high frequency correlation and shows slows decay compared with perpendicular polarization. Once the reorientation process was complete, the FFCFs for parallel and perpendicular polarization merged, as the decays at longer waiting times were solely influenced by environmental fluctuations.

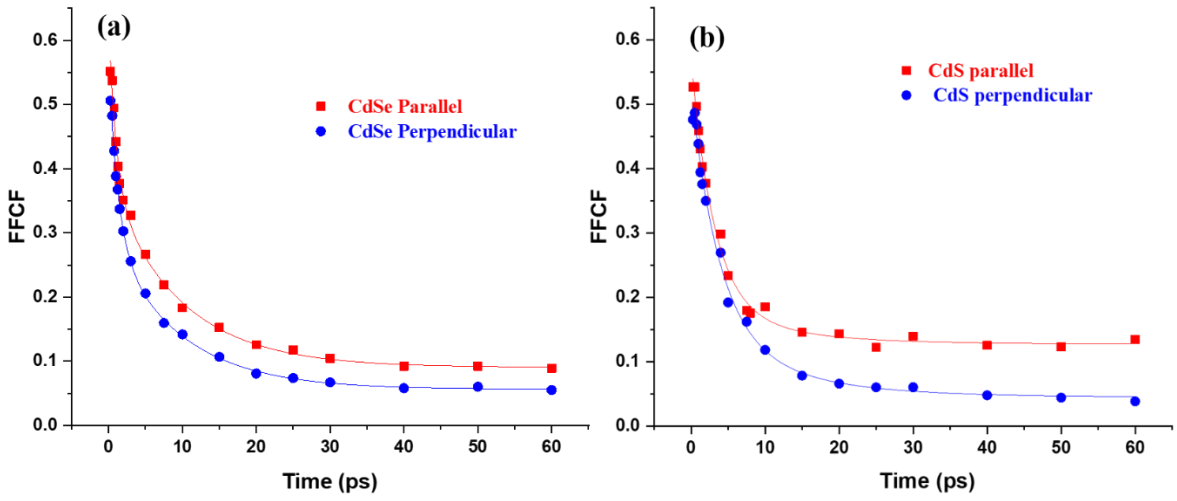

Figure 4.5 Polarization dependent FFCF decay curves of CdSe-SCN and CdS-SCN for parallel (red) and perpendicular (blue) polarization conditions.

Interestingly, Figure 4.5 reveals that the FFCF for parallel and perpendicular conditions do not merge even at large waiting times. A constant static offset is observed between the parallel and perpendicular polarization FFCFs up to 60 ps. This phenomenon has been previously reported by Garrett-Roe and colleagues for colloidal suspensions of charged surfactant molecules in ionic liquids, probed by thiocyanate ions using polarization-selective 2D IR.[32-33]

To explain the discrepancy in FFCF at long waiting times, a non-isotropic distribution of thiocyanate probes in a local electric field is considered. For both polarizations, the FFCF decays are not identical at long waiting times, and they remain different even after the reorientation dynamics are completed. The presence of a strong electric field results in potential energy changes for the probe molecules based on the angle between the dipole moment of the probe and the local electric field. Consequently, this non-isotropic distribution of molecular dipoles in the probe is created due to the potential energy difference.

Recently, Fayer's group further investigated the results reported by Garrett-Roe and coworkers by considering the effects of the steric and electrostatic environment of the probe molecule on RISD.[34] They found that when the probe molecule interacts sterically, it has minimal effect on RISD, whereas electrostatically interacting probe molecules exhibit a significant impact on RISD.

To explore the possibility of SCN ions interacting with the ammonium cation ($NH4^+$), and thereby showing polarization-dependent spectral diffusion, we conducted polarization-dependent 2D IR experiments on 100mM NH_4SCN in DMF. Interestingly, we observed polarization-independent spectral diffusion, indicating that the Cd cation-rich facet (111) of both CdS and CdSe creates a strong electric field, and SCN ions interact electrostatically with Cd cations.

The polarization-selective 2D IR results for SCN^-passivated CdS and CdSe quantum dots directly probe the electrostatically ordered SCN ions in the electrical double layer within the polar solvent. This provides valuable insights into the interactions and dynamics of the electrical double layer in these systems.

4.4 Conclusion

In summary, the FTIR spectra of both SCN-capped CdS and CdSe nanocrystals, which are of similar size, reveal the presence of both bound and free populations of SCN ligands. The FWHM of the free peak in both NCs is larger by ~3 cm^{-1} compared to NH_4SCN in DMF. Notably, polarization-selective 2D IR experiments for both NCs demonstrate different FFCF decays, and these decays do not become identical even after completing the reorientation time of SCN ions. This observation strongly suggests that the SCN ions interact electrostatically with Cd cations in both CdS and CdSe nanocrystals.

In the past, the electrostatic stabilization of quantum dots by short inorganic ligands has been explained by reporting the zeta potential. However, direct proof of these electrostatically interacting ions has not been reported yet. These results highlight the effectiveness of polarization-selective 2D IR in directly probing the electrostatically interacting short inorganic ligands on the surface of quantum dots.

Overall, this study provides valuable insights into the interactions between quantum dots and their surface ligands, shedding light on the mechanism of electrostatic stabilization and paving the way for further understanding and optimizing the performance of quantum dot-based devices.

4.5 References

1. Fafarman, A. T.; Koh, W.-k.; Diroll, B. T.; Kim, D. K.; Ko, D.-K.; Oh, S. J.; Ye, X.; Doan-Nguyen, V.; Crump, M. R.; Reifsnyder, D. C.; Murray, C. B.; Kagan, C. R., Thiocyanate-Capped Nanocrystal Colloids: Vibrational Reporter of Surface Chemistry and Solution-Based Route to Enhanced Coupling in Nanocrystal Solids. *J. Am. Chem. Soc.* ***2011,*** *133*, 15753-15761.
2. Koh, W.-k.; Saudari, S. R.; Fafarman, A. T.; Kagan, C. R.; Murray, C. B., Thiocyanate-Capped PbS Nanocubes: Ambipolar Transport Enables Quantum Dot Based Circuits on a Flexible Substrate. *Nano Lett.* **2011,** *11*, 4764-4767.
3. Dambhare, N. V.; Sharma, A.; Mahajan, C.; Rath, A. K., Thiocyanate- and Thiol-Functionalized p-Doped Quantum Dot Colloids for the Development of Bulk Homojunction Solar Cells. *Energy Technol.* **2022,** *10*, 2200455.
4. Chen, F.; Boopathi, K. M.; Imran, M.; Lauciello, S.; Salerno, M., Thiocyanate-Treated Perovskite-Nanocrystal-Based Light-Emitting Diodes with Insight in Efficiency Roll-Off. *Materials* **2020,** *13*, 367.
5. Dey, A.; Ye, J.; De, A.; Debroye, E.; Ha, S. K.; Bladt, E.; Kshirsagar, A. S.; Wang, Z.; Yin, J.; Wang, Y.; Quan, L. N.; Yan, F.; Gao, M.; Li, X.; Shamsi, J.; Debnath, T.; Cao, M.; Scheel, M. A.; Kumar, S.; Steele, J. A.; Gerhard, M.; Chouhan, L.; Xu, K.; Wu, X.-g.; Li, Y.; Zhang, Y.; Dutta, A.; Han, C.; Vincon, I.; Rogach, A. L.; Nag, A.; Samanta, A.; Korgel, B. A.; Shih, C.-J.; Gamelin, D. R.; Son, D. H.; Zeng, H.; Zhong, H.; Sun, H.; Demir, H. V.; Scheblykin, I. G.; Mora-Seró, I.; Stolarczyk, J. K.; Zhang, J. Z.; Feldmann, J.; Hofkens, J.; Luther, J. M.; Pérez-Prieto, J.; Li, L.; Manna, L.; Bodnarchuk, M. I.; Kovalenko, M. V.; Roeffaers, M. B. J.; Pradhan, N.; Mohammed, O. F.; Bakr, O. M.; Yang, P.; Müller-Buschbaum, P.; Kamat, P. V.; Bao, Q.; Zhang, Q.; Krahne, R.; Galian, R. E.; Stranks, S. D.; Bals, S.; Biju, V.; Tisdale, W. A.; Yan, Y.; Hoye, R. L. Z.; Polavarapu, L., State of the Art and Prospects for Halide Perovskite Nanocrystals. *ACS Nano* **2021,** *15*, 10775-10981.

6. Koscher, B. A.; Swabeck, J. K.; Bronstein, N. D.; Alivisatos, A. P., Essentially Trap-Free CsPbBr3 Colloidal Nanocrystals by Postsynthetic Thiocyanate Surface Treatment. *J. Am. Chem. Soc.* **2017,** *139*, 6566-6569.
7. Patra, B. K.; Agrawal, H.; Zheng, J.-Y.; Zha, X.; Travesset, A.; Garnett, E. C., Close-Packed Ultrasmooth Self-assembled Monolayer of CsPbBr3 Perovskite Nanocubes. *ACS Appl. Mater. Interfaces* **2020,** *12*, 31764-31769.
8. Zheng, X.; Yuan, S.; Liu, J.; Yin, J.; Yuan, F.; Shen, W.-S.; Yao, K.; Wei, M.; Zhou, C.; Song, K.; Zhang, B.-B.; Lin, Y.; Hedhili, M. N.; Wehbe, N.; Han, Y.; Sun, H.-T.; Lu, Z.-H.; Anthopoulos, T. D.; Mohammed, O. F.; Sargent, E. H.; Liao, L.-S.; Bakr, O. M., Chlorine Vacancy Passivation in Mixed Halide Perovskite Quantum Dots by Organic Pseudohalides Enables Efficient Rec. 2020 Blue Light-Emitting Diodes. *ACS Energy Lett.* **2020,** *5*, 793-798.
9. Lu, M.; Guo, J.; Lu, P.; Zhang, L.; Zhang, Y.; Dai, Q.; Hu, Y.; Colvin, V. L.; Yu, W. W., Ammonium Thiocyanate-Passivated CsPbI3 Perovskite Nanocrystals for Efficient Red Light-Emitting Diodes. *J. Phys. Chem. C* **2019,** *123*, 22787-22792.
10. Deshmukh, S. H.; Chatterjee, S.; Ghosh, D.; Bagchi, S., Ligand Dynamics Time Scales Identify the Surface–Ligand Interactions in Thiocyanate-Capped Cadmium Sulfide Nanocrystals. *J. Phys. Chem. Lett.* **2022,** *13*, 3059-3065.
11. Sayevich, V.; Cai, B.; Benad, A.; Haubold, D.; Sonntag, L.; Gaponik, N.; Lesnyak, V.; Eychmüller, A., 3D Assembly of All-Inorganic Colloidal Nanocrystals into Gels and Aerogels. *Angew. Chem. Int. Ed.* **2016,** *55*, 6334-6338.
12. Nag, A.; Kovalenko, M. V.; Lee, J.-S.; Liu, W.; Spokoyny, B.; Talapin, D. V., Metal-free Inorganic Ligands for Colloidal Nanocrystals: S2â€“, HSâ€“, Se2â€“, HSeâ€“, Te2â€“, HTeâ€“, TeS32â€“, OHâ€“, and NH2â€“ as Surface Ligands. *Journal of the American Chemical Society 133* (27), 10612-10620.
13. Wang, W.; Zhang, M.; Pan, Z.; Biesold, G. M.; Liang, S.; Rao, H.; Lin, Z.; Zhong, X., Colloidal Inorganic Ligand-Capped Nanocrystals: Fundamentals, Status, and Insights into Advanced Functional Nanodevices. *Chem. Rev.* **2022,** *122*, 4091-4162.
14. Zhang, H.; Jang, J.; Liu, W.; Talapin, D. V., Colloidal Nanocrystals with Inorganic Halide, Pseudohalide, and Halometallate Ligands. *ACS Nano 8* (7), 7359-7369.
15. Lokteva, I.; Radychev, N.; Witt, F.; Borchert, H.; Parisi, J.; Kolny-Olesiak, J., Surface Treatment of CdSe Nanoparticles for Application in Hybrid Solar Cells: The Effect of Multiple Ligand Exchange with Pyridine. *J. Phys. Chem. C* **2010,** *114*, 12784-12791.
16. Zhao, L.; Hu, L.; Fang, X., Growth and Device Application of CdSe Nanostructures. *Adv. Funct. Mater.* **2012,** *22*, 1551-1566.
17. Wang, Y. F.; Yang, R. Q.; Wang, Y. J.; Shi, Z. X.; Liu, J. J., Application of CdSe nanoparticle suspension for developing latent fingermarks on the sticky side of adhesives. *Forensic Science International* **2009,** *185* (1), 96-99.
18. Cosseddu, S.; Pascazio, R.; Giansante, C.; Manna, L.; Infante, I., Ligand dynamics on the surface of CdSe nanocrystals. *Nanoscale* **2023,** *15*, 7410-7419.
19. Goldzak, T.; McIsaac, A. R.; Van Voorhis, T., Colloidal CdSe nanocrystals are inherently defective. *Nat Commun* **2021,** *12*, 890.
20. Liu, L.; Zhuang, Z.; Xie, T.; Wang, Y.-G.; Li, J.; Peng, Q.; Li, Y., Shape Control of CdSe Nanocrystals with Zinc Blende Structure. *J. Am. Chem. Soc.* **2009,** *131*, 16423-16429.
21. Mahajan, C.; Sharma, A.; Rath, A. K., Solution-Phase Hybrid Passivation for Efficient Infrared-Band Gap Quantum Dot Solar Cells. *ACS Applied Materials & Interfaces 12* (44), 49840-49848.

22. Choi, M.-J.; GarcÃ-a de Arquer, F. P.; Proppe, A. H.; Seifitokaldani, A.; Choi, J.; Kim, J.; Baek, S.-W.; Liu, M.; Sun, B.; Biondi, M.; Scheffel, B.; Walters, G.; Nam, D.-H.; Jo, J. W.; Ouellette, O.; Voznyy, O.; Hoogland, S.; Kelley, S. O.; Jung, Y. S.; Sargent, E. H., Cascade surface modification of colloidal quantum dot inks enables efficient bulk homojunction photovoltaics. *Nature Communications 11* (1), 103.
23. Kyung-Koo, L.; Kwang-Hee, P.; Donghyun, K.; Jun-Ho, C.; Hyewon, S.; Sungnam, P.; Minhaeng, C., Ion-pairing dynamics of Li+ and SCNâˆ’ in dimethylformamide solution: Chemical exchange two-dimensional infrared spectroscopy. *The Journal of Chemical Physics 134* (6), 064506.
24. Park, S.; Ji, M.; Gaffney, K. J., Ligand Exchange Dynamics in Aqueous Solution Studied with 2DIR Spectroscopy. *The Journal of Physical Chemistry B 114* (19), 6693-6702.
25. Kyungwon, K.; Sungnam, P.; Ilya, J. F.; Fayer, M. D., Frequency-frequency correlation functions and apodization in two-dimensional infrared vibrational echo spectroscopy: A new approach. *The Journal of Chemical Physics* **2007,** *127* (12), 124503.
26. Kramer, P. L.; Nishida, J.; Giammanco, C. H.; Tamimi, A.; Fayer, M. D., Observation and theory of reorientation-induced spectral diffusion in polarization-selective 2D IR spectroscopy. *J. Chem. Phys.* **2015,** *142*.
27. Shin, J. Y.; Yamada, S. A.; Fayer, M. D., Carbon Dioxide in a Supported Ionic Liquid Membrane: Structural and Rotational Dynamics Measured with 2D IR and Pump–Probe Experiments. *J. Am. Chem. Soc.* **2017,** *139*, 11222-11232.
28. Shin, J. Y.; Yamada, S. A.; Fayer, M. D., Dynamics of a Room Temperature Ionic Liquid in Supported Ionic Liquid Membranes vs the Bulk Liquid: 2D IR and Polarized IR Pump–Probe Experiments. *J. Am. Chem. Soc.* **2017,** *139*, 311-323.
29. Kramer, P. L.; Nishida, J.; Fayer, M. D., Separation of experimental 2D IR frequency-frequency correlation functions into structural and reorientation-induced contributions. *J. Chem. Phys.* **2015,** *143*.
30. Tamimi, A.; Bailey, H. E.; Fayer, M. D., Alkyl Chain Length Dependence of the Dynamics and Structure in the Ionic Regions of Room-Temperature Ionic Liquids. *J. Phys. Chem. B* **2016,** *120*, 7488-7501.
31. Sakpal, S. S.; Deshmukh, S. H.; Chatterjee, S.; Ghosh, D.; Bagchi, S., Transition of a Deep Eutectic Solution to Aqueous Solution: A Dynamical Perspective of the Dissolved Solute. *J. Phys. Chem. Lett.* **2021,** *12*, 8784-8789.
32. Ren, Z.; Kelly, J.; Gunathilaka, C. P.; Brinzer, T.; Dutta, S.; Johnson, C. A.; Mitra, S.; Garrett-Roe, S., Ultrafast dynamics of ionic liquids in colloidal dispersion. *Phys. Chem. Chem. Phys.* **2017,** *19*, 32526-32535.
33. Ren, Z.; Garrett-Roe, S., Reorientation-induced spectral diffusion of non-isotropic orientation distributions. *J. Chem. Phys.* **2017,** *147*.
34. Hoffman, D. J.; Fica-Contreras, S. M.; Pan, J.; Fayer, M. D., Distinguishing steric and electrostatic molecular probe orientational ordering via their effects on reorientation-induced spectral diffusion. *J. Chem. Phys.* **2021,** *154*.

Chapter 5

Orientational Dynamics of Electrostatically Interacting Ligands in Size Dependent CdSe Nanocystals

5.1 Introduction

The colloidal nanocrystals possess unique optical, electronic, thermal, magnetic, and chemical properties, making them highly desirable as primary elementary units for optoelectronic device applications.[1-7] The shape, size, surface ligand, and composition-dependent optical and electronic properties of NCs make them interesting materials in various fields, which is why they have gained significant attention from both industry and academia.[8] NCs have been designed for efficient use in a wide range of applications, spanning from biomedicine to sensing and energy.[9] Surface ligands used during the synthesis of NCs play a crucial role in their properties and behavior. Carefully selecting ligands is essential in controlling the nucleation and growth processes, ultimately influencing the shape and size of the nanocrystals.[10-11] Several experimental and theoretical reports have been dedicated to understanding the behavior of ligands.[12-13] To enhance the practical applications of NCs-based devices, efficient charge carrier mobility, interparticle coupling, and good electronic communication are necessary.[14] However, the long and bulky ligands used in the synthesis can hinder carrier mobility. A solution to this issue is to replace the long ligands with shorter inorganic ligands. Talapin's group pioneered this approach in 2009 by demonstrating that the conductivity between individual nanocrystals can be significantly enhanced by using compact inorganic ligands. Halides, Pseudohalides, chalcogenide chalcogenidometallates are used as short ligands for NCs surface covering.[15] These short, compact ligands cut down the interpaticle distance, improve the electronic coupling and enhance the carrier mobility. Kagan and co-workers replaced the bulky ligands with SCN^- ions where film conductivity and carrier mobility increased by many fold.[14, 16]

In Chapters 3 and 4 of this publication, we have studied SCN^- capped CdS and CdSe NCs using FTIR, 2D IR spectroscopy, and quantum mechanical calculations. The results revealed the presence of three types of ligands: strongly bound, weakly bound, and freely diffusing.[17] Polarization-selective 2D IR spectroscopy further validated that the strongly and weakly bound ligands form an electrical double layer (EDL) around the NCs. The strongly bound ligands directly attach to the positively charged Cd-rich 111 facet of the CdS and CdSe NCs, while the weakly bound ligands are held near the NC surface by the electric field exerted by the charged facets.

Surface ligand alters the absolute energy levels of NCs electronic states.[16, 18-19] This energy change has an electrostatic origin. Electric dipoles are created by surface-bound ligand. The electric field potential shifts all energy levels down if dipoles are oriented towards the NC centre, and vice versa if they are not. The orientation and the magnitude of a surface dipole is the contribution of interfacial dipole (associated with surface atom and ligand head group) and intrinsic dipole (associated with ligand molecular structure).[20] Electric field dynamics at a metal-semiconductor interface and characterisation of the semiconductor interface has been reported using the second harmonic generation.[21-22] Interfacial electric field at Au/SAM interfaces reported using vibrational stark spectroscopy.[23] A substantial amount of research in both electrochemistry and surface science has been done on the electrical double layer (EDL), an extremely crucial interfacial area involved in many electrochemical reactions, and short ligand capped NCs stabilization in polar solvents. However, it is difficult to directly measure interfacial electric fields in the EDL. Electric field distributions in the double layer of a single-crystal electrode has been probed using Raman spectroscopy.[24]

The electric field strength across the electric double layer of electrode-electrolyte interfaces has been reported.[25] Observation of an electric field within the diffuse double-layer at SAM-modified Ag electrode surfaces has been investigated.[26] Like, electrode colloidal NCs are not static, they possess Brownian movement all the time. In this case, the entire ensemble of each NCs with its electric double layer moves throughout the sample under the Brownian movement. Due to this Brownian motion, measuring the electric field experienced by short ligands in EDL is quite challenging. The effect of the surface electric field of NCs on the weakly interacting ligand (present in EDL) is not reported yet.

In this study, we have explored the effect of the core size of CdSe NCs on the orientation of SCN^- ions in the electrical double layer using polarization-selective ultrafast pump-probe spectroscopy. The pump-probe spectroscopy measures the population decay as a function of time for parallel and perpendicular polarizations, providing valuable information about the local environment and the orientation of probes.[27-28] The replacement of bulky hydrocarbon surface ligands with SCN^- ions as short inorganic ligands allows us to conduct label-free experiments, avoiding the need for external probes that may perturb the systems equilibrium. The unique properties of SCN^- ions, such as a strong extinction coefficient, good vibrational lifetime, and short linear structure, make them ideal vibrational reporters for time-resolved spectroscopic investigations.[17, 29-32]

5.2 Materials and Method

5.2.1 Chemicals

Cadmium oxide (CdO, 99.5%), Trioctylphosphine oxide (TOPO, 99%), Trioctylphosphine (TOP,90%), 1-octadecene (ODE, 90%), Oleic acid (90%), Selenium powder mesh (99.99%), Octaadecylamine (ODA, >95%), toluene, hexane, methanol, acetone chloropropanethiol (CPT).

5.2.2 CdSe nanocrystals synthesis

Synthesis method for CdSe NCs is same as reported in previous chapter. For three different size synthesis ODE volume changed. For smaller size 14-15 mL ODE used and for bigger size around 10-12 mL ODE used as solvent. As, High concentration of precursors, more nuclei and faster growth as they are closer to each other. The reaction was monitored with time using absorbance or PL and quenched reaction after getting desired size. Final nanocrystal size determined by HRTEM analysis.

5.2.3 Ligand Exchange

The ligand exchange procedure was performed using the method reported in previous chapter. For all three sizes of CdSe NCs ligand exchange method is same.

5.2.4 IR spectroscopy

IR absorption spectra was measured at room temperature on a Bruker Vertex 70 FTIR spectrometer. For each sample, ~90 μL of the sample solution was loaded into a demountable cell consisting of two windows (CaF_2, 3 mm thickness) separated by a mylar spacer of 100 μm thickness. Same sample cell used for pump-probe experiments.

5.2.5 Pump- probe spectroscopy

Pump probe data acquired by using same laser setup. The time delay between pump and probe was controlled by motorised delay stage present in pump path. Parallel and perpendicular polarization controlled by polarizer and half wave plate.

5.3 Results and discussion

In this work, we prepared CdSe NCs of three different sizes using a synthesis method reported by Peng with some modifications.[33] Detailed procedure of synthesis has been given in materials and method section. After synthesis of CdSe NCs due to hydrophobic bulky surface ligands shows good stability in non-polar solvents like hexane. Exchange of bulky insulating ligands with short, compact and conductive inorganic ligands is a pivotal step in solution phase ligand exchange for inorganic ligand covered NCs. This method is extremely popular due to its robustness for preparing highly concentrated NCs ink along with complete removal of initial ligands and providing a homogeneous ligand coverage to the NCs surface.[34] The solution phase ligand exchange did similarly as reported by the Kagan group, using ammonium thiocyanate as a short inorganic ligand and finally dispersed in DMF. Figure 5.1a represents the absorption spectrum before and after ligand exchange for three different diameters of NCs, which shows that excitonic features remain the same after ligand exchange. In each size of CdSe NCs the excitonic features remain the same after ligand exchange. Normalized UV–vis spectra of the CdSe NCs with three different diameters shown in figure 5.1 b.

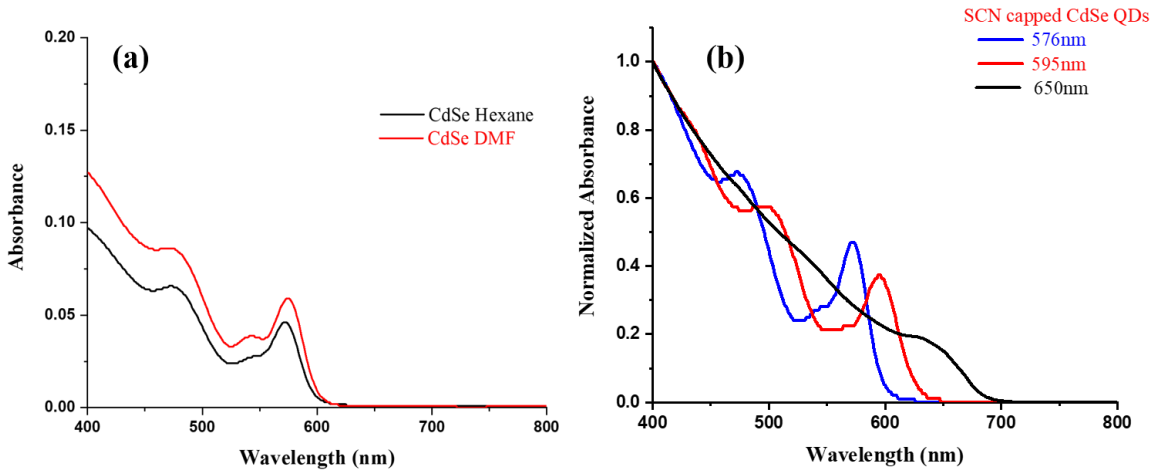

Figure 5.1 (a) UV–vis spectra of the CdSe NCs dispersed in hexane (before exchange) and DMF (after exchange) solutions. (b) Normalized UV–vis spectra of the CdSe NCs with three different diameters. The diameters of the CdSe NCs were determined to be 3.6 nm (576 nm), 4.3 nm (595 nm), and 7.7 nm (650 nm).

The XRD pattern and particle size distribution reported in Figure 5.2 (a). XRD pattern represent the (111), (220) and (311) planes, which is the characteristic signature of are cubic zinc blend crystal structure.[35] High intense (111) facet indicate cation rich plane. The particle size distribution for the UV-vis spectrum of 576, 595 and 650 nm is 3.6, 4.3 and 7.7 nm calculated from HRTEM images and the size distribution of CdSe NCs is relatively narrow. Figure 5.3(d,e,f)

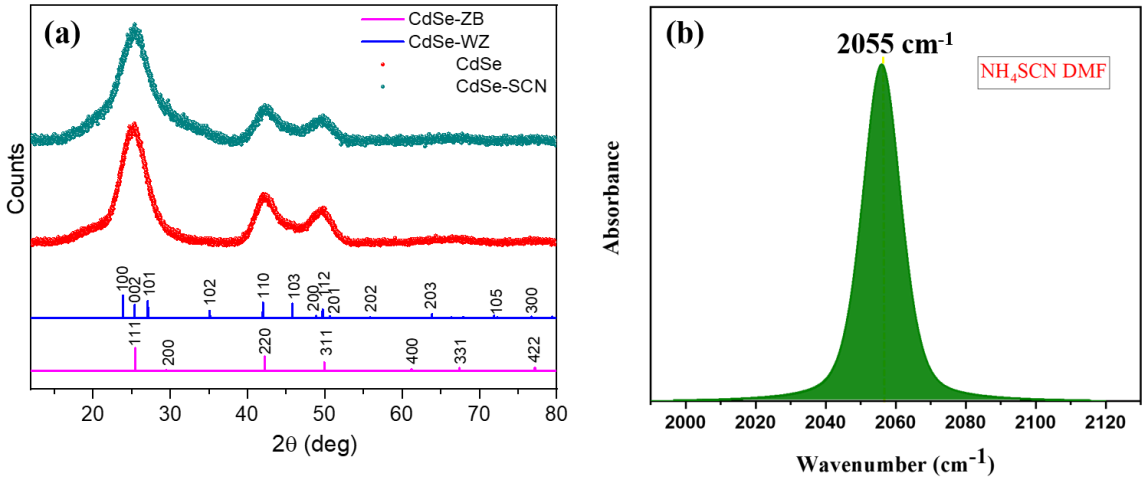

Figure 5.2 (a) XRD pattern of the CdSe NCs (b) only NH_4SCN in DMF.

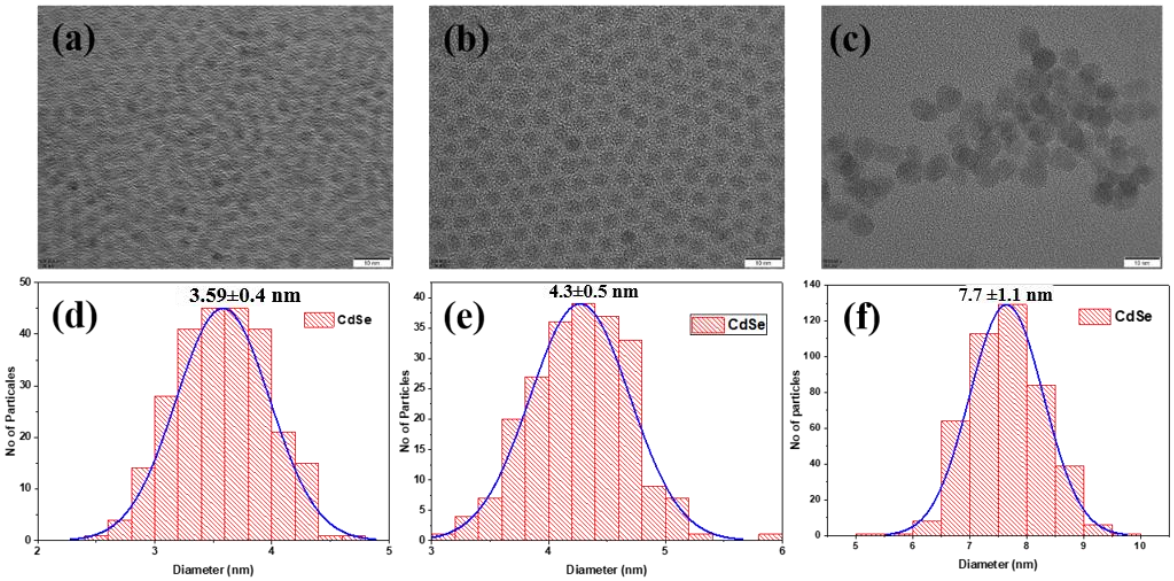

Figure 5.3 HRTEM images of CdSe NCs with the UV-Vis absorption wavelength at (a) 576 nm, (b) 595 nm and (c) 650 nm. Size distributions of the CdSe NCs from the HRTEM results with typical diameters at (d) 3.6 nm, (e) 4.3 nm and (f) 7.7 nm.

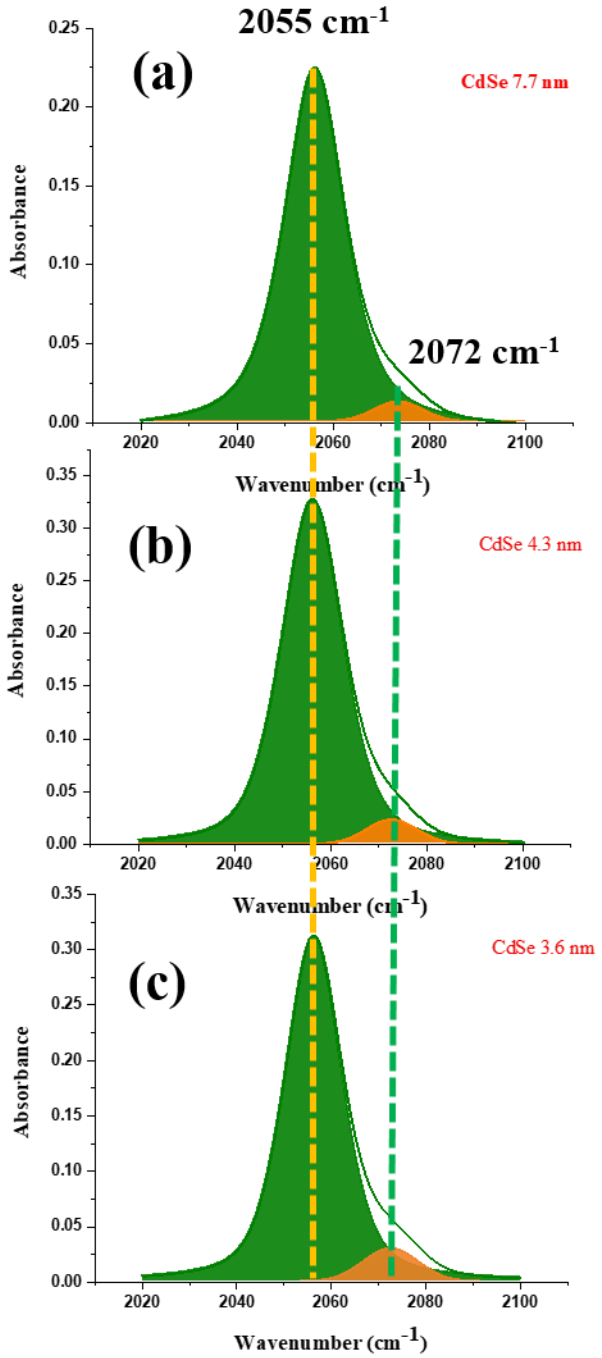

Figure 5.4 FTIR spectrum of SCN capped CdSe NCs (a) 7.7 nm (b) 4.3 nm and (c) 3.6 nm.

The FTIR spectrum of thiocyanate capped CdSe NCs dispersed in DMF with different core diameters is shown in Figure 5.4. Only NH_4SCN in DMF is also shown in Figure 5.2 (b). The

FTIR spectrum shows an asymmetric peak having a tail at the higher wavenumber. FTIR peak frequency at 2055 cm^{-1} represents free SCN^- ions, which agree with previous reports.[28, 36] However, the 2072 cm^{-1} peak corresponds to the surface bound thiocyanate ions. It is well known that CN stretching frequency shows blue shift in bound state compared to that of the unbound state.[36-37] SCN^- ions have the possibility to bind through S or N terminal. The Tetrathiocyanatocadmate (II) complex in DMF and DMSO prefers N end binding over S end due to different solvation capacities at each end of SCN^- ions.[38] In Chapter 3, we discussed that in thiocyanate capped CdS NCs ligands bind through N end by using quantum chemical calculation. The peak at 2055 cm^{-1} in each NCs has higher FWHM compared to only NH_4SCN in DMF (Table 5.1). This broadening is due to a weakly interacting ligand with, NCs surface this observation we explained in the previous article. The NCs core diameter do not affect the CN stretch at 2055 cm^{-1} and 2072 cm^{-1}. These results are in agreement with the thiocyanate capped ZnSe NCs where the diameter of NCs does not affect bound and free peaks positions.[28]

Table 5.1 FTIR peak positions and FWHM of three size of SCN capped CdSe NCs

system	FTIR peak position (cm^{-1})	FWHM (cm^{-1})
NH_4SCN in DMF	2055.6	13.50
CdSe-SCN 3.6 nm	2055.6	16.40
CdSe-SCN 4.3 nm	2055.6	16.42
CdSe-SCN 7.7 nm	2055.7	16.39

Here, we are interested in the orientation dynamics of weakly interacting SCN ions with the surface of NCs with different NCs diameters. This population is present in 2055 cm^{-1} peak. This subpopulation can't be resolved by free SCN^- ions due to solvent separated and free ions have

similar vibrational stretch.[36, 39] For weakly interacting species, solvent molecules are presents between ions and NCs surfaces which mimic the solvent separated ion pair scenario. As a result, these two have a similar vibrational frequency (2055 cm^{-1}). We did not consider the bound population for this report. However, rotational dynamics of the SCN bound population in ZnSe with three different diameters has been revealed by the Bain group.[28] Here, anisotropy decay of weakly interacting thiocyanate ions for three NCs is determined by polarization selective pump probe spectroscopy. It reports the orientation dynamics of thiocyanate ions with varying CdSe NCs diameters. For pump probe spectroscopy, parallel $I_{\parallel}$(t) and perpendicular $I_{\perp}$(t) signals can be expressed using the following equations

$$I_{\parallel}(t) = P(t)[1 + 0.8C_2(t)] \quad (1)$$

$$I_{\perp}(t) = P(t)[1 - 0.4C_2(t)] \quad (2)$$

where P(t) is the isotropic pump−probe decay and C_2(t) is the second-order Legendre polynomial orientation correlation function of the transition dipole moment.

By using Eqs. 1 and 2, we get

$$[I_{\parallel}(t) + 2I_{\perp}(t)] = 3P(t) \quad (3)$$

$$[I_{\parallel}(t) - I_{\perp}(t)] = 1.2P(t)C_2(t) \quad (4)$$

Anisotropy $r(t)$ can subsequently obtained from Eqs. 3 and 4

$$r(t) = \frac{I_{\parallel}(t) - I_{\perp}(t)}{I_{\parallel}(t) + 2I_{\perp}(t)} = 0.4\, C_2(t) \quad (5)$$

$C_2(t)$ is orientational correlation function. At t=0 anisotropy value starts from 0.4, However drop from 0.4 is due to inertial motions happens on a faster time scale than the temporal resolution of laser pulses that cannot capture. Figure 5.5 represent the normalized anisotropy decay of weakly interacting ligands for three different CdSe NCs.

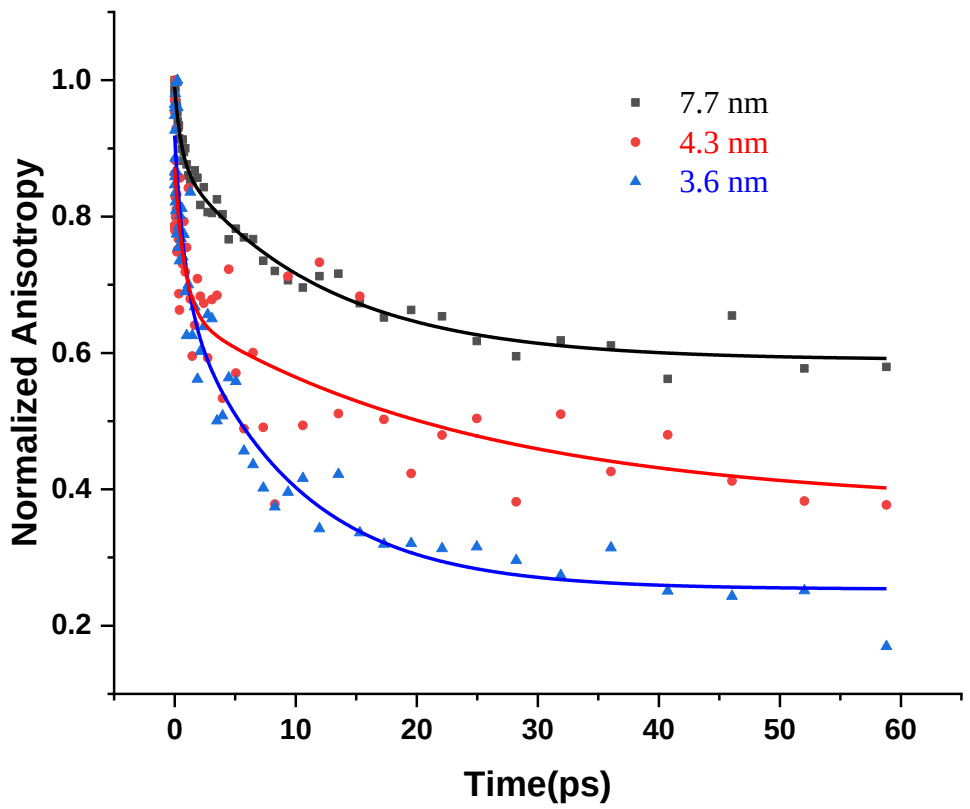

Figure 5.5 Rotational anisotropy decay of the SCN ligands with different CdSe NCs diameters.

Anisotropy decay of SCN ligands in an electric double layer is reported using a biexponential decay function. Bi-exponential decays fitting parameter given in table 5.2. Interestingly, with increasing the core diameter, the offset of bi-exponential fit increases. If the vibrational probe is present in zero electric field environments, then there is no directional orientation of the probe and at sufficient time delay it will complete its orientation and anisotropy decays gradually to zero. In the case of non-zero electric field a probe molecules try to orient towards the direction of the field and it unable to complete its orientation even at long time. In this scenario, we have static offset.

Table 5.2 Fitting results for the anisotropy decay of the SCN in three different sizes of CdSe NC

CdSe (nm)	a_1	a_2	τ_1 (ps)	τ_2 (ps)	y_0
3.6	0.22±0.06	0.43±0.06	0.84±0.42	9.3±2	0.25 ±0.020
4.3	0.21±0.04	0.28±0.04	0.82±0.40	24.3±7	0.37 ±0.003
7.7	0.11±0.01	0.28±0.01	0.567±0.12	12.17±1.2	0.58 ±0.008

In stronger electric fields, anisotropy decay has significant offset and never decay zero within the experimental time window.[40] The same situation is present in thiocyanate capped CdSe NCs with different diameters. The weakly interacting ligands stay away from the NCs surface. The cationic Cd rich facet (111) of CdSe exerts the electric field.

Our results indicate that the electric field experienced by ligands further away from the surface is stronger for in larger sized NCs, as compared to the small sized ones. This scenario is counterintuitive as the charge density of the NCs decrease with the increase in NC size. However, our results can be rationalized when the size-dependent surface curvature of the NCs are considered. The smaller sized NCs have a larger curvature. Therefore, the adjacent ligands are at a larger angle between one another, thereby reducing the steric and electronic repulsion. This allows a larger surface coverage of the bound ligands which shield the electric field to a larger extent from the weakly bound layer. In the case of larger NCs, ligands get a flatter surface for binding and a large number of ligands create the electronic repulsion with each other, which affects the shielding layer of ligand at the NCs surface. Therefore, larger NCs have an ineffective shielding layer of bound thiocyanate ligands which is observed in the experimental trends.

We have also measure the zeta-potential for the three different sizes of thiocyanate capped CdSe NCs. The zeta potential of inorganic ligand-passivated nanocrystals can vary as a function of their core size. However, it is important to note that the specific relationship between zeta potential and core size can be influenced by various factors, including the type of nano crystal, the ligand used for passivation, and the surrounding medium. Here we the core size of CdSe NCs change, other things, like ligand and solvent is same. Zeta potential is the electrical potential at the slipping plane. In other words, this plane represents the boundary or surface that divides the fluid that can move freely (mobile fluid) from the fluid that adheres or remains attached to the surface (bound fluid).

Table 5.3 Zeta potential value for three different size NCs

CdSe NCs size (nm)	Zeta potential value (mV)
3.6	-16.62
4.3	-20.00
7.7	-32.29

With increase in size of CdSe NCs observed zeta potential value also increases respectively (Table 5.3). Which show the similar trend observed in our results. For small NCs surface charge is more shielded as results zeta potential value is less, however for the large NCs the shielding is weak showing the higher value of zeta potential.

5.4 Conclusion

This chapter explains that ultrafast pump-probe spectroscopy can directly monitor the orientational dynamics of electrostatic interaction of inorganic ligands with NCs surface as a function of the NCs diameter. In thiocyanate-capped CdSe NCs the electrostatic interaction becomes stronger with the increase in the diameter of NCs. These results provide a molecular level understanding of the interactions of the SCN^- ligands with the NCs.

5.5 References

1. Wilkes, J. S.; Zaworotko, M. J., Air and Water Stable 1-Ethyl-3-methylimidazolium Based Ionic Liquids. *J. Chem. Soc., Chem. Commun.* **1992,** *13*, 965.
2. Konstantatos, G.; Howard, I.; Fischer, A.; Hoogland, S.; Clifford, J.; Klem, E.; Levina, L.; Sargent, E. H., Ultrasensitive solution-cast quantum dot photodetectors. *Nature. 2006 Jul 13;442(7099):180-3. doi: 10.1038/nature04855.*
3. Kovalenko, M. V.; Manna, L.; Cabot, A.; Hens, Z.; Talapin, D. V.; Kagan, C. R.; Klimov, V. I.; Rogach, A. L.; Reiss, P.; Milliron, D. J.; Guyot-Sionnnest, P.; Konstantatos, G.; Parak, W. J.; Hyeon, T.; Korgel, B. A.; Murray, C. B.; Heiss, W., Prospects of Nanoscience with Nanocrystals. *ACS Nano 9* (2), 1012-1057.
4. Talapin, D. V.; Lee, J.-S.; Kovalenko, M. V.; Shevchenko, E. V., Prospects of Colloidal Nanocrystals for Electronic and Optoelectronic Applications. *Chemical Reviews 110* (1), 389-458.
5. Gao, X.; Cui, Y.; Levenson, R. M.; Chung, L. W. K.; Nie, S., In vivo cancer targeting and imaging with semiconductor quantum dots. *Nature Biotechnology* **2004,** *22* (8), 969-976.
6. Howes, P. D.; Chandrawati, R.; Stevens, M. M., Colloidal nanoparticles as advanced biological sensors. *Science 346* (6205), 1247390.
7. Bell, A. T., The Impact of Nanoscience on Heterogeneous Catalysis. *Science* **2003,** *299* (5613), 1688-1691.
8. Jasieniak, J.; Smith, L.; van Embden, J.; Mulvaney, P.; Califano, M., Re-examination of the Size-Dependent Absorption Properties of CdSe Quantum Dots. *J. Phys. Chem. C* **2009,** *113*, 19468-19474.
9. Ben-Shahar, Y.; Stone, D.; Banin, U., Rich Landscape of Colloidal Semiconductor–Metal Hybrid Nanostructures: Synthesis, Synergetic Characteristics, and Emerging Applications. *Chem. Rev.* **2023,** *123*, 3790-3851.
10. Heuer-Jungemann, A.; Feliu, N.; Bakaimi, I.; Hamaly, M.; Alkilany, A.; Chakraborty, I.; Masood, A.; Casula, M. F.; Kostopoulou, A.; Oh, E.; Susumu, K.; Stewart, M. H.; Medintz, I. L.; Stratakis, E.; Parak, W. J.; Kanaras, A. G., The Role of Ligands in the Chemical Synthesis and Applications of Inorganic Nanoparticles. *Chem. Rev.* **2019,** *119*, 4819-4880.
11. Baig, N.; Kammakakam, I.; Falath, W., Nanomaterials: a review of synthesis methods, properties, recent progress, and challenges. *Mater. Adv.* **2021,** *2*, 1821-1871.
12. Pang, Z.; Zhang, J.; Cao, W.; Kong, X.; Peng, X., Partitioning surface ligands on nanocrystals for maximal solubility. *Nat Commun* **2019,** *10*, 2454.

13. Giansante, C., Library Design of Ligands at the Surface of Colloidal Nanocrystals. *Acc. Chem. Res.* **2020,** *53*, 1458-1467.
14. Fafarman, A. T.; Koh, W.-k.; Diroll, B. T.; Kim, D. K.; Ko, D.-K.; Oh, S. J.; Ye, X.; Doan-Nguyen, V.; Crump, M. R.; Reifsnyder, D. C.; Murray, C. B.; Kagan, C. R., Thiocyanate-Capped Nanocrystal Colloids: Vibrational Reporter of Surface Chemistry and Solution-Based Route to Enhanced Coupling in Nanocrystal Solids. *Journal of the American Chemical Society 133* (39), 15753-15761.
15. Zhang, H.; Jang, J.; Liu, W.; Talapin, D. V., Colloidal Nanocrystals with Inorganic Halide, Pseudohalide, and Halometallate Ligands. *ACS Nano 8* (7), 7359-7369.
16. Boles, M. A.; Ling, D.; Hyeon, T.; Talapin, D. V., The surface science of nanocrystals. *Nature Materials 15* (2), 141-153.
17. Deshmukh, S. H.; Chatterjee, S.; Ghosh, D.; Bagchi, S., Ligand Dynamics Time Scales Identify the Surface–Ligand Interactions in Thiocyanate-Capped Cadmium Sulfide Nanocrystals. *J. Phys. Chem. Lett.* **2022,** *13*, 3059-3065.
18. Luo, M.-Y.; Tang, B.; Liu, A.-A.; Zhao, J.-Y.; Zhang, Z.-L.; Pang, D.-W., A robust and unique approach for tuning the energy level of Ag2Se quantum dots via “on-surface” manipulation of nitrogen-containing groups of surface-coordinated ligands. *Nano Research* **2023**.
19. Owen, J., Nanocrystal structure. The coordination chemistry of nanocrystal surfaces. *Science. 2015 Feb 6;347(6222):615-6. doi: 10.1126/science.1259924.*
20. Brown, P. R.; Kim, D.; Lunt, R. R.; Zhao, N.; Bawendi, M. G.; Grossman, J. C.; Bulović, V., Energy Level Modification in Lead Sulfide Quantum Dot Thin Films through Ligand Exchange. *ACS Nano* **2014,** *8*, 5863-5872.
21. de Jong, W.; van Etteger, A. F.; van 't Hof, C. A.; van Hall, P. J.; Rasing, T., Electric field dynamics at a metal-semiconductor interface probed by femtosecond optical second harmonic generation. *Surface Science* **1995,** *331-333*, 1372-1376.
22. Lüpke, G., Characterization of semiconductor interfaces by second-harmonic generation. *Surface Science Reports* **1999,** *35* (3-4), 75-161.
23. Staffa, J. K.; Lorenz, L.; Stolarski, M.; Murgida, D. H.; Zebger, I.; Utesch, T.; Kozuch, J.; Hildebrandt, P., Determination of the Local Electric Field at Au/SAM Interfaces Using the Vibrational Stark Effect. *J. Phys. Chem. C* **2017,** *121*, 22274-22285.
24. Wen, B.-Y.; Lin, J.-S.; Zhang, Y.-J.; Radjenovic, P. M.; Zhang, X.-G.; Tian, Z.-Q.; Li, J.-F., Probing electric field distributions in the double layer of a single-crystal electrode with angstrom spatial resolution using Raman spectroscopy. *J. Am. Chem. Soc* **2020,** *142*, 11698-11702.
25. Bhattacharyya, D.; Videla, P. E.; Palasz, J. M.; Tangen, I.; Meng, J.; Kubiak, C. P.; Batista, V. S.; Lian, T., Sub-nanometer mapping of the interfacial electric field profile using a vibrational stark shift ruler. *J. Am. Chem. Soc.* **2022,** *144*, 14330-14338.
26. Oklejas, V.; Sjostrom, C.; Harris, J. M., SERS detection of the vibrational stark effect from nitrile-terminated SAMs to probe electric fields in the diffuse double-layer. *J. Am. Chem. Soc.* **2002,** *124*, 2408-2409.
27. Weng, W.; Weberg, A. B.; Gera, R.; Tomson, N. C.; Anna, J. M., Probing Ligand Effects on the Ultrafast Dynamics of Copper Complexes via Midinfrared Pump–Probe and 2DIR Spectroscopies. *J. Phys. Chem. B* **2021,** *125* (44), 12228-12241.

28. Hao, H.; Ai, J.; Shi, C.; Zhou, D.; Meng, L.; Bian, H.; Fang, Y., Structural Dynamics of Short Ligands on the Surface of ZnSe Semiconductor Nanocrystals. *J. Phys. Chem. Lett.* **2022,** *13*, 3158-3164.
29. Bian, H.; Chen, H.; Zhang, Q.; Li, J.; Wen, X.; Zhuang, W.; Zheng, J., Cation Effects on Rotational Dynamics of Anions and Water Molecules in Alkali (Li+, Na+, K+, Cs+) Thiocyanate (SCNâ€“) Aqueous Solutions. *The Journal of Physical Chemistry B 117* (26), 7972-7984.
30. Pienpinijtham, P.; Han, X. X.; Ekgasit, S.; Ozaki, Y., Highly Sensitive and Selective Determination of Iodide and Thiocyanate Concentrations Using Surface-Enhanced Raman Scattering of Starch-Reduced Gold Nanoparticles. *Analytical Chemistry 83* (10), 3655-3662.
31. Ren, Z.; Brinzer, T.; Dutta, S.; Garrett-Roe, S., Thiocyanate as a Local Probe of Ultrafast Structure and Dynamics in Imidazolium-Based Ionic Liquids: Water-Induced Heterogeneity and Cation-Induced Ion Pairing. *The Journal of Physical Chemistry B 119* (13), 4699-4712.
32. Wang, Z.; Liu, T.; Long, X.; Li, Y.; Bai, F.; Yang, S., Understanding the Diverse Coordination Modes of Thiocyanate Anion on Solid Surfaces. *The Journal of Physical Chemistry C 123* (14), 9282-9291.
33. Qu, L.; Peng, X., Control of Photoluminescence Properties of CdSe Nanocrystals in Growth. *J. Am. Chem. Soc.* **2002,** *124*, 2049-2055.
34. Wang, W.; Zhang, M.; Pan, Z.; Biesold, G. M.; Liang, S.; Rao, H.; Lin, Z.; Zhong, X., Colloidal Inorganic Ligand-Capped Nanocrystals: Fundamentals, Status, and Insights into Advanced Functional Nanodevices. *Chem. Rev* **2022,** *122*, 4091-4162.
35. Liu, L.; Zhuang, Z.; Xie, T.; Wang, Y.-G.; Li, J.; Peng, Q.; Li, Y., Shape Control of CdSe Nanocrystals with Zinc Blende Structure. *J. Am. Chem. Soc.* **2009,** *131*, 16423-16429.
36. Lee, K.-K.; Park, K.-H.; Kwon, D.; Choi, J.-H.; Son, H.; Park, S.; Cho, M., Ion-pairing dynamics of Li+ and SCN− in dimethylformamide solution: Chemical exchange two-dimensional infrared spectroscopy. *J. Chem. Phys.* **2011,** *134*.
37. Deb, P.; Haldar, T.; Kashid, S. M.; Banerjee, S.; Chakrabarty, S.; Bagchi, S., Correlating Nitrile IR Frequencies to Local Electrostatics Quantifies Noncovalent Interactions of Peptides and Proteins. *J. Phys. Chem. B* **2016,** *120*, 4034-4046.
38. Ohtaki, H., Structural studies on solvation and complexation of metal ions in nonaqueous solutions. *Pure&AppI. Chem.*, **1987,** *59*, 1143-1150.
39. Park, S.; Ji, M.; Gaffney, K. J., Ligand Exchange Dynamics in Aqueous Solution Studied with 2DIR Spectroscopy. *The Journal of Physical Chemistry B 114* (19), 6693-6702.
40. Ren, Z.; Garrett-Roe, S., Reorientation-induced spectral diffusion of non-isotropic orientation distributions. *J. Chem. Phys.* **2017,** *147*.

Chapter 6

Summary and Future Scope

6.1 Summary

Nanocrystals gain a tremendous amount of interest by industry and academia due to their size-dependent properties that range from optical to magnetic properties.[1-2] The surface modification of nanocrystals is becomes a subject of intense research interest given its importance for wide range of applications. The native organic ligands are routinely replaced with inorganic short ligands to maintain the desired distance for efficient charge transport.[3] The surface ligand interaction plays the key role in organic/inorganic capped nanocrystals to tune the optical and electronic properties of nanocrystlas. The understanding the surface chemistry of NCs for better optimization and efficiency improvement is a central need of today's world. Investigation of surface chemistry of organic capped ligands for a wide range of NCs with different NCs has been reported using NMR spectroscopy.[4-6] The understanding of the surface chemistry of inorganic capped ligands is not explored yet even though they are playing a pivotal role in optical and electronic technology due to unavailability of spectroscopic techniques.

In this thesis investigation of ligand-surface interaction of inorganic capped nanocrystals is reported using ultrafast 2D IR and pump-probe spectroscopy.

In chapter 3, we have investigated the ligand surface interaction in thiocyanate capped CdS nanocrystals using ultrafast 2D IR spectroscopy. As SCN^- is able to bind either S or N side to the surface of CdS, quantum chemical calculation and FTIR spectral shift reports the binding to the NCs surface through N end. Based upon the dynamical time scale of ligands, they are classified as strongly bound, weakly bound and free thiocyanate ligands. We create a model using these results which shows that the overall stability for NCs is provided by bound ligand, electrostatically interacting ligand (weak bound) and free ligands. These ligands are in dynamic

equilibrium with each other. However, the exchange time scale is higher than the NMR time scale and lower than the 2D IR time scale.

In chapter 4, electrostatically interacting ligands in thiocyanate capped nanocrystals are probed using polarization selective 2D IR spectroscopy. We choose CdS and CdSe as two different nanocrystals to observe electrostatic effects. Frequency- frequency correlation decay for parallel and perpendicular polarization is different, and it shows static offset for a long waiting time for both CdS and CdSe nanocrystals. This indicates the SCN^- ion provides the electrostatic stabilization to the nanocrystal. This study provides direct proof of the presence of electrostatically interacting ligands in inorganic capped nanocrystals.

Chapter 5 deals with the understanding the effect of an electric field extorted by the cationic facet of size-dependent CdSe nanocrystals on the reorientational dynamics of electrostatically interaction thiocyanate ligands in thiocyanate capped CdSe nanocrystals dispersed in polar solvent DMF. We use polarization selective pump probe spectroscopy for instigation of reorientational dynamics. Reorientation dynamics (anisotropy decay) show an increase in offset with the increase in NCs size. The slowing down of the reorientational dynamics indicates that the layer farther away from the NC surface experiences a larger electric field with increase of the NC size. This is counterintuitive when we consider the size-dependent charge density of the NCs. In this chapter, we have shown that ineffective shielding in larger NCs by the bound thiocyanate layer contributes to the experimentally observed trend.

6.2 Future Scope

6.2.1 Understanding the molecular level picture of azide (different inorganic ligand) capped nanocrystals.

For the specific application of NCs based devices, bulky insulating organic ligands are replaced by short ligands for the last two decades.[3, 7] These short ligands are halides, Psudohalides, chalcogenide, chalcogenidometallates.[3] All these ligands might binds to NCs by different coordination and geometry, however relative binding strength of these ligands could be different. How SCN^- ligands stabilize the CdS nanocrystals is revealed by 2D IR spectroscopy. Molecular level insights of SCN^- capped CdS NCs is, it stabilizes the NCs by direct binding to the cationic facet along with electrostatic interaction with the charged facet. Three different populations observed strongly bind, weakly bind and free. Surface capping ligands modify the optical and electronic properties of NCs, which is needed for specific applications. Azide is also a popular vibrational probe due to its clear spectral window, simple linear structure and as a result, it has been used as a vibrational reporter in many complex systems.[8-12] The azide is also used as a short inorganic ligand for surface capping of nanocrystals.[3] We will use azide capped NCs which will provides better understanding of molecular level insights of NCs surface ligand interface. This study will help to understand, modify and control the specific parameters for better applications.

6.2.2 Estimation of effect the organic and inorganic capped ligands on Cd nuclei of CdS and CdSe nanocrystals by Cd NMR spectroscopy.

In the modern world of technology, nanomaterial chemistry has gained much attention due to a use of nanocrystal-based technology in day to day life. To enhance the efficiency of energy-based devices, research labs are working continuously for molecular level understanding and modifying the size, shape and facets of NCs, changing the surface ligands and NCs. Surface

chemistry of different ligands of NCs is studied by many techniques.[13-15] How the NCs surface - ligand interface behaves with long bulky ligands and short ligands is known. The core of NCs has paramount importance in the NCs field and fundamental understanding of the core of cadmium nanocrystals has been reported using ^{113}Cd NMR spectroscopy.[16-18] The nanocrystals like CdSe, CdS and CdTe have been widely used NCs in many applications. We will use ^{113}Cd NMR for bulky organic capped NCs and short inorganic ligands to understand the effect of lignads on the surface and core of NCS. Understanding the changes in the core and surface by changing capping-ligand will help to stretch the working window of NCs-based technologies.

6.2.3 Probing the electric field exerted by size dependent NCs by 4 mercaptobenzonitrile (4MBN) as ligand and Vibrational reporter.

The surface of NCs is always an interesting part of nanomaterials chemistry. Surface of NCs gain special attention due to the high surface to volume ratio of NCs and understanding the surface nature of NCs becomes the igniting subject of the nanomaterial community. On the surface, NCs consist of different facets, which carry different charges. The charged surfaces of NCs, exerts the electric field to its surrounding environment. For short ligands, NCs sustain their colloidal stability due to electrostatic interaction of these short ligands with the electric field of their respective facet. Understanding the electric field effect created by the charged facet of NCs is very interesting, however, it is not explored yet. 4 mercaptobenzonitrile (4MBN) is widely used as a vibrational stark reporter, for change in the electric field of the surroundings by observing corresponding changes in CN stretch in many complex system.[19-21] Here, 4 mercaptobenzonitrile will play the dual role of vibrational reporter and capping ligands. This experiment will allow us

to conduct perturbation-free measurements. The external probe will not require an extrinsic vibrational signature of 4MBN ligand will provide information about the electric field. We will use different ligands along with 4MBN to reveal the electric field directed from the charged facet to its surroundings. The effects of electric fields will be monitored by changing the size/shape of NCs. In this work we will use FTIR, 2D IR and pump –probe spectroscopy.

6.3 References

1. Efros, A. L.; Brus, L. E., Nanocrystal Quantum Dots: From Discovery to Modern Development. *ACS Nano* **2021,** *15*, 6192-6210.
2. Baek, W.; Chang, H.; Bootharaju, M. S.; Kim, J. H.; Park, S.; Hyeon, T., Recent Advances and Prospects in Colloidal Nanomaterials. *JACS Au* **2021,** *1*, 1849-1859.
3. Zhang, H.; Jang, J.; Liu, W.; Talapin, D. V., Colloidal Nanocrystals with Inorganic Halide, Pseudohalide, and Halometallate Ligands. *ACS Nano* **2014,** *8*, 7359-7369.
4. Dhaene, E.; Coppenolle, S.; Deblock, L.; De Buysser, K.; De Roo, J., Binding Affinity of Monoalkyl Phosphinic Acid Ligands toward Nanocrystal Surfaces. *Chem. Mater.* **2023,** *35*, 558-569.
5. Kessler, M. L.; Dempsey, J. L., Mapping the Topology of PbS Nanocrystals through Displacement Isotherms of Surface-Bound Metal Oleate Complexes. *Chem. Mater.* **2020,** *32*, 2561-2571.
6. Hartley, C. L.; Kessler, M. L.; Dempsey, J. L., Molecular-Level Insight into Semiconductor Nanocrystal Surfaces. *J. Am. Chem. Soc.* **2021,** *143*, 1251-1266.
7. Fafarman, A. T.; Koh, W.-k.; Diroll, B. T.; Kim, D. K.; Ko, D.-K.; Oh, S. J.; Ye, X.; Doan-Nguyen, V.; Crump, M. R.; Reifsnyder, D. C.; Murray, C. B.; Kagan, C. R., Thiocyanate-Capped Nanocrystal Colloids: Vibrational Reporter of Surface Chemistry and Solution-Based Route to Enhanced Coupling in Nanocrystal Solids. *J. Am. Chem. Soc.* **2011,** *133*, 15753-15761.
8. Li, S.; Schmidt, J. R.; Piryatinski, A.; Lawrence, C. P.; Skinner, J. L., Vibrational Spectral Diffusion of Azide in Water. *J. Phys. Chem. B* **2006,** *110*, 18933-18938.
9. Sando, G. M.; Dahl, K.; Owrutsky, J. C., Vibrational Spectroscopy and Dynamics of Azide Ion in Ionic Liquid and Dimethyl Sulfoxide Water Mixtures. *J. Phys. Chem. B* **2007,** *111*, 4901-4909.
10. Lee, C.; Son, H.; Park, S., Effect of Hydrogen Bonds on the Vibrational Relaxation and Orientational Relaxation Dynamics of HN3 and N3– in Solutions. *J. Phys. Chem. B* **2016,** *120*, 9723-9731.
11. Weng, W.; Weberg, A. B.; Gera, R.; Tomson, N. C.; Anna, J. M., Probing Ligand Effects on the Ultrafast Dynamics of Copper Complexes via Midinfrared Pump–Probe and 2DIR Spectroscopies. *J. Phys. Chem. B* **2021,** *125* (44), 12228-12241.

12. Zhou, D.; Zhao, B.; Bai, Y.; Mukherjee, S.; Liu, J.; Bian, H.; Fang, Y., Exploring the Structure and Complexation Dynamics of Azide Anion Recognition by Calix[4]pyrroles in Solution. *J. Phys. Chem. Lett.* **2022,** *13*, 669-675.
13. De Roo, J.; Yazdani, N.; Drijvers, E.; Lauria, A.; Maes, J.; Owen, J. S.; Van Driessche, I.; Niederberger, M.; Wood, V.; Martins, J. C.; Infante, I.; Hens, Z., Probing Solvent–Ligand Interactions in Colloidal Nanocrystals by the NMR Line Broadening. *Chem. Mater.* **2018,** *30*, 5485-5492.
14. Deshmukh, S. H.; Chatterjee, S.; Ghosh, D.; Bagchi, S., Ligand Dynamics Time Scales Identify the Surface–Ligand Interactions in Thiocyanate-Capped Cadmium Sulfide Nanocrystals. *J. Phys. Chem. Lett.* **2022,** *13*, 3059-3065.
15. De Roo, J., The Surface Chemistry of Colloidal Nanocrystals Capped by Organic Ligands. *Chem. Mater.* **2023,** *35*, 3781-3792.
16. Blanc, F., CdSe Semiconductor Nanocrystals: The Surface and the Core. *ACS Cent. Sci.* **2018,** *4*, 1081-1083.
17. Xing, B.; Ge, S.; Zhao, J.; Yang, H.; Song, J.; Geng, Y.; Qiao, Y.; Gu, L.; Han, P.; Ma, G., Alloyed Crystalline CdSe1-xSx Semiconductive Nanomaterials – A Solid State 113Cd NMR Study. *ChemistryOpen* **2020,** *9*, 1018-1026.
18. Hanrahan, M. P.; Chen, Y.; Blome-Fernández, R.; Stein, J. L.; Pach, G. F.; Adamson, M. A. S.; Neale, N. R.; Cossairt, B. M.; Vela, J.; Rossini, A. J., Probing the Surface Structure of Semiconductor Nanoparticles by DNP SENS with Dielectric Support Materials. *J. Am. Chem. Soc.* **2019,** *141*, 15532-15546.
19. Staffa, J. K.; Lorenz, L.; Stolarski, M.; Murgida, D. H.; Zebger, I.; Utesch, T.; Kozuch, J.; Hildebrandt, P., Determination of the Local Electric Field at Au/SAM Interfaces Using the Vibrational Stark Effect. *J. Phys. Chem. C* **2017,** *121*, 22274-22285.
20. Voegtle, M. J.; Pal, T.; Pennathur, A. K.; Menachekanian, S.; Patrow, J. G.; Sarkar, S.; Cui, Q.; Dawlaty, J. M., Interfacial Polarization and Ionic Structure at the Ionic Liquid–Metal Interface Studied by Vibrational Spectroscopy and Molecular Dynamics Simulations. *J. Phys. Chem. B* **2021,** *125*, 2741-2753.
21. Wright, D.; Sangtarash, S.; Mueller, N. S.; Lin, Q.; Sadeghi, H.; Baumberg, J. J., Vibrational Stark Effects: Ionic Influence on Local Fields. *J. Phys. Chem. Lett.* **2022,** *13* (22), 4905-4911.

ABSTRACT

Name of the Student: Samadhan Haridas Deshmukh **Registration No**.:10CC18A26005

Faculty of Study: Chemical Science **Year of Submission**: 2023

AcSIR academic centre/CSIR Lab: CSIR-National Chemical Laboratory, Pune

Name of the Supervisor: Dr. Sayan Bagchi

Title of the thesis: Revealing the molecular picture of surface-ligand interactions in thiocyanate-capped nanocrystals by 2D IR spectroscopy

---

Semiconducting nanocrystals (NCs) are gaining much interest due to their significant role for wide range of applications. Ample amounts of NCs are synthesized using different semiconducting materials. The optoelectronic properties of NCs can be tuned by changing the material, composition, size, shape and surface-covering ligands. Surface ligands are an integral component of nanocrystals, as they provide stability by preventing agglomeration and crystal defects. They also enable size and shape control during synthesis, which influences the properties of the nanocrystals. Surface ligands passivate the nanocrystal surface, enhancing electronic and optical properties. Additionally, they allow for solubility, dispersion, and biofunctionalization, making nanocrystals suitable for diverse applications such as drug delivery and bioimaging. Long bulky organic surface ligands are often replaced with short inorganic ligands, which enhance the electronic communication between the NCs. This ultimately increases the efficiency of these NC-based devices by many folds. However, simply creating more materials does not necessarily enhance our understanding of their unique physical properties and their role in optoelectronic devices. Despite our comprehensive knowledge of physical structure of NCs, the specific details regarding the interaction between ligands and the NCs surfaces have remained enigmatic, defying a clear understanding. This thesis employs a unique 2D IR spectroscopy method to reveal surface ligand interactions in thiocyanate-capped NCs. Due to the absence of hydrogen, ^{1}H NMR spectroscopy cannot be employed, and ^{13}C NMR spectroscopy does not provide any conclusive data. From dynamical viewpoint, the specific timescale of ligand dynamics provides information about the ligand subpopulation around the NCs. Surface ligands (vibrational probe) reorient and fluctuate in the surrounding environment, which can lead to the frequency evolution of the vibrational reporter. Polarization-selective 2D IR experiments selectively probe the electrostatically interacting ligands to the surface of NCs. Time-resolved polarization-selective pump-probe spectroscopy can differentiate the reorientation of weakly interacting ligands as a function of NC size. In a nutshell, this thesis provides a detailed report on the surface ligand interaction of thiocyanate-capped nanocrystals using time-resolved spectroscopic techniques. This molecular-level understanding will help to improve the device performance.

List of Publication(s) in SCI Journal(s) Emanating from the Thesis Work

1. **Samadhan H. Deshmukh,** Srijan Chatterjee, Deborin Ghosh* and Sayan Bagchi*, *Ligand Dynamics Time Scales Identify the Surface−Ligand Interactions in Thiocyanate-Capped Cadmium Sulfide Nanocrystals, J. Phys. Chem. Lett.*, 13, 3059 - 3065 (2022).

List of Publications Non-Emanating from the Thesis Work

1. Srijan Chatterjee, Deborin Ghosh, Tapas Haldar, Pranab Deb, Sushil S.Sakpal, **Samadhan H. Deshmukh,** Somnath M. Kashid* and Sayan Bagchi*, *Hydrocarbon Chain-Length Dependence of Solvation Dynamics in Alcohol-Based Deep Eutectic Solvents: A Two-Dimensional Infrared Spectroscopic Investigation, J. Phys. Chem. B.*, 123, 9355 – 9363 (2019).
2. Sushil S. Sakpal[#], **Samadhan H. Deshmukh**[#] , Srijan Chatterjee, Deborin Ghosh and Sayan Bagchi*, *Transition of a Deep Eutectic Solution to Aqueous Solution: A Dynamical Perspective of the Dissolved Solute, J. Phys. Chem. Lett.*, 12, 8784 - 8789 (2021). (**First equal author**)
3. Deborin Ghosh, Sushil S. Sakpal, Srijan Chatterjee, **Samadhan H. Deshmukh,** Hyejin Kwon , Yung Sam Kim* and Sayan Bagchi*, *Association–Dissociation Dynamics of Ionic Electrolytes in Low Dielectric Medium, J. Phys. Chem. B.*, 126, 239 - 248 (2022).
4. Suranjana Chakrabarty[#], **Samadhan H. Deshmukh**[#], Anjan Barman, Sayan Bagchi*, Anup Ghosh*, On–Off Infrared Absorption of the S═O Vibrational Probe of Dimethyl Sulfoxide, *J. Phys. Chem. B., 126*, 4501-4508 (2022) (**First equal author**)
5. Srijan Chatterjee*, **Samadhan H. Deshmukh** and Sayan Bagchi*, *Does Viscosity Drive the Dynamics in an Alcohol-Based Deep Eutectic Solvent, J. Phys. Chem. B.*, 126, 8331 - 8337 (2022).
6. Shivshankar Kore, **Samadhan H. Deshmukh**, Sushil S. Sakpal, Srijan Chatterjee, Atanu Das* and Sayan Bagchi*, *Elucidation of pH-Induced Protein Structural Changes: A Combined 2D IR and Computational Approach, Biochemistry*, 62, 451 - 461 (2023).

7. Shivshankar Kore, Rudhi Ranjan Sahoo , Binit Santra , Archishman Sarkar, Tubai Chowdhury, **Samadhan H. Deshmukh** ,Sulagna Hazarika ,Srijan Chatterjee*, Sayan Bagchi *, *Solvation structure and dynamics of a small ion in an organic electrolyte*, *J. Photochem. Photobiol. A: Chem.*, 440, 114666 (2023).
8. Tubai Chowdhury, Srijan Chatterjee, Samadhan H. Deshmukh, Sayan Bagchi *, *A Systematic Study on the Role of Hydrogen Bond Donors in Dictating the Dynamics of Choline-based Deep Eutectic Solvents.* (communicated)

Book Chapter

1. Deborin Ghosh, **Samadhan H. Deshmukh**, Srijan Chatterjee, Sushil S. Sakpal, Tapas Haldar, Ambuj Dhakad, Somnath M. Kashid, Sayan Bagchi*, *Two Dimensional Infrared Spectroscopy: A Structure Sensitive Technique with Ultrafast Time Resolution*; Modern Techniques of Spectroscopy. Progress in Optical Science and Photonics, vol 13. Springer, Singapore, 2021.

List of papers with abstract presented (oral or poster) at national or international conferences/seminars.

1. Oral Presentation in **"NCL Research Foundation"** organised by CSIR NCL pune. (2023)
2. Oral presentation in **"Chem-Dojo Conference 2022"** held at, Pune India and organised by the CSIR-NCL Pune, IIT Bombay and TIFR Mumbai.
3. Poster presentation in **"NCL Research Foundation"** organised by CSIR NCL pune. (2020)

THE JOURNAL OF PHYSICAL CHEMISTRY LETTERS
A JOURNAL OF THE AMERICAN CHEMICAL SOCIETY

pubs.acs.org/JPCL Letter

Ligand Dynamics Time Scales Identify the Surface–Ligand Interactions in Thiocyanate-Capped Cadmium Sulfide Nanocrystals

Samadhan H. Deshmukh, Srijan Chatterjee, Deborin Ghosh,* and Sayan Bagchi*

Cite This: *J. Phys. Chem. Lett.* 2022, 13, 3059–3065 Read Online

ACCESS | Metrics & More | Article Recommendations | Supporting Information

ABSTRACT: The nanocrystal surface, which acts as an interface between the semiconductor lattice and the capping ligands, plays a significant role in the attractive photophysical properties of semiconductor nanocrystals for use in a wide range of applications. Replacing the long-chain organic ligands with short inorganic variants improves the conductivity and carrier mobility of nanocrystal-based devices. However, our current understanding of the interactions between the inorganic ligands and the nanocrystals is obscure due to the lack of experiments to directly probe the inorganic ligands. Herein, using two-dimensional infrared spectroscopy, we show that the variations in the inorganic ligand dynamics within the heterogeneous nanocrystal ensemble can identify the diversities in the inorganic ligand–nanocrystal interactions. The ligand dynamics time scale in SCN^- capped CdS nanocrystals identifies three distinct ligand populations and provides molecular insight into the nanocrystal surface. Our results demonstrate that the SCN^- ligands engage in a dynamic equilibrium and stabilize the nanocrystals by neutralizing the surface charges through both direct binding and electrostatic interaction.

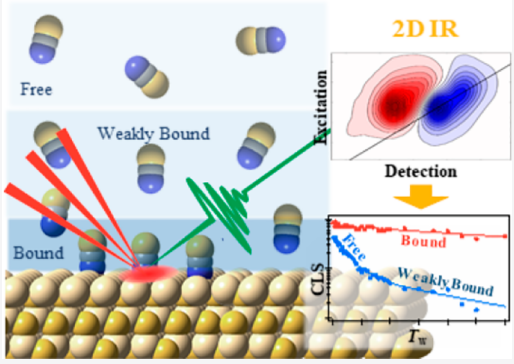

Semiconductor nanocrystals (NCs) are composed of a semiconductor lattice whose surface is passivated with molecular capping ligands. Selection of the capping ligands, semiconductor material, size, and dimension provides highly tunable optical and electronic properties of the NCs. These characteristics make the NCs an emerging class of building blocks in various optoelectronic, photovoltaic, photocatalytic, and biodiagnostic applications.[1−7] The last few decades have witnessed advances in controlling the reproducibility of size and shape dispersity in NC synthesis.[8] However, one of the most defining features of the properties and reactivity of the NCs is the surface, which acts as an interface between the semiconductor lattice and the capping ligands.[9] Unlike conventional molecules, heterogeneity exists across the surface of an individual NC. In addition, a dynamic equilibrium exists between the ligands bound to the NC surface and the free ligands in the surrounding media.[8,10] Detailed insight into the heterogeneity in ligand–NC interactions is essential to improve the current NC-based technologies.

Long-chain organic ligands are usually used for stabilizing NCs during their preparation. However, replacing the long-chain ligands with shorter variants improves the conductivity and carrier mobility, thereby increasing NC-based device performance.[11−14] In the past decade, solution-based ligand exchange has routinely been used to replace the long-chain organic ligands with the shorter inorganic variants (e.g., halides, pseudohalides, azides, halometalates).[15−17] Thiocyanate (SCN^-) ligand has been recently utilized to prepare colloidal quantum ink, which showed superior carrier mobility.[15] Despite the importance of the NC surface, the heterogeneous ligand–NC interactions are poorly understood due to a lack of molecular-level information.[8] ^{1}H NMR has recently been utilized for long-chain organic ligands (acids and thiolates) to distinguish between surface-bound and freely diffusing ligands.[8,9,18−23] However, ^{1}H NMR cannot be applied to short inorganic pseudohalide ligands like thiocyanates which are devoid of hydrogen atoms. The interactions of these short ligands at the NC surfaces have been qualitatively explained based on the hard and soft acids and bases (HSAB) principle.[9,16] However, a recent quantum chemical study has reported that the coordination of the SCN^- ligand only partly follows the HSAB principle, which cannot be generalized to inorganic solid materials.[24] Quantitative information on the binding modes and the coordination number of inorganic ligands is required to understand their influence on the NC properties.

The use of Fourier transform infrared (FTIR) and Raman spectroscopies has been reported to access purity, ligand identity, and static coordination environments at the NC surface.[15,21,25] Although most of the ligands (both long chain

Received: February 18, 2022
Accepted: March 25, 2022
Published: March 30, 2022

Downloaded via NATL CHEMICAL LABORATORY on July 18, 2023 at 09:21:45 (UTC).
See https://pubs.acs.org/sharingguidelines for options on how to legitimately share published articles.

ACS Publications © 2022 American Chemical Society

https://doi.org/10.1021/acs.jpclett.2c00493
J. Phys. Chem. Lett. 2022, 13, 3059−3065

acids and short pseudohalides) have distinct vibrational signatures, these steady-state vibrational techniques are most helpful in understanding ligand−NC interactions when used in complement with other experiments and quantum calculations. Beyond probing the static coordination environments, transient IR (TRIR) spectroscopy has been successfully used for the long-chain oleic acid ligands.[26,27] However, no time-resolved IR studies have been reported on the short inorganic variants. Among the available time-resolved IR methodologies, two-dimensional infrared (2D IR) spectroscopy provides a unique route to obtain an in-depth understanding of the inorganic ligand−NC interactions. A particular mode of ligand−NC interaction is manifested as a symmetric peak in the FTIR spectrum. Due to the inherent heterogeneity in the NC ensemble, subensembles exist within each absorption band. These subensembles exchange on specific time scales (spectral diffusion) depending on the strength of interaction of the ligand to the NC surface (Figure 1a). The stronger the ligand−NC interaction, the slower the time scale (Figure 1b). The changes in the 2D IR line shapes can directly provide the spectral diffusion time scales and identify the relative strength of the ligand−NC interaction. Herein, we successfully demonstrate that the ligand dynamics time scales obtained from 2D IR spectroscopy in SCN^- capped CdS NCs quantitatively distinguish three distinct inorganic ligand−NC interactions within the heterogeneous ensemble.

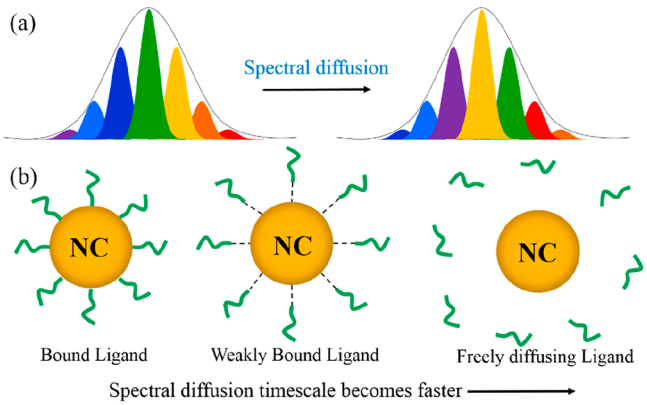

Figure 1. Schematic representations of (a) the exchanging heterogeneous subensembles (different colors) within a symmetric frequency distribution (solid black line representing an absorption band) leading to spectral diffusion and (b) the changes in the spectral diffusion time scales with variations in ligand−NC interactions.

For this work, oleic acid capped CdS NCs (CdS-OA) are synthesized with minor modifications to previously reported procedures.[28] CdS-OA in hexane is combined with a solution of ammonium thiocyanate (NH_4SCN) in DMF (detailed procedure in the Supporting Information) to exchange the organic ligands. After ligand exchange, ^1H NMR shows no characteristic peak for vinyl hydrogen of oleate around 5 to 6 ppm confirming full removal of oleate from the NCs surface (Figure S1). We choose the short SCN^- ligand because of its ability to form stable solution-phase NCs and its impressive electron mobility, which is required for optoelectronic applications.[15,29] Moreover, SCN^- is a highly sensitive local vibrational probe of the surface heterogeneity.[30,31] Figure 2a shows that the excitonic features of the CdS NCs were preserved after ligand exchange. The X-ray diffraction (XRD) pattern of the SCN^- capped CdS (CdS-SCN) was identical to that of CdS-OA (Figure 2b). HRTEM images of CdS NCs (Figure S2) before and after ligand exchange exhibit good crystallinity with well-defined lattice fringes. The size distributions of the NCs are shown in Figure 2c. In agreement with the previous literature, the fringe spacing and XRD correspond to (111), (220), and (311) planes of the zinc blend structure.[32] The XRD pattern reveals (111) to be the predominant facet.

The FTIR spectrum of the CdS-SCN in DMF shows an asymmetric peak in the CN stretch ($\bar{\nu}_{CN}$) region (Figure 2d) which could be fitted (Table S1) to two Gaussians centered at 2055 cm^{-1} ($\bar{\nu}_L$) and 2072 cm^{-1} ($\bar{\nu}_H$). The full width at half-maximum (fwhm) of the peaks at $\bar{\nu}_L$ and $\bar{\nu}_H$ are 16.5 and 14.6 cm^{-1}, respectively. In the absence of NCs, NH_4SCN shows a symmetric peak at 2055 cm^{-1} ($\bar{\nu}_F$) in DMF with a fwhm of 13.5 (Figures 2d). Previous studies of M^+SCN^- (M = Li^+, Na^+, Mg^{2+}) in different solvents reported a blue-shift in $\bar{\nu}_{CN}$ due to the formation of contact ion pairs.[33−38] Thus, the peaks at $\bar{\nu}_L$ and $\bar{\nu}_H$ in CdS-SCN can plausibly be assigned to the freely diffusing ligands and the ligands interacting with the NCs, respectively. However, these assignments based on peak positions are speculative. Further, it should be noted that although the presence of NCs makes the fwhm of the peak at $\bar{\nu}_L$ larger by 3 cm^{-1} than that of the peak at $\bar{\nu}_F$ (Table S1), the origin of this broadening cannot be explained from FTIR results.

We have acquired 2D IR spectra of CdS-SCN at different time delays (T_w) to obtain a detailed understanding of the ligand−NC interactions. A typical 2D IR spectrum consists of a peak pair corresponding to ground-state bleach and stimulated emission (blue peak, ν = 0 to ν = 1) and excited-state absorption (red peak, ν = 1 to ν = 2) separated by vibrational anharmonicity. The existence of multiple binding modes introduces multiple overlapping peak pairs (2D IR) in the spectra. The 2D IR spectrum shows two peak pairs (Figure 3, left column), with the blue peaks centered at frequencies corresponding to the FTIR peak positions ($\bar{\nu}_L$ and $\bar{\nu}_H$) and the red peaks shifted along the detection axis by the respective anharmonicities. The spectral diffusion (within each peak) lowers the diagonal tilt of the peaks with increasing T_w without changing the peak positions (white lines in Figure 3). The spectral diffusion time scales are quantified using center line slope (CLS) formalism where the inverse of the T_w-dependent white lines' slopes are fitted to exponential decays.[39] We have performed additional control experiments and analyses in the absence of NCs on NH_4SCN in DMF (Figure 3, right column).

The CLS of the peak at $\bar{\nu}_H$ fits well to a single exponential decay indicating that the spectral diffusion with this ligand population happens at a 114 ps time scale (Figure 4a). The CLS of the peak at $\bar{\nu}_L$ shows a biexponential decay, consisting of two decay time scales, 5 and 39 ps (Figure 4a). The faster (5 ps) time scale shows an excellent agreement with that obtained from the CLS of the peak ($\bar{\nu}_F$) in the absence of NCs, thereby confirming the existence of freely diffusing ligands. It is worth mentioning that the freely diffusing ligands can be paired with the NH_4^+ countercation. A previous study reported a much faster spectral diffusion in DMF (1 ps), albeit using transition metal carbonyl as the vibrational probe.[40] A future study involving variation in the cation size/charge density can provide a clearer picture. Direct binding to the NC surface should restrict the ligand movement and slow down the spectral diffusion. Thus, the slowest time scale corresponding

https://doi.org/10.1021/acs.jpclett.2c00493
J. Phys. Chem. Lett. 2022, 13, 3059−3065

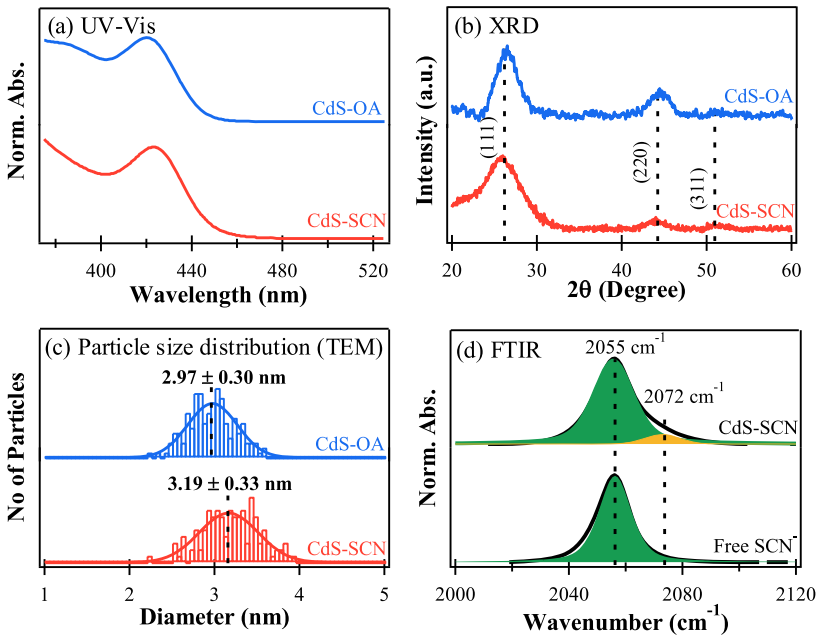

Figure 2. (a) UV−vis absorption spectra, (b) XRD patterns, and (c) particle size distributions obtained from HRTEM analysis of CdS NCs before (blue) and after (red) ligand exchange. (d) FTIR spectra of the nitrile stretch ($\bar{\nu}_{CN}$) of SCN^- in the presence (up) and absence (down) of NCs.

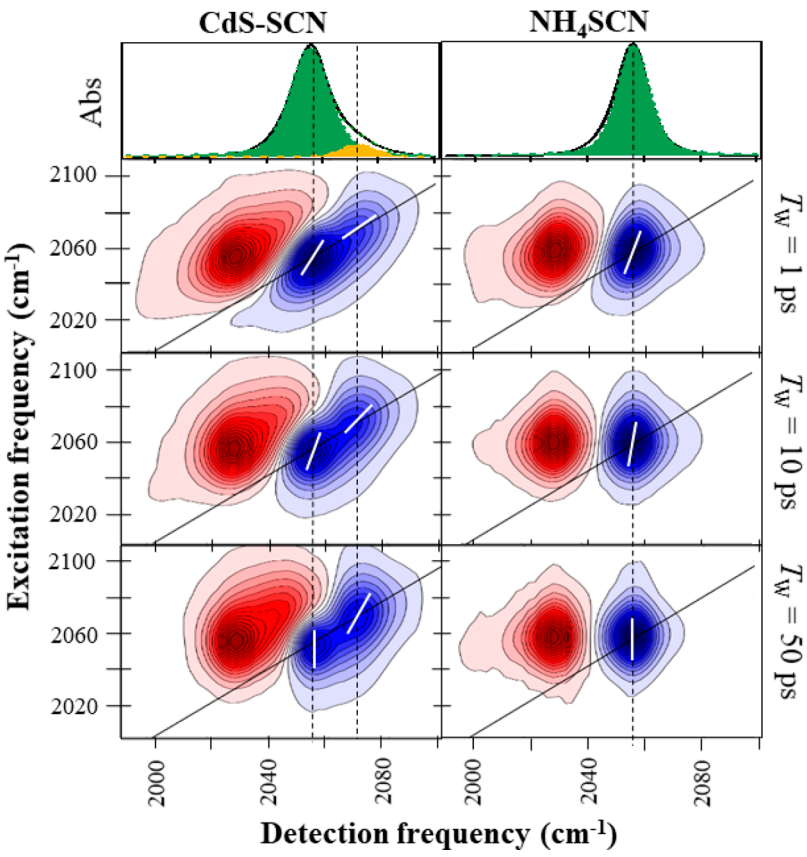

Figure 3. 2D IR spectra of CdS-SCN (left column) and NH_4SCN (right column) in DMF at three different waiting times (T_w). T_w increases from the top to the bottom along each column. FTIR spectra are shown at the respective top panels such that the peak positions of the FTIR and 2D IR spectra are vertically aligned.

to the peak at $\bar{\nu}_H$ arises due the strongly bound ligands. The negatively charged SCN^- likely binds (making X-type interaction) to the Cd-rich positively charged (111) surface, giving rise to this distinct ligand population. The intermediate time scale of 39 ps for the peak at $\bar{\nu}_L$ indicates a ligand population which is neither freely diffusing nor strongly bound to the NC surface. The ligand interacting weakly with the NCs would be less restricted than those bound strongly to the NCs

https://doi.org/10.1021/acs.jpclett.2c00493
J. Phys. Chem. Lett. 2022, 13, 3059−3065

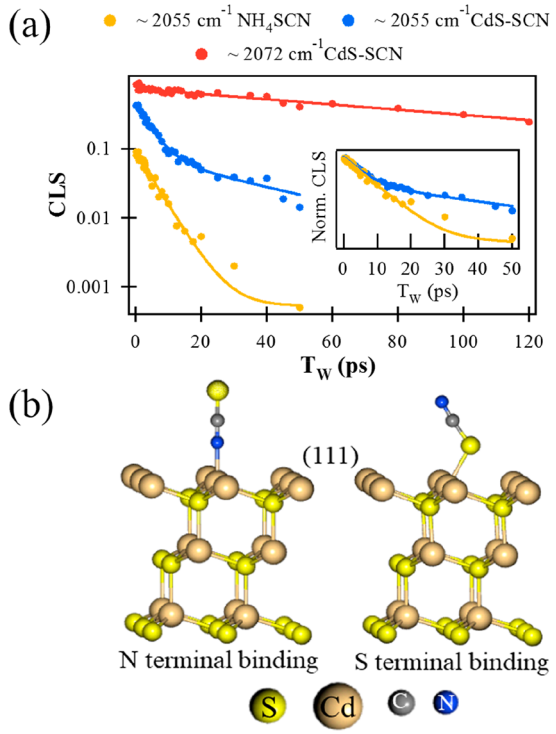

Figure 4. (a) T_w dependent CLS decays of the 2055 and 2072 cm^{-1} peaks of CdS-SCN are shown in blue and red, respectively. CLS decay of NH_4SCN (2055 cm^{-1}, yellow) has been appended for easy comparison with the blue decay. The *y*-axis is shown in log scale for clear visualization of the number of exponential decays. The inset represents the normalized CLS decays at 2055 cm^{-1} in the presence and absence of NCs. (b) Optimized slab structure of the N-terminated and S-terminated SCN^- capped (111) facet of the CdS crystal. We set $a = b = 8.40$ Å, $c = 60$ Å, and $\alpha = \beta = \gamma = 90°$ to construct the slab with chelating ligands. The vacuum spacing is about 45 Å, and thus the image effect is eliminated. The plane wave basis set is used with a kinetic energy cutoff of 25 Ry.

but would have slower dynamics than that of the freely diffusing ligands. The absorption of the weakly interacting ligands at a frequency similar to that of the freely diffusing ones makes these two ligand populations indistinguishable in the FTIR spectra. It has been previously reported that free thiocyanate anions cannot be spectrally distinguished from solvent separated ion pairs.[34,38] The only indication in the steady-state spectrum was the broadening of the peak at $\bar{\nu}_L$ as compared to that at $\bar{\nu}_F$. However, the ligand dynamics time scales obtained from 2D IR allows us to directly identify the variations in the ligand populations.

Interestingly, the freely diffusing ligands do not have any apparent interaction with the NCs, as indicated from the spectral diffusion time scales. We tried decreasing the ligand concentration during ligand exchange to remove the freely diffusing ligands. However, only a partial transfer of the NCs to the DMF phase was observed, which shows identical normalized FTIR spectra (Figure S3) irrespective of the ligand concentration. This result suggests that the free-diffusing ligands are an integral part of the heterogeneous NC system. A zeta potential value of −57.6 mV for CdS-SCN indicates that the ligands can provide electrostatic stabilization to the NCs. Our results demonstrate that the electrostatically bound ligands (39 ps time scale) are in dynamic equilibrium with the freely diffusing ligands (5 ps time scale). Thus, the free ligands could not be eliminated by reducing the ligand concentration during ligand exchange.

In addition to the distinct time scale upon binding to the NCs, the separation between the respective blue and red peaks (vibrational anharmonicity) for SCN^- is known to decrease with proximity to the cations.[41] The estimated anharmonicity (Table S1) is the lowest for the peak at $\bar{\nu}_H$, confirming that this peak arises from strongly bound ligands to the NCs. The anharmonicities of the weakly bound and the free ligands are the same, within the experimental error limit. Additional information is obtained from the amplitudes of the CLS decays (Figure 4a). Although the CLS value at $T_w = 0$ should be unity as no spectral diffusion is possible, it usually decreases from unity due to the presence of ultrafast homogeneous fluctuations. A larger decrease from unity at $T_w = 0$ indicates a larger homogeneous contribution to the line shape of the IR peak. It is intriguing to observe that the ultrafast fluctuations decrease with the increasing strength of ligand−NC interaction, thereby decreasing the homogeneous contribution to the IR line shape.

The ratio of the areas of the peaks at $\bar{\nu}_H$ and $\bar{\nu}_L$ is estimated to be 0.1 from the FTIR spectrum of CdS-SCN. In addition, the amplitudes of the biexponential CLS decay for the peak at $\bar{\nu}_L$ show that the weakly bound ligands contribute ∼20% while the rest comes from the freely diffusing ligands. Combining the two results, the population ratio of strongly bound ligands:weakly bound ligands:free ligands is estimated to be 1:2:7. A large fraction of free ligands is needed to stabilize the NCs as the free ligands are in dynamic equilibrium with both the strongly bound and the weakly interacting ligands. Although the IR spectra of CdS-SCN show two peaks arising from three overlapping transitions, a single peak in ^{13}C NMR[15] confirms the presence of a dynamic equilibrium between the three ligands populations. We therefore estimate a nanosecond time scale for the exchange process, i.e., faster than the NMR time scale and slower than picoseconds as no cross peaks from chemical exchange are seen up to 80 ps in 2D IR.

Although we have identified the strongly bound ligand population directly from the ligand dynamics time scales, the ambidentate SCN^- can bind to the positively charged (111) NC surface (X-type interaction) either through the sulfur (S) or the nitrogen (N) atom. Density functional theory (DFT) calculations on Cd^{2+}-SCN^- ion pairs (see Table S2 for calculated frequencies) predict a blue-shift in $\bar{\nu}_{CN}$ for SCN^- interacting with Cd^{2+} either through the S end or through the N end. To mimic the experimental condition, additional DFT calculations have been performed using Quantum-Expresso on the (111) facet of zinc-blende shaped CdS-NC. For simplification, a slab model has been used to optimize the NC structure.[42] PBE[43] was used as the exchange-correlation functional, and ultrasoft pseudopotentials[44] described the electron−ion interaction. Two different models considering the binding nature of SCN^- (S-bound and N-bound) have been constructed, and their optimized structures are presented in Figure 4b. Small fragments of the slabs were utilized to calculate the $\bar{\nu}_{CN}$ at the B3LYP/lanl2dz level of calculation with the Gaussian 16 package.[45] The calculated values of $\bar{\nu}_{CN}$ are presented in Table S2. A close resemblance of $\bar{\nu}_{CN}$ for the N-bound SCN^- (2079.36 cm^{-1}) to the (111) surface has been observed with an experimental band at 2072 cm^{-1}, indicating that the ligands are bound to the NC surface through the N atom, making an X type interaction with the (111) facet.

https://doi.org/10.1021/acs.jpclett.2c00493
J. Phys. Chem. Lett. 2022, 13, 3059−3065

Our results successfully demonstrate that the variations in the inorganic ligand−NC interactions at the NC surface can be successfully deciphered from the variations in the ligand dynamics (Figure 5). A unique spectral diffusion time scale,

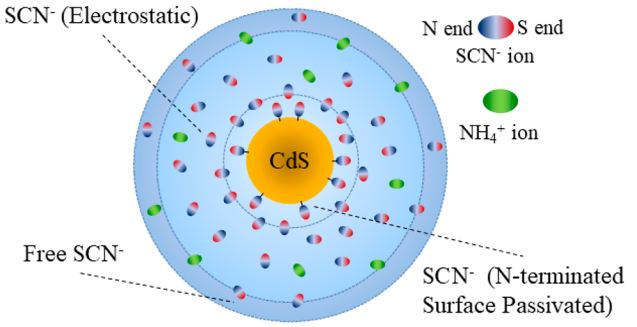

Figure 5. Schematic representation of different SCN^- populations in the CdS-SCN system.

associated with any ligand−NC interactions, depends on how strongly the ligand is interacting with the NC. A stronger interaction slows down the spectral diffusion such that the excitation and detection frequencies remain correlated for a longer time. We have identified three distinct populations of pseudohalide ligands—strongly bound, electrostatically interacting, and freely diffusing—in the CdS-SCN NCs. These ligand populations were found to be present in the NC system in the ratio 1:2:7. Furthermore, control experimental results indicate a dynamic equilibrium where all the three ligand populations exchange at nanosecond time scales. Interestingly, although the freely diffusing ligands do not apparently interact with NCs, the presence of the dynamic equilibrium between the various ligand populations make these free ligands an intrinsic part of the NC system. Results obtained from quantum chemical calculations show an excellent agreement with our 2D IR interpretations. In addition, the theoretical results indicate that the ambidentate SCN^- ligand binds through the N atom, making an X-type interaction with the NCs. This work demonstrates that 2D IR spectroscopy can directly provide a detailed molecular-level picture of how small inorganic ligands stabilize the NCs. In CdS-SCN, the stabilization of the NCs comes from passivating the surface charges through direct binding as well as electrostatic interaction. This study opens up a new avenue to investigate the interaction of small inorganic ligands with the NCs of varying shapes, sizes, and semiconductor materials.

■ ASSOCIATED CONTENT

Supporting Information

The Supporting Information is available free of charge at https://pubs.acs.org/doi/10.1021/acs.jpclett.2c00493.

Materials and methods, experimental details, material characterization of NCs (NMR and HR-TEM) and FTIR spectra, and results of quantum chemical calculations on NCs (PDF)

Transparent Peer Review report available (PDF)

■ AUTHOR INFORMATION

Corresponding Authors

Deborin Ghosh − *Physical and Materials Chemistry Division, National Chemical Laboratory (CSIR-NCL), Pune 411008, India*; Email: deborin88@gmail.com

Sayan Bagchi − *Physical and Materials Chemistry Division, National Chemical Laboratory (CSIR-NCL), Pune 411008, India; Academy of Scientific and Innovative Research (AcSIR), Ghaziabad 201002, India*; orcid.org/0000-0001-6932-3113; Email: s.bagchi@ncl.res.in

Authors

Samadhan H. Deshmukh − *Physical and Materials Chemistry Division, National Chemical Laboratory (CSIR-NCL), Pune 411008, India; Academy of Scientific and Innovative Research (AcSIR), Ghaziabad 201002, India*; orcid.org/0000-0002-0326-6125

Srijan Chatterjee − *Physical and Materials Chemistry Division, National Chemical Laboratory (CSIR-NCL), Pune 411008, India; Academy of Scientific and Innovative Research (AcSIR), Ghaziabad 201002, India*; orcid.org/0000-0001-9701-4158

Complete contact information is available at: https://pubs.acs.org/10.1021/acs.jpclett.2c00493

Notes

The authors declare no competing financial interest.

■ ACKNOWLEDGMENTS

S.B. thanks CSIR-NCL and SERB, India (EMR/2016/000576), for financial support. D.G. acknowledges SERB India (PDF/2018/000046) for financial support. The support and the resources provided by the "PARAM Brahma Facility" under the National Supercomputing Mission, Government of India, at the Indian Institute of Science Education and Research (IISER) Pune are gratefully acknowledge. S.H.D. acknowledges CSIR for a research fellowship. We would like to thank Dr. Arup Kumar Rath, Neha V. Dambhare, Debranjan Mandal, and Chandan Mahajan from CSIR-NCL, Pune, for their support in NC synthesis. We acknowledge Prof. Naresh Kumar Patwari from IIT Bombay for giving the access of Gaussian 16.

■ REFERENCES

(1) Gur, I.; Fromer, N. A.; Geier, M. L.; Alivisatos, A. P. Air-Stable All-Inorganic Nanocrystal Solar Cells Processed from Solution. *Science* **2005**, *310*, 462−465.

(2) Konstantatos, G.; Howard, I.; Fischer, A.; Hoogland, S.; Clifford, J.; Klem, E.; Levina, L.; Sargent, E. H. Ultrasensitive Solution-cast Quantum Dot Photodetectors. *Nature* **2006**, *442*, 180−183.

(3) Kovalenko, M. V.; Manna, L.; Cabot, A.; Hens, Z.; Talapin, D. V.; Kagan, C. R.; Klimov, V. I.; Rogach, A. L.; Reiss, P.; Milliron, D. J.; Guyot-Sionnnest, P.; Konstantatos, G.; Parak, W. J.; Hyeon, T.; Korgel, B. A.; Murray, C. B.; Heiss, W. Prospects of Nanoscience with Nanocrystals. *ACS Nano* **2015**, *9*, 1012−1057.

(4) Talapin, D. V.; Lee, J.-S.; Kovalenko, M. V.; Shevchenko, E. V. Prospects of Colloidal Nanocrystals for Electronic and Optoelectronic Applications. *Chem. Rev.* **2010**, *110*, 389−458.

(5) Gao, X.; Cui, Y.; Levenson, R. M.; Chung, L. W. K.; Nie, S. In Vivo Cancer Targeting and Imaging with Semiconductor Quantum Dots. *Nat. Biotechnol.* **2004**, *22*, 969−976.

(6) Howes, P. D.; Chandrawati, R.; Stevens, M. M. Colloidal Nanoparticles as Advanced Biological Sensors. *Science* **2014**, *346*, 1247390.

(7) Bell, A. T. The Impact of Nanoscience on Heterogeneous Catalysis. *Science* **2003**, *299*, 1688−1691.

(8) Hartley, C. L.; Kessler, M. L.; Dempsey, J. L. Molecular-Level Insight into Semiconductor Nanocrystal Surfaces. *J. Am. Chem. Soc.* **2021**, *143*, 1251−1266.

(9) Boles, M. A.; Ling, D.; Hyeon, T.; Talapin, D. V. The Surface Science of Nanocrystals. *Nat. Mater.* **2016**, *15*, 141−153.
(10) Anderson, N. C.; Hendricks, M. P.; Choi, J. J.; Owen, J. S. Ligand Exchange and the Stoichiometry of Metal Chalcogenide Nanocrystals: Spectroscopic Observation of Facile Metal-Carboxylate Displacement and Binding. *J. Am. Chem. Soc.* **2013**, *135*, 18536−18548.
(11) Noone, K. M.; Strein, E.; Anderson, N. C.; Wu, P.-T.; Jenekhe, S. A.; Ginger, D. S. Broadband Absorbing Bulk Heterojunction Photovoltaics Using Low-Bandgap Solution-Processed Quantum Dots. *Nano Lett.* **2010**, *10*, 2635−2639.
(12) Lu, H.; Joy, J.; Gaspar, R. L.; Bradforth, S. E.; Brutchey, R. L. Iodide-Passivated Colloidal PbS Nanocrystals Leading to Highly Efficient Polymer: Nanocrystal Hybrid Solar Cells. *Chem. Mater.* **2016**, *28*, 1897−1906.
(13) Seo, J.; Cho, M. J.; Lee, D.; Cartwright, A. N.; Prasad, P. N. Efficient Heterojunction Photovoltaic Cell Utilizing Nanocomposites of Lead Sulfide Nanocrystals and a Low-Bandgap Polymer. *Adv. Mater.* **2011**, *23*, 3984−3988.
(14) Itskos, G.; Papagiorgis, P.; Tsokkou, D.; Othonos, A.; Hermerschmidt, F.; Economopoulos, S. P.; Yarema, M.; Heiss, W.; Choulis, S. Size-Dependent Charge Transfer in Blends of PbS Quantum Dots with a Low-Gap Silicon-Bridged Copolymer. *Adv. Energy Mater.* **2013**, *3*, 1490−1499.
(15) Fafarman, A. T.; Koh, W.-k.; Diroll, B. T.; Kim, D. K.; Ko, D.-K.; Oh, S. J.; Ye, X.; Doan-Nguyen, V.; Crump, M. R.; Reifsnyder, D. C.; Murray, C. B.; Kagan, C. R. Thiocyanate-Capped Nanocrystal Colloids: Vibrational Reporter of Surface Chemistry and Solution-Based Route to Enhanced Coupling in Nanocrystal Solids. *J. Am. Chem. Soc.* **2011**, *133*, 15753−15761.
(16) Nag, A.; Kovalenko, M. V.; Lee, J.-S.; Liu, W.; Spokoyny, B.; Talapin, D. V. Metal-free Inorganic Ligands for Colloidal Nanocrystals: S^{2-}, HS^{-}, Se^{2-}, HSe^{-}, Te^{2-}, HTe^{-}, TeS_3^{2-}, OH^{-}, and NH_2^{-} as Surface Ligands. *J. Am. Chem. Soc.* **2011**, *133*, 10612−10620.
(17) Zhang, H.; Jang, J.; Liu, W.; Talapin, D. V. Colloidal Nanocrystals with Inorganic Halide, Pseudohalide, and Halometallate Ligands. *ACS Nano* **2014**, *8*, 7359−7369.
(18) De Roo, J.; Yazdani, N.; Drijvers, E.; Lauria, A.; Maes, J.; Owen, J. S.; Van Driessche, I.; Niederberger, M.; Wood, V.; Martins, J. C.; Infante, I.; Hens, Z. Probing Solvent - Ligand Interactions in Colloidal Nanocrystals by the NMR Line Broadening. *Chem. Mater.* **2018**, *30*, 5485−5492.
(19) Elimelech, O.; Aviv, O.; Oded, M.; Banin, U. A Tale of Tails: Thermodynamics of CdSe Nanocrystal Surface Ligand Exchange. *Nano Lett.* **2020**, *20*, 6396−6403.
(20) Zherebetskyy, D.; Scheele, M.; Zhang, Y.; Bronstein, N.; Thompson, C.; Britt, D.; Salmeron, M.; Alivisatos, P.; Wang, L.-W. Hydroxylation of the Surface of PbS Nanocrystals Passivated with Oleic Acid. *Science* **2014**, *344*, 1380−1384.
(21) Zhang, J.; Zhang, H.; Cao, W.; Pang, Z.; Li, J.; Shu, Y.; Zhu, C.; Kong, X.; Wang, L.; Peng, X. Identification of Facet-Dependent Coordination Structures of Carboxylate Ligands on CdSe Nanocrystals. *J. Am. Chem. Soc.* **2019**, *141*, 15675−15683.
(22) Fritzinger, B.; Capek, R. K.; Lambert, K.; Martins, J. C.; Hens, Z. Utilizing Self-Exchange to Address the Binding of Carboxylic Acid Ligands to CdSe Quantum Dots. *J. Am. Chem. Soc.* **2010**, *132*, 10195−10201.
(23) Giansante, C.; Infante, I. Surface Traps in Colloidal Quantum Dots: A Combined Experimental and Theoretical Perspective. *J. Phys. Chem. Lett.* **2017**, *8*, 5209−5215.
(24) Wang, Z.; Liu, T.; Long, X.; Li, Y.; Bai, F.; Yang, S. Understanding the Diverse Coordination Modes of Thiocyanate Anion on Solid Surfaces. *J. Phys. Chem. C* **2019**, *123*, 9282−9291.
(25) Pienpinijtham, P.; Han, X. X.; Ekgasit, S.; Ozaki, Y. Highly Sensitive and Selective Determination of Iodide and Thiocyanate Concentrations Using Surface-Enhanced Raman Scattering of Starch-Reduced Gold Nanoparticles. *Anal. Chem.* **2011**, *83*, 3655−3662.
(26) Leger, J. D.; Friedfeld, M. R.; Beck, R. A.; Gaynor, J. D.; Petrone, A.; Li, X.; Cossairt, B. M.; Khalil, M. Carboxylate Anchors Act as Exciton Reporters in 1.3 nm Indium Phosphide Nanoclusters. *J. Phys. Chem. Lett.* **2019**, *10*, 1833−1839.
(27) Kennehan, E. R.; Munson, K. T.; Doucette, G. S.; Marshall, A. R.; Beard, M. C.; Asbury, J. B. Dynamic Ligand Surface Chemistry of Excited PbS Quantum Dots. *J. Phys. Chem. Lett.* **2020**, *11*, 2291−2297.
(28) Murray, C. B.; Norris, D. J.; Bawendi, M. G. Synthesis and Characterization of Nearly Monodisperse CdE (E = Sulfur, Selenium, Tellurium) Semiconductor Nanocrystallites. *J. Am. Chem. Soc.* **1993**, *115*, 8706−8715.
(29) Sun, B.; Voznyy, O.; Tan, H.; Stadler, P.; Liu, M.; Walters, G.; Proppe, A. H.; Liu, M.; Fan, J.; Zhuang, T.; Li, J.; Wei, M.; Xu, J.; Kim, Y.; Hoogland, S.; Sargent, E. H. Pseudohalide-Exchanged Quantum Dot Solids Achieve Record Quantum Efficiency in Infrared Photovoltaics. *Adv. Mater.* **2017**, *29*, 1700749.
(30) Wu, B.; Breen, J. P.; Xing, X.; Fayer, M. D. Controlling the Dynamics of Ionic Liquid Thin Films via Multilayer Surface Functionalization. *J. Am. Chem. Soc.* **2020**, *142*, 9482−9492.
(31) Kim, H.; Cho, M. Infrared Probes for Studying the Structure and Dynamics of Biomolecules. *Chem. Rev.* **2013**, *113*, 5817−5847.
(32) Kumar, N.; Alam, F.; Dutta, V. Photoluminescence Study of Oleic Acid Capped and Hexanoic Acid Washed CdS Quantum Dots. *RSC Adv.* **2016**, *6*, 28316−28321.
(33) Yuan, R.; Yan, C.; Fayer, M. Ion−Molecule Complex Dissociation and Formation Dynamics in LiCl Aqueous Solutions from 2D IR Spectroscopy. *J. Phys. Chem. B* **2018**, *122*, 10582−10592.
(34) Lee, K.-K.; Park, K.-H.; Kwon, D.; Choi, J.-H.; Son, H.; Park, S.; Cho, M. Ion-pairing Dynamics of Li^{+} and SCN^{-} in Dimethylformamide Solution: Chemical Exchange Two-dimensional Infrared Spectroscopy. *J. Chem. Phys.* **2011**, *134*, 064506.
(35) Firman, P.; Xu, M.; Eyring, E. M.; Petrucci, S. Thermodynamics of Dimerization of Sodium Thiocyanate in Some Acyclic Polyethers Studied by Infrared Spectroscopy. *J. Phys. Chem.* **1992**, *96*, 8631−8639.
(36) Saar, D.; Petrucci, S. Infrared and Ultrasonic Spectra of Sodium Thiocyanate and Lithium Thiocyanate in Tetrahydrofuran. *J. Phys. Chem.* **1986**, *90*, 3326−3330.
(37) Sun, Z.; Zhang, W.; Ji, M.; Hartsock, R.; Gaffney, K. J. Contact Ion Pair Formation between Hard Acids and Soft Bases in Aqueous Solutions Observed with 2DIR Spectroscopy. *J. Phys. Chem. B* **2013**, *117*, 15306−15312.
(38) Park, S.; Ji, M.; Gaffney, K. J. Ligand Exchange Dynamics in Aqueous Solution Studied with 2DIR Spectroscopy. *J. Phys. Chem. B* **2010**, *114*, 6693−6702.
(39) Kwak, K.; Park, S.; Finkelstein, I. J.; Fayer, M. D. Frequency-frequency Correlation Functions and Apodization in Two-dimensional Infrared Vibrational Echo Spectroscopy: A New Approach. *J. Chem. Phys.* **2007**, *127*, 124503.
(40) Dunbar, J. A.; Arthur, E. J.; White, A. M.; Kubarych, K. J. Ultrafast 2D-IR and Simulation Investigations of Preferential Solvation and Cosolvent Exchange Dynamics. *J. Phys. Chem. B* **2015**, *119*, 6271−6279.
(41) Roy, V. P.; Kubarych, K. J. Interfacial Hydration Dynamics in Cationic Micelles Using 2D-IR and NMR. *J. Phys. Chem. B* **2017**, *121*, 9621−9630.
(42) Giannozzi, P.; Baroni, S.; Bonini, N.; Calandra, M.; Car, R.; Cavazzoni, C.; Ceresoli, D.; Chiarotti, G. L.; Cococcioni, M.; Dabo, I.; Dal Corso, A.; de Gironcoli, S.; Fabris, S.; Fratesi, G.; Gebauer, R.; Gerstmann, U.; Gougoussis, C.; Kokalj, A.; Lazzeri, M.; Martin-Samos, L.; Marzari, N.; Mauri, F.; Mazzarello, R.; Paolini, S.; Pasquarello, A.; Paulatto, L.; Sbraccia, C.; Scandolo, S.; Sclauzero, G.; Seitsonen, A. P.; Smogunov, A.; Umari, P.; Wentzcovitch, R. M. QUANTUM ESPRESSO: A Modular and Open-source Software Project for Quantum Simulations of Materials. *J. Phys.: Condens. Matter* **2009**, *21*, 395502.
(43) Perdew, J. P.; Burke, K.; Ernzerhof, M. Generalized Gradient Approximation Made Simple. *Phys. Rev. Lett.* **1996**, *77*, 3865−3868.

https://doi.org/10.1021/acs.jpclett.2c00493
J. Phys. Chem. Lett. 2022, 13, 3059−3065

(44) Vanderbilt, D. Soft Self-consistent Pseudopotentials in a Generalized Eigenvalue Formalism. *Phys. Rev. B* **1990**, *41*, 7892−7895.

(45) Frisch, M. J.; Trucks, G. W.; Schlegel, H. B.; Scuseria, G. E.; Robb, M. A.; Cheeseman, J. R.; Scalmani, G.; Barone, V.; Petersson, G. A.; Nakatsuji, H.; Li, X.; Caricato, M.; Marenich, A. V.; Bloino, J.; Janesko, B. G.; Gomperts, R.; Mennucci, B.; Hratchian, H. P.; Ortiz, J. V.; Izmaylov, A. F.; Sonnenberg, J. L.; Williams-Young, D.; Ding, F.; Lipparini, F.; Egidi, F.; Goings, J.; Peng, B.; Petrone, A.; Henderson, T.; Ranasinghe, D.; Zakrzewski, V. G.; Gao, J.; Rega, N.; Zheng, G.; Liang, W.; Hada, M.; Ehara, M.; Toyota, K.; Fukuda, R.; Hasegawa, J.; Ishida, M.; Nakajima, T.; Honda, Y.; Kitao, O.; Nakai, H.; Vreven, T.; Throssell, K.; Montgomery, J. A., Jr.; Peralta, J. E.; Ogliaro, F.; Bearpark, M. J.; Heyd, J. J.; Brothers, E. N.; Kudin, K. N.; Staroverov, V. N.; Keith, T. A.; Kobayashi, R.; Normand, J.; Raghavachari, K.; Rendell, A. P.; Burant, J. C.; Iyengar, S. S.; Tomasi, J.; Cossi, M.; Millam, J. M.; Klene, M.; Adamo, C.; Cammi, R.; Ochterski, J. W.; Martin, R. L.; Morokuma, K.; Farkas, O.; Foresman, J. B.; Fox, D. J. *Gaussian 16*, Revision A.03; Gaussian, Inc.: Wallingford, CT, 2016.

Recommended by ACS

Influence of Capping Ligands, Solvent, and Thermal Effects on CdSe Quantum Dot Optical Properties by DFT Calculations

Didac A. Fenoll, Xavier Solans-Monfort, *et al.*

MARCH 17, 2023
ACS OMEGA
READ

Spontaneous Patterning of Binary Ligand Mixtures on CdSe Nanocrystals: From Random to Janus Packing

Orian Elimelech, Uri Banin, *et al.*

MARCH 09, 2023
ACS NANO
READ

Reexamination of the Giant Oscillator Strength Effect in CdSe Nanoplatelets

Benjamin T. Diroll and Richard D. Schaller

FEBRUARY 22, 2023
THE JOURNAL OF PHYSICAL CHEMISTRY C
READ

***In Situ* Optical and X-ray Spectroscopy Reveals Evolution toward Mature CdSe Nanoplatelets by Synergetic Action of Myristate and Acetate Ligands**

Johanna C. van der Bok, Andries Meijerink, *et al.*

APRIL 28, 2022
JOURNAL OF THE AMERICAN CHEMICAL SOCIETY
READ

Get More Suggestions >

https://doi.org/10.1021/acs.jpclett.2c00493
J. Phys. Chem. Lett. 2022, 13, 3059−3065